


Summer 2009

## Inhibition of Yeast Hexokinase by the Antimalarial Drug Artemisinin: Probing Mechanism of Action with a Model Enzyme

Jennifer S. Spence  
*Old Dominion University*

Follow this and additional works at: [https://digitalcommons.odu.edu/biology\\_etds](https://digitalcommons.odu.edu/biology_etds)

 Part of the [Biochemistry Commons](#), [Microbiology Commons](#), [Molecular Biology Commons](#), and the [Parasitic Diseases Commons](#)

---

### Recommended Citation

Spence, Jennifer S.. "Inhibition of Yeast Hexokinase by the Antimalarial Drug Artemisinin: Probing Mechanism of Action with a Model Enzyme" (2009). Master of Science (MS), Thesis, Biological Sciences, Old Dominion University, DOI: 10.25777/mftx-4d14  
[https://digitalcommons.odu.edu/biology\\_etds/285](https://digitalcommons.odu.edu/biology_etds/285)

This Thesis is brought to you for free and open access by the Biological Sciences at ODU Digital Commons. It has been accepted for inclusion in Biological Sciences Theses & Dissertations by an authorized administrator of ODU Digital Commons. For more information, please contact [digitalcommons@odu.edu](mailto:digitalcommons@odu.edu).

# **INHIBITION OF YEAST HEXOKINASE BY THE ANTIMALARIAL DRUG ARTEMISININ: PROBING MECHANISM OF ACTION WITH A MODEL ENZYME**

by

Jennifer S. Spence  
B.S. May 2003, George Washington University  
B.A. January 2001, University of Virginia

A Thesis Submitted to the Faculty of  
Old Dominion University in Partial Fulfillment of the  
Requirement for the Degree of

MASTER OF SCIENCE

BIOLOGY

OLD DOMINION UNIVERSITY  
August 2009

Approved by:

\_\_\_\_\_  
Roland A. Cooper (Director)

\_\_\_\_\_  
Wayne L. Hynes (Member)

\_\_\_\_\_  
Christopher J. Osgood (Member)

## ABSTRACT

### INHIBITION OF YEAST HEXOKINASE BY THE ANTIMALARIAL DRUG ARTEMISININ: PROBING MECHANISM OF ACTION WITH A MODEL ENZYME

Jennifer S. Spence  
Old Dominion University, 2009  
Director: Dr. Roland A. Cooper

A leading infectious cause of death, malaria threatens approximately half of the world's population, and drug-resistant strains of *Plasmodium falciparum* have created immense difficulty in chemotherapy of the disease. The artemisinin (ART) class of antimalarials may represent a powerful solution. In addition to their safety, effectiveness, and moderate cost, they are the only drugs in use for which there has been no widespread evidence of clinical resistance. The exact parasitocidal mechanism of ART is highly contested, but evidence suggests that protein alkylation may play a role in cytotoxicity. *In vitro* assays were performed using yeast hexokinase (HK) to demonstrate a hypothesized relationship between alkylation by ART and activity inhibition of a model enzyme. ART, in the presence of ferrous iron, irreversibly inhibited HK phosphotransferase activity. The drug's endoperoxide bridge was essential for activity against HK, indicating that inhibition is mediated by radicals. MALDI-TOF mass spectrometry failed to detect ART adducts of inhibited HK, however, which suggests that alkylation may not be responsible for inhibition of enzymatic activity. Further, although alkylation of thiols by ART has been confirmed and was hypothesized as the means of inhibition of HK, solvolysis-released adducts of ART and Thiopropyl Sepharose 6B resin were not observed by thin-layer chromatography. Loss of protein function through ART-induced oxidation, which has already been implicated in membrane damage, is therefore proposed as a component of the *in vivo* mechanism of ART.

## TABLE OF CONTENTS

	Page
LIST OF FIGURES .....	v
I. INTRODUCTION .....	1
LIFE CYCLE OF MALARIAL PARASITES .....	1
THE PATHOLOGY OF MALARIA .....	2
DRUG MANAGEMENT OF MALARIA .....	3
ARTEMISININ BACKGROUND .....	5
ARTEMISININ PHARMACOKINETICS .....	6
POSSIBLE MECHANISMS OF ARTEMISININ ACTION .....	6
POTENTIAL TARGETS OF ARTEMISININ .....	11
AIMS AND RATIONALE .....	15
II. MATERIALS AND METHODS .....	19
HEXOKINASE ASSAYS .....	19
DIALYSIS OF ARTEMISININ-TREATED HEXOKINASE .....	20
SOLVOLYSIS OF ARTEMISININ-TREATED RESIN-LINKED THIOLS .....	21
TWO-DIMENSIONAL ELECTROPHORESIS OF ARTEMISININ- TREATED HEXOKINASE .....	23
MASS SPECTROMETRY OF ARTEMISININ-TREATED HEXOKINASE .....	24
III. RESULTS .....	26
INHIBITION OF HEXOKINASE ACTIVITY BY ARTEMISININ .....	26
ARTEMISININ REACTION WITH THIOPROPYL SEPHAROSE RESIN .....	40
ALKYLATION OF ARTEMISININ-TREATED HEXOKINASE .....	44
MASS SPECTROMETRY OF DRUG-TREATED HEXOKINASE .....	47
IV. DISCUSSION .....	53
INHIBITION OF HEXOKINASE ACTIVITY BY ARTEMISININ .....	54
ALKYLATION OF HEXOKINASE BY ARTEMISININ .....	57
DETECTION OF COVALENT HEXOKINASE-ARTEMISININ ADDUCTS .....	59
MASS SPECTROMETRIC STUDIES OF COVALENT ARTEMISININ BINDING .....	60
OXIDATIVE DAMAGE TO HEXOKINASE BY ARTEMISININ RADICALS .....	61
PATHWAYS IN ARTEMISININ-INDUCED OXIDATIVE DAMAGE .....	62
SIGNIFICANCE OF ARTEMISININ ALKOXYL RADICALS <i>IN VIVO</i> .....	64
<i>IN VIVO</i> CORRELATIONS OF THE <i>IN VITRO</i> HEXOKINASE ASSAY .....	67
V. CONCLUSIONS .....	71
VI. REFERENCES .....	74

	Page
VII. APPENDICES .....	85
APPENDIX I: ADDITIONAL DRUG STRUCTURES.....	85
APPENDIX II: MALDI-TOF OF HEXOKINASE.....	86
VIII. VITA .....	107

## LIST OF FIGURES

Figure	Page
1. Life cycle of <i>Plasmodium falciparum</i> .....	2
2. Structure of ART and derivatives .....	7
3. Proposed heterolytic activation of ART by ferrous iron complexation .....	8
4. Proposed pathways in the Fe <sup>(II)</sup> -mediated homolytic activation of ART....	10
5. Structure of a heme-ART adduct.....	12
6. SDS-PAGE and autoradiograph of <i>P. falciparum</i> lysates.....	14
7. Coupled-enzyme reaction used in HK studies.....	19
8. Overview of the reactions involved in thiopropyl sepharose 6B resin preparation, drug treatment, and derivative release .....	22
9. Plot of NADPH absorbance over time at varying HK concentrations .....	27
10. Dose-dependent inhibition of HK activity by ninhydrin .....	28
11. Dose-dependent inhibition of HK activity by iodoacetamide.....	28
12. Time-dependent loss of HK activity in the presence of ART and/or ferrous iron .....	29
13. HK activity following incubation with ferrous iron and varying concentrations of ART .....	30
14. HK activity following incubation with ART and varying concentrations of ferrous iron .....	31
15. HK activity following incubation with ferrous iron and ART or dDHA.....	32
16. HK activity following incubation with ART and ferrous or ferric iron .....	33
17. HK activity following incubation with ART and FeCl <sub>2</sub> or hemin.....	34
18. Protection of HK activity against inhibition by ART and iron by pre- treatment with ATP .....	35

Figure	Page
19. Protection of HK activity against inhibition by ART and iron by pre-treatment with mannose .....	36
20. Inability of ATP to reverse inhibition of HK treated with ART and iron.....	37
21. Inability of mannose to reverse inhibition of HK treated with ART and iron .....	38
22. Inability of dialysis to restore activity to ART- and iron-treated HK.....	39
23. TLC of ART-thiopropyl sepharose resin solvolysis reaction products .....	42
24. TLC of ART following 24 h incubation with varying concentrations of $\text{FeCl}_2$ .....	43
25. Two-dimensional electrophoresis of drug-treated HK (first gel set).....	44
26. Two-dimensional electrophoresis of drug-treated HK (second gel set)....	46
27. MALDI-TOF spectrum of untreated HK-A, fragment mass 900-2200.....	48
28. MALDI-TOF spectrum of untreated HK-A, fragment mass 2200-3800.....	49
29. MALDI-TOF peptide matches to the amino acid sequence of HK-A .....	51
30. Proposed pathways in the ferrous iron-mediated activation of ART to oxygen radicals capable of HK activity inhibition .....	65
31. MALDI-TOF spectrum of spot 1, fragment mass 900-2200.....	86
32. MALDI-TOF spectrum of spot 1, fragment mass 2200-3800.....	87
33. MALDI-TOF spectrum of spot 3, fragment mass 900-2200.....	88
34. MALDI-TOF spectrum of spot 3, fragment mass 2200-3800.....	89
35. MALDI-TOF spectrum of spot 4, fragment mass 900-2200.....	90
36. MALDI-TOF spectrum of spot 4, fragment mass 2200-3800.....	91
37. MALDI-TOF spectrum of spot 5, fragment mass 900-2200.....	92
38. MALDI-TOF spectrum of spot 5, fragment mass 2200-3800.....	93

Figure	Page
39. MALDI-TOF spectrum of spot 6, fragment mass 900-2200.....	94
40. MALDI-TOF spectrum of spot 6, fragment mass 2200-3800.....	95
41. MALDI-TOF spectrum of spot 7, fragment mass 900-2200.....	96
42. MALDI-TOF spectrum of spot 7, fragment mass 2200-3600.....	97
43. MALDI-TOF spectrum of spot 8, fragment mass 900-2200.....	98
44. MALDI-TOF spectrum of spot 8, fragment mass 2200-3600.....	99
45. MALDI-TOF spectrum of spot 9, fragment mass 900-2200.....	100
46. MALDI-TOF spectrum of spot 9, fragment mass 2200-3600.....	101
47. MALDI-TOF spectrum of spot 10, fragment mass 900-2200.....	102
48. MALDI-TOF spectrum of spot 10, fragment mass 2200-3600.....	103
49. MALDI-TOF spectrum of spot 11, fragment mass 900-2200.....	104
50. MALDI-TOF spectrum of spot 11, fragment mass 2200-3600.....	105
51. MALDI-TOF spectrum of spot 12, fragment mass 900-2200.....	106
52. MALDI-TOF spectrum of spot 12, fragment mass 2200-3600.....	107



## INTRODUCTION

Responsible for 500 million infections and 1-3 million deaths annually [1], malaria is the world's leading parasitic cause of morbidity and mortality. Nearly half of the global population lives in regions endemic to malaria, mainly sub-Saharan Africa, southeast Asia, and parts of Central and South America. Disease etiology derives from protozoans of the genus *Plasmodium*; of the four species infecting man, *P. vivax*, *P. malariae*, and *P. ovale* rarely cause death [2]. *P. falciparum*, on the other hand, represents the greatest threat, accounting for approximately 50% of all clinical cases and the vast majority of fatalities [1].

### Life Cycle of Malarial Parasites

Transmitted to man only by mosquitoes of the genus *Anopheles*, *Plasmodium* demonstrates a unique heteroxenous life cycle (Fig. 1) that necessitates vertebrate hosts [2]. Following entry into the human circulatory system, sporozoites from mosquito salivary glands penetrate hepatocytes for a nonpathological phase that first involves metamorphosis into trophozoites. Mature trophozoites replicate exponentially through schizogony into merozoites, with each trophozoite producing approximately 30,000 daughter merozoites. Merozoites are released from hepatocytes to invade erythrocytes. Inside blood cells, the parasite undergoes ring, trophozoite, and schizont stages, the latter of which results in clonal reproduction and release of more daughter merozoites (8-

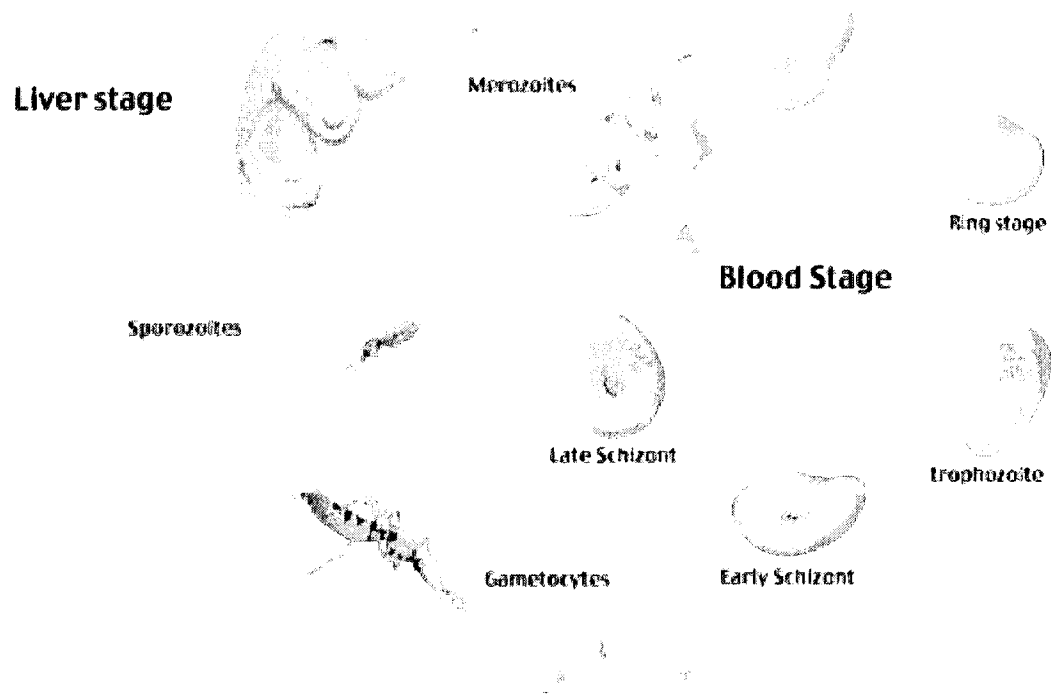


Fig. 1 - Life cycle of *Plasmodium falciparum*. From <http://www.pasteur.fr/recherche/unites/ImmStr/en/projects/malaria.html>.

32 produced). In select circumstances, merozoites may differentiate into gametocytes, which are infective to the anopheline mosquito and can engage in sexual reproduction within their insect host.

### The Pathology of Malaria

Intraerythrocytic forms of *Plasmodium* are solely responsible for disease

pathology. The classic malarial symptom of periodic fevers is caused by massive hemolysis upon synchronized merozoite release [2]. Infections can be characterized by species, in part, by whether paroxysms occurs every 48 or 72 hours. Loss of erythrocytes also leads to anemia. In addition to extremely high levels of blood parasitemia (> 60% of cells may be infected, while 25% parasitemia is usually fatal), the severity of *falciparum* malaria stems from parasite-induced alteration of the erythrocyte ultrastructure. Knob-like erythrocyte membrane protrusions cause cytoadherence of parasitized cells to the cerebral microvasculature. Neurological symptoms include seizures and coma, which frequently precede death. Prenatal malaria is a leading cause of maternal death and poor infant development and mortality in Africa, primary location of the world's malaria burden [1] and most *P. falciparum* infections. As with most infectious diseases, malaria poses the greatest risk to children and the immunocompromised, while adults in endemic regions of sub-Saharan Africa may have partial immunity due to repeated, long-term exposure to the parasite [2].

### **Drug Management of Malaria**

Most classes of antimalarial drugs target the more metabolically-active intra-erythrocytic forms of the parasite. The parasite endocytoses and catabolizes the hemoglobin within erythrocytes to meet its need for amino acids and must sequester the toxic heme moiety in a less harmful form in its digestive vacuole (DV) [2]. Quinine, chloroquine, and other quinolines interfere with the

crystallization of heme into inert hemozoin [3]. Atovaquone, a ubiquinone analog, affects protozoal mitochondrial electron transport [4]. Because *Plasmodium* is unable to synthesize purines *de novo*, drugs such as proguanil, sulfadoxine, and pyrimethamine target purine salvage [5]. Other antibiotic agents, among them doxycycline, have also proven useful against the parasite. [6,7]. Vaccines represent an ideal form of prophylaxis but have yet to show more than limited efficacy in clinical trials [8].

Clinical malaria treatments, as well as attempts to combat the disease on a global scale, have been severely hampered by the emergence and spread of drug resistant parasites. *P. falciparum* displays a remarkable capacity for rendering antimalarials clinically ineffective. Mutations in *pfcr*, which encodes the *P. falciparum* chloroquine resistance transporter spanning the DV membrane, allow increased quinoline drug efflux, reducing antimalarial effects [9]. Mutated P-glycoprotein homologue Pgh1, the product of the *pfmdr1* (multidrug resistance transporter) gene, also has been implicated in reduced effectiveness for several types of drug [10]. Additionally, due to a common point mutation in cytochrome *b* [4], clinical resistance to atovaquone was observed mere months after the drug's release for prophylaxis [11]. In particular, the unfortunate advent of resistance to chloroquine, previously the gold standard among antimalarials, created arguably the largest obstacle to worldwide malaria eradication [12]. Despite disease resurgence, the rediscovery of an ancient folk remedy is giving rise to a new era in malaria treatment.

## Artemisinin Background

Preparations of sweet wormwood (*Artemisia annua* L.) have been used as antipyretics, thus accidental antimalarials, in China for more than 2000 years [13], but only in the last three decades has the plant's active component been isolated and identified [14]. Artemisinin (ART) and its derivatives are the only agents for which no widespread clinical resistance has been demonstrated in *P. falciparum* [15], although recent studies indicate that resistance may be developing in limited foci [16, 17]. The World Health Organization currently advocates the use of ART combination therapies (ACTs), typically employing the quinoline amodiaquine, the quinoline-like lumefantrine, or sulfadoxine/pyrimethamine, as a first-line defense against malaria [1]. ACTs usually feature the derivatives artesunate (ARS) or artemether (ARM) due to poor solubility of the parent compound. The combination of ART derivatives, which have particularly short half-lives, with slower-clearing, mechanistically-unrelated drugs is meant to improve treatment efficacy and decrease the possibility of widespread resistance [18]. ART itself is highly potent, with an  $IC_{50}$  frequently lower than that of chloroquine [18], it eliminates parasites from the blood quickly, and its specific targeting of *Plasmodium* produces few side effects on hosts [19]. Further, good shelf stability and moderate cost make ART attractive to healthcare providers in malaria-endemic areas [1]. The precise manner in which this excellent drug works, however, has yet to be resolved conclusively.

## Artemisinin Pharmacokinetics

Derivatives of ART are most commonly administered orally, but intravenous, intramuscular, or suppository dosage can be used in severe malaria or with infants. ART drugs are hydrolyzed to dihydroartemisinin (DHA) in the stomach (quickly) and blood (more slowly), with maximal blood concentrations for oral doses occurring after two hours [20]. Intramuscular oil suspensions are absorbed at a much slower rate, and DHA blood levels peak after six hours [21]. Once in the blood, DHA has a half-life of approximately one hour [20].

ART derivatives enter erythrocytes by means of passive diffusion, as their basic chemical structures are highly lipophilic [22]. *Plasmodium* actively takes up the drug from inside the blood cell via a tubulovesicular network of membranes that extend from the parasitophorous vacuole to the erythrocyte periphery [23]. It is presumed that uptake occurs through a carrier-mediated process [22]. Only after entering the parasite does the drug unleash its selective cytotoxicity.

## Possible Mechanisms of Artemisinin Action

ART (Fig. 2) is a sesquiterpene lactone featuring an endoperoxide bridge within a 1,2,4-trioxane ring. The endoperoxide moiety is essential for antiparasitic activity [24], as derivatives lacking one or both of the peroxy oxygens are pharmacologically inactive. In general, peroxides are unstable and can easily form reactive oxygen species (ROS), and this structural feature of ART led to theories of radical-induced parasite death [14, 25]. Formation of ROS is enhanced by Fenton reagents, such as ferrous heme iron, which is available in

the parasite through hemoglobin metabolism [26]. The drug is commonly believed to be converted to radicals via reductive cleavage of the endoperoxide

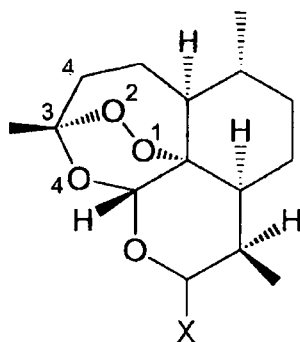


Fig. 2 - Structure of ART and derivatives. X = O (ART), OH (DHA), OCH<sub>3</sub> (ARM), OCOCH<sub>2</sub>CH<sub>2</sub>COOH (ARS). Oxygens 1 and 2 comprise the endoperoxide bridge, while oxygens 1, 2, and 4 are part of the trioxane moiety. Carbons 3 and 4 of the sesquiterpene lactone structure are also labeled.

moiety—possibly due to heme or an endogenous parasitic iron source such as catalase or cytochromes [27]. Evidence in favor of iron activation is seen in the reduction of ART-induced damage to erythrocyte membranes by metal chelators [28]. The drug is also effective *in vitro* against many types of cancer cells, which have higher cytosolic iron levels due to increased transferrin receptor expression [29]; addition of iron can further enhance drug potency against cancer cells [30, 31]. Following peroxide bond cleavage, ART undergoes rearrangement to free-radical intermediates, which are thought to account for cytotoxicity. Heterolytic

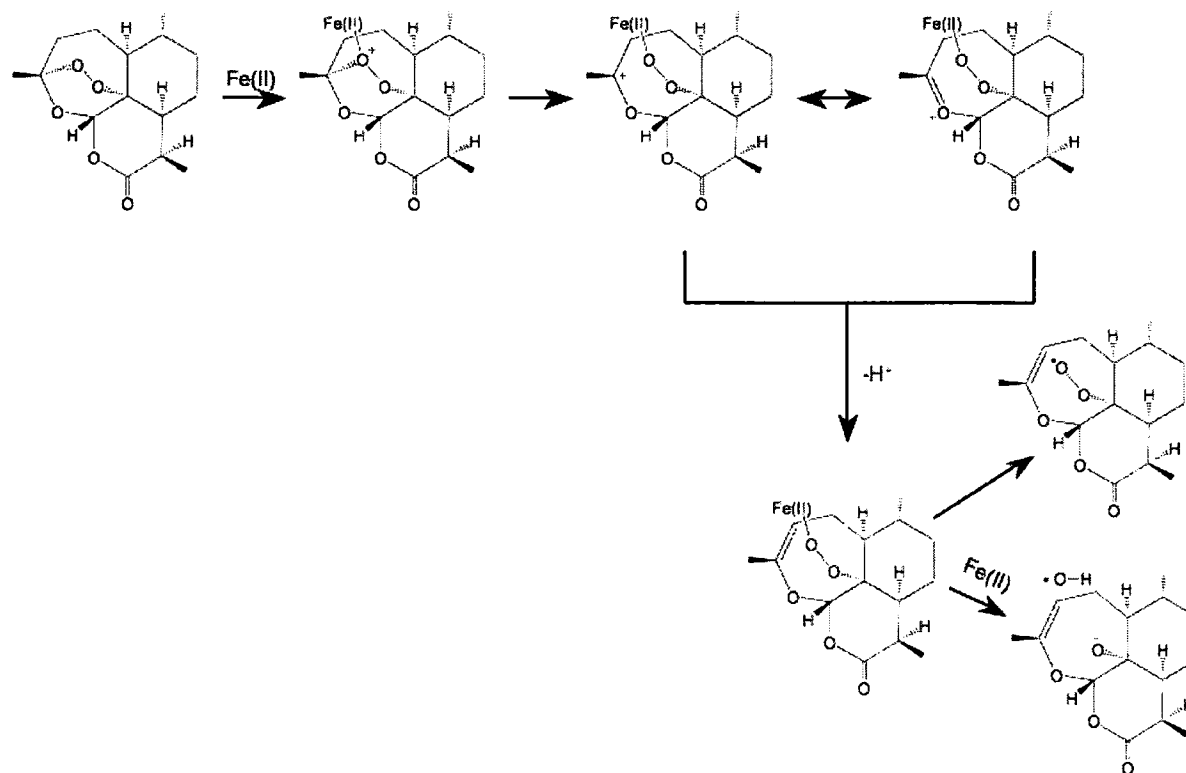


Fig. 3 - Proposed heterolytic activation of ART by ferrous iron complexation. This pathway generates a metalloperoxide that decomposes to a carbocation and/or oxygen free radicals capable of oxidatively damaging biomolecules. Adapted from Olliaro *et al.* [32]



cleavage of the endoperoxide has been suggested as a mode of reduced iron activation (Fig. 3) [32]. In this scheme, O4 of the trioxane ring stabilizes the positive charge added by iron complexation and facilitates ring opening. Intermolecular rearrangement creates a metalloperoxide that can further decompose to a carbocation or oxygen free radicals. Most experimental evidence, however, appears to support homolytic bond cleavage (Fig. 4). Attack by reduced iron produces a radical at either oxygen, depending on reaction conditions, and alkoxy drug radicals can rearrange to form carbon-centered radicals. Oxygen-centered radicals of ART have been shown to increase oxidative stress within the parasite [34] and damage erythrocyte membranes [35]. Adducts of alkoxy radicals have been proposed, including the iron-oxo species  $\text{Fe(IV)=O}$ , formed as a leaving group during radical rearrangement [32]. However, carbon-centered radicals may provide a more suitable explanation of the means by which ART effects parasite death.

Much has been made of the greater stability of carbon-centered ART radicals over their oxygen-centered precursors [36]. Being less transient, they may have a greater likelihood of interacting with targets prior to degradation or quenching. In order to demonstrate the importance of carbon radicals in ART cytotoxicity, Posner *et al.* synthesized two sets of trioxanes: in the first set (Appendix I), two of three compounds were unable to complete the O1 pathway due to lack of an appropriate hydrogen for abstraction at C4, while in the second set, two of three compounds were unable to complete the O2 pathway due to steric hindrance at C3 [37]. Within each set, only the compounds that were capable of producing

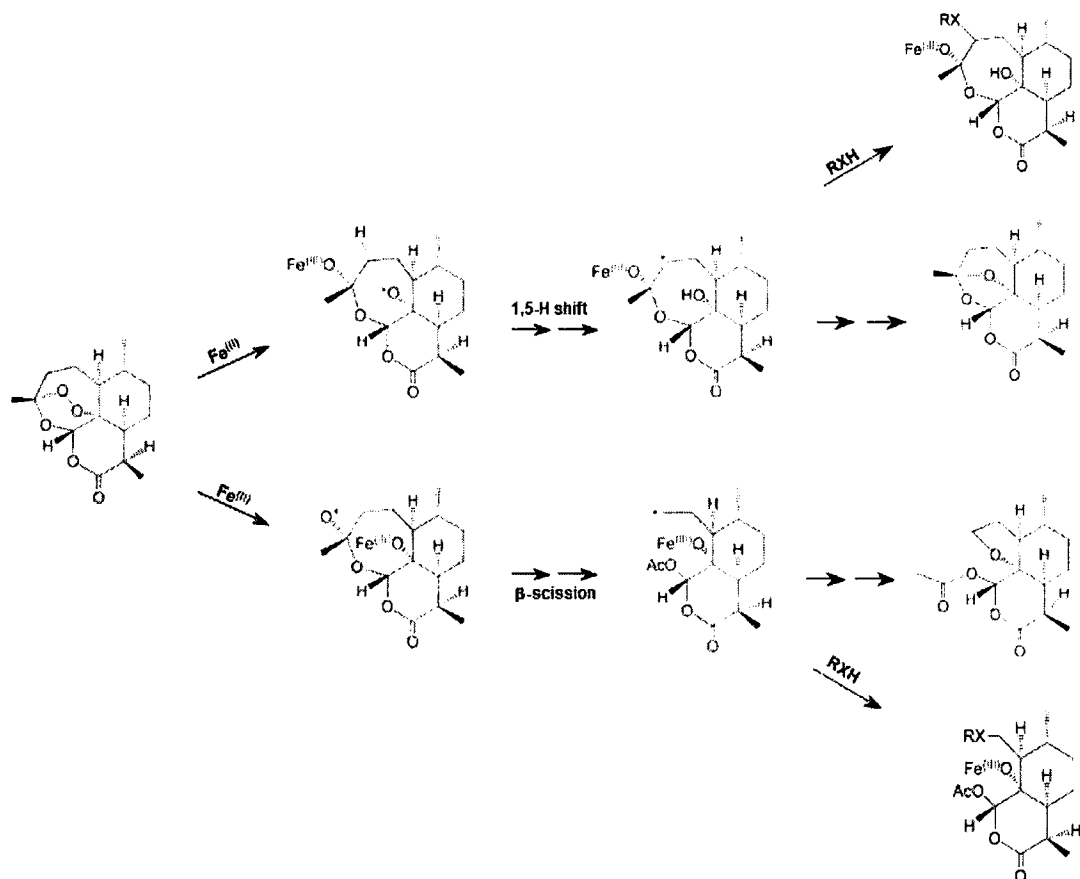


Fig. 4 - Proposed pathways in the Fe<sup>II</sup>-mediated homolytic activation of ART. In the top pathway (O1 path), following cleavage of the endoperoxide, abstraction of a hydrogen from C4 to O1 creates a C4 radical. In the bottom pathway (O2 path), transfer of the radical from O2 to C3 causes bond scission between C3 and C4 and subsequent rearrangement to a separate C4 radical. Drug radicals may react with a variety of nucleophiles (RXH, where X = O, NH, S) or self-quench.

Adapted from Tonmuphean *et al.* [33].

self-quenched metabolites following reaction with iron acted as potent antimalarials. Posner *et al.* took these findings to indicate an importance for carbon radicals, because they could not be formed by the inactive trioxanes. As alkylating species, carbon-centered radicals can react with a wide variety of biological molecules bearing nucleophiles such as thiolates, amines, phosphates, and carboxylates [38], and alkylation is an established mode of cytotoxicity [39, 40].

### **Potential Targets of Artemisinin**

Because ART has the ability to form species capable of alkylation, a definitive target for its action has been long sought. Heme was identified early as a prospective target, since it serves a target for a number of antimalarials and possesses a central iron molecule that might activate the drug. ART has, in fact, been demonstrated to bind to heme [41, 42], and heme-ART adducts (Fig. 5) have been recovered from the spleen (which removes parasitized erythrocytes) and urine of *P. vinckei*-infected, but not healthy, mice [42]. The parasite DV has been proposed as a primary site of ART activation and/or action, as the earliest signs of drug-induced morphological alteration are seen in this organelle [43]. Asawamahasakda *et al.* showed greatest localization of the drug occurring in the DV fraction of parasite lysates [45]. In that study, only a minor percentage of ART was covalently-associated with heme, and drug localization within the parasite has been disputed by other researchers [46]. In spite of demonstrated

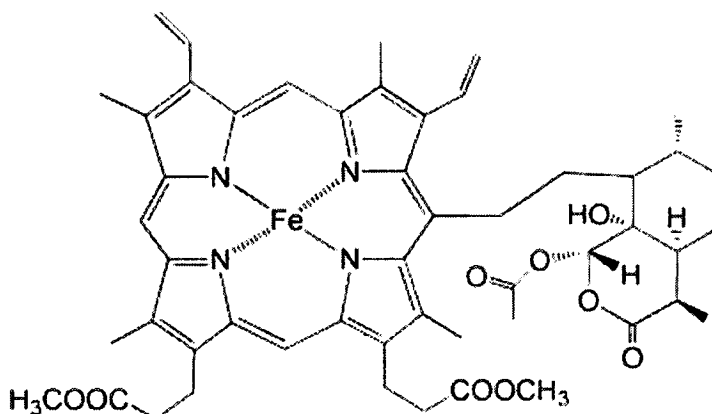


Fig. 5 - Structure of a heme-ART adduct. Adapted from Bousejra-El Harah *et al.* [44].

alkylation, a role for ART in interference with heme sequestration is debatable, as the drug has little effect on hemozoin formation [47, 48]. Heme-ART binding may contribute to oxidative damage within the parasite, since peroxidase activity of heme increases in the presence of ART [35].

An early study by Asawamahasakda *et al.* [45] demonstrated alkylation of six parasite proteins by radiolabeled ART derivatives. The proteins were not among the most abundant in the parasite, suggesting a high degree of reaction specificity. While the other labeled proteins are still unknown, one was identified as the *P. falciparum* translationally-controlled tumor protein homologue (TCTP) [49], found in the cytosol and DV membrane [50]. ART binds to the thiols of the protein, but TCTP function and whether ART alkylation of it contributes to parasite death are uncertain.

Recently, the *P. falciparum* sarco-endoplasmic reticulum  $\text{Ca}^{2+}$ -dependent ATPase (SERCA) orthologue PfATP6 has received support as a purported ART target. Inhibition of this ATPase by ART was demonstrated when the protein was expressed in *Xenopus* oocytes [46]. Eckstein-Ludwig *et al.* also showed pharmacological antagonism between ART and thapsigargin, another sesquiterpene lactone and a known SERCA inhibitor, and the two drugs are predicted to occupy the same binding site [51]. An amino acid substitution in PfATP6 may be associated with decreased parasite susceptibility to ART [51], but sensitivity to the drug appears to be modulated by more than a single protein, as Pgh1 has also been implicated in increased ART tolerance by *Plasmodium* [10].

Several other proteins have been offered as possible ART targets, among them, the heme-binding histidine-rich protein II [52] and cysteine proteases [53], which are present in the DV. Cysteine is of particular interest, as ART has been demonstrated to alkylate it *in vitro* [54]. The amino acid possesses a highly nucleophilic sulfhydryl group, making it an exceptionally good target for free radicals. Alkylation of glutathione has been reported [55], and ART may potentially bind to a number of cysteine-bearing proteins or other biomolecules. The notion of ART having multiple targets within the parasite or being a nonspecific alkylator is also a distinct possibility. Building on the research of Asawamahasakda *et al.* [45], previous work by this laboratory showed moderate alkylation of a wide range of parasite proteins following incubation with [ $^3\text{H}$ ]DHA (R. Cooper, unpublished results, Fig. 6). As Figure 6 indicates, ART may have

abundant protein targets in the parasite. Further evidence against a specific target, such as PfATP6, was provided by pure 1,2,4-trioxane enantiomers synthesized by O'Neill *et al.* [56]. The enantiomers were structurally related to and exhibited similar potency as ART. The latter observation would be unlikely if there were a single parasite target, which would require stereospecificity for chiral recognition of the drug by the target. Most importantly, the fact that clinical resistance to ART has rarely arisen in *Plasmodium* infections supports the theory that the drug acts on a multiplicity of targets.

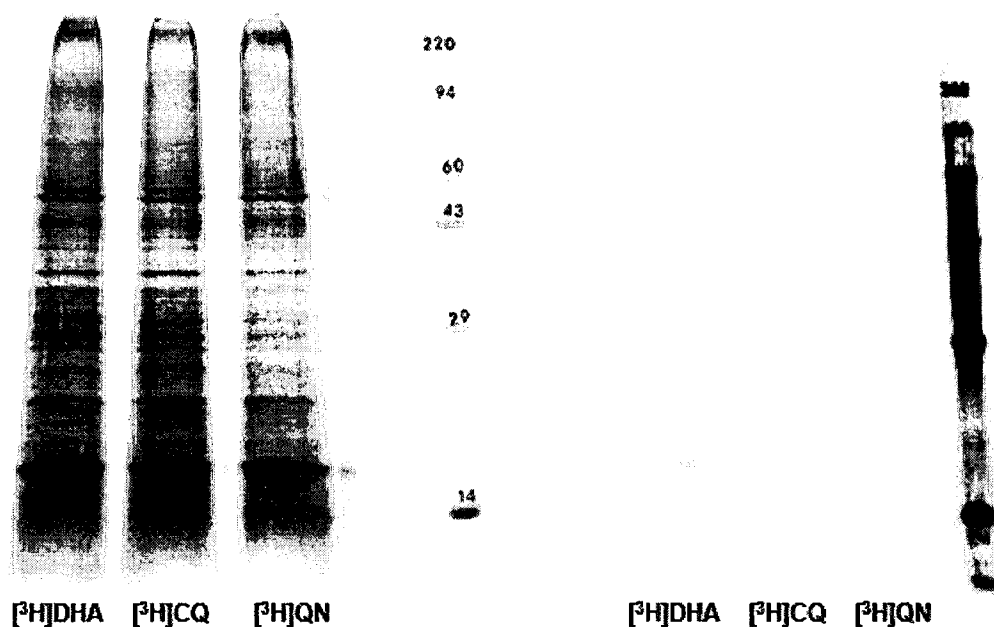


Fig. 6 - SDS-PAGE (left) and autoradiograph (right) of *P. falciparum* lysates. Parasites were isolated following 12 h exposure to  $[^3\text{H}]\text{DHA}$ ,  $[^3\text{H}]\text{chloroquine}$  (CQ), or  $[^3\text{H}]\text{quinine}$  (QN). Drug-bound proteins are visible in the autoradiograph.

In addition to *Plasmodium* and cancer cells, ART is effective against a variety of other pathogens. ART has been shown to cause calcium imbalances in trypanosomes [57] and *Toxoplasma gondii* [58], which suggests a role for it in impairing  $\text{Ca}^{2+}$ -dependent ATPases, much like that purported in *Plasmodium*. The drug also reduces *Schistosoma* burdens in mice [59]. Although schistosomes, as blood flukes, generate hemozoin [60], ART toxicity appears to be completely unrelated to heme metabolism in these parasites. Instead, schistosomes exhibit tegumental damage [61]. Cutaneous *Leishmania* promastigotes and amastigotes are susceptible to ART, as well [62]. Additionally, the drug possesses antiviral action against hepatitis B [63] and C [64] viruses and bovine viral diarrhea virus [65] *in vitro*. No ART-induced cytotoxicity is observed in host cells, while both viral production and cytopathy due to the viruses are significantly reduced. In particular, hepatitis C virus polymerase exhibits activity loss upon exposure to the drug [64]. ART effectiveness against so many disparate pathogens appears to support selective activation, which precludes damage to host cells, and nonspecific targeting, as parasite proteins such as PfATP6 have no viral homologue.

### **Aims and Rationale**

The three aims of our research were investigation of the effect of ART on protein function, demonstration of covalent binding of ART to protein targets, and characterization of ART adducts. In particular, we examined protein alkylation by ART radicals as a possible component of cytotoxicity and malarial parasite death.

To date, researchers have shown covalent ART binding to proteins without characterizing the effect on their biological roles, or they have established inhibition of protein function without providing incontrovertible evidence of alkylation. We intended to bridge previous findings on the drug's interaction with proteins and demonstrate that functional inhibition of vital proteins due to alkylation could be an important mode of drug action within the parasite.

For our first aim, investigation of the effect of ART on protein function, a model enzyme system was used in place of direct experimentation with parasite proteins. The failure thus far to validate targets or pathways of ART points toward inherent complexities of *in vivo* drug metabolism. Instead of an attempt to identify, isolate, and investigate the activity of one or a few parasite proteins from the multitude alkylated by the drug (Fig. 6), a model *in vitro* system might better serve to explore the effects of ART on protein function—specifically, enzymatic activity. Because the drug appears to be a moderate, nonspecific alkylator, its inhibitory effect on a single essential enzyme may be representative of its effect on other proteins.

Yeast hexokinase (HK, E.C. 2.7.1.1., from *Saccharomyces cerevisiae*), which catalyzes the initial reaction of glycolysis, was selected as the model enzyme with which to investigate the effects of proposed ART alkylation on catalytic activity. It was chosen on the basis of several notable properties: the enzyme is able to be alkylated—typically at its cysteine residues [66]; alkylated HK can exhibit a measurable decrease in phosphotransferase activity [67, 68]; and enzyme activity is easily assayed. The sensitivity of HK to alkylation gives the



enzyme the advantage of being well-studied with a range of alkylators. Further, HK has been useful in demonstrating cytotoxicity for a variety of compounds [69, 70]. Agents such as alloxan, ninhydrin, and lonidamine, the latter of which is also effective against trypanosomes [71], act specifically on hexokinase to induce cytopathy [71, 72].

Building upon the first aim, the second aim of our research was investigation of covalent binding of ART to HK. Matrix-assisted laser desorption-ionization–time-of-flight (MALDI-TOF) mass spectrometry, frequently used to verify covalent modification of proteins, was intended to provide evidence of alkylation of HK by ART. Because the amino acid sequence of HK is known [73, 74], identification of any alkylated residues was theorized.

Finally, our third aim was the characterization of ART adducts in order to identify the pathway(s) involved in drug activation in this system. As a complement to the HK experiments, resin-linked sulfhydryl groups were used to capture drug radicals under *in vitro* conditions. Adducts were cleaved from solid matrix-bound thiols for structural confirmation through chromatographic methods.

We hypothesized that nonspecific covalent binding of carbon-centered ART radicals, particularly to protein sulfhydryl groups, causes inhibition of enzymatic activity. A purified model enzyme system, along with solid-matrix thiols for radical trapping, was used to enable a simplified and unified investigation of structural and functional aspects of the drug's mechanism of action. Cumulative deleterious effects resulting from moderate alkylation of essential proteins by ART may be responsible, in part, for cytotoxicity toward parasites. After decades of research,

ART remains an enigmatic drug, and thorough understanding of its mechanistic properties is essential if it is to be wielded effectively against malaria, as well as other diseases.

## MATERIALS AND METHODS

### Hexokinase Assays

Purified HK (MP Biomedicals) was incubated at 28°C in 125 mM Tris-HCl buffer, pH 6.8, (Quality Biologicals), in the presence and absence of ART and FeCl<sub>2</sub>, FeCl<sub>3</sub> or hemin chloride, separately or combined. Reagents were obtained from Sigma-Aldrich unless noted. Because ART (Acros) was dissolved in absolute EtOH to a concentration of 50 µM prior to addition to enzyme solutions, control samples with equivalent EtOH concentrations were included. HK was initially incubated 96 h with ART and/or iron, and enzyme activity was assessed at various time points in order to establish optimal incubation time in this *in vitro* system. All subsequent experiments employed 24 h incubation of HK with reagents. Residual enzyme activity was measured at 340 nm in 96-well non-protein binding microplates (Corning) with a Fluostar spectrophotometric plate reader (BMG LabTech). A coupled-enzyme reaction (Fig. 7) with glucose-6-

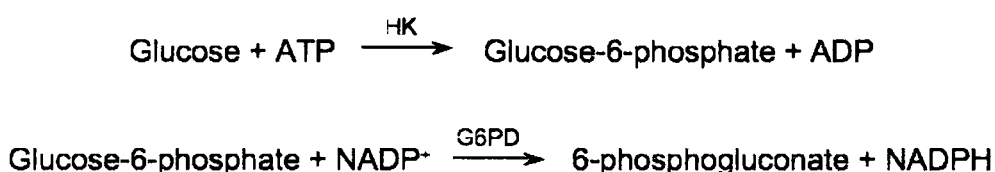


Fig. 7 - Coupled-enzyme reaction used in HK studies. The reduction of NADP<sup>+</sup> to NADPH creates a spectrophotometrically-detectable product.

phosphate dehydrogenase (G6PD) was used to assess HK activity by methods adapted from Mulcahy *et al.* [75].

Drug-treated and control HK was added to reaction solutions immediately prior to measurement. UV absorbance readings were taken every 45 s for 15 cycles, and each sample was measured in duplicate at room temperature. The final concentrations in each well were: 0.005 U HK, 0.156 U G6PD (MP Biomedicals), 0.290 mM ATP (MP Biomedicals), 0.680 mM NADP<sup>+</sup> (Calbiochem), 4.8 mM glucose, and 9.7 mM MgCl<sub>2</sub> in pH 7.5 125 mM Tris-HCl. For substrate protection assays, HK was pre-incubated 20 min with ATP or mannose prior to receiving any other treatment. For activity restoration assays, HK was incubated 24 h with ART and iron prior to 20 min treatment with ATP or mannose. Absorbance values were plotted over time, and slope values were derived by linear regression (Prism 4.0). Residual HK activity rates were normalized by establishing the slope value of untreated HK control samples as 100%. Activity rates of treated samples were reported as percentages of control activity rates. Mean enzyme activity values were analyzed for statistically significant differences using ANOVA ( $p < 0.05$ ) with a *post hoc* Tukey test.

### **Dialysis of Artemisinin-Treated Hexokinase**

Dialysis was performed using 10 kD MWCO Slide-A-Lyzer cassettes (Pierce). Cassettes were dialyzed 30 min against dH<sub>2</sub>O to remove excess membrane glycerol prior to use. Following 24 h incubation at 28°C with 350 μM ART and/or

35  $\mu\text{M}$   $\text{FeCl}_2$ , HK samples (15  $\mu\text{g}$  in 3 mL 125 mM Tris-HCl, pH 6.8) were injected into cassettes and dialyzed 3 h at 28°C in 1 L 125 mM Tris-HCl buffer, pH 7.5, with hourly buffer changes. HK activity was assessed post-dialysis, and protein content of dialyzed samples was verified by means of Bradford assay. Mean enzyme activity values for each assay time point were analyzed for statistically significant differences using ANOVA ( $p < 0.05$ ). Pre- and post-dialysis values for each sample were analyzed for statistically significant differences using paired  $t$ -test ( $p < 0.05$ ).

### **Solvolysis of Artemisinin-Treated Resin-Linked Thiols**

A solvolysis reaction (Fig. 8) was performed to isolate ART adducts from thiol groups using methods adapted from Mattocks and Jukes [76]. Thiopropyl sepharose 6B resin (GE Healthcare) was washed and activated with  $\beta\text{ME}$  according to manufacturer's instructions. Aliquots of resin samples (each with a dry weight of 200 mg) were incubated 24 h on a rocker at 28°C and contained 1 mL 125 mM Tris-HCl (pH 6.8) with 350  $\mu\text{M}$  ART and/or 35  $\mu\text{M}$  or 350  $\mu\text{M}$   $\text{FeCl}_2$ . The resin was washed with 50 mL each  $\text{dH}_2\text{O}$  followed by MeOH to remove any unbound drug and incubated 20 min with 11 mL 134 mM  $\text{AgNO}_3$  in 90% MeOH. The solvolysis reaction was stopped with 2 mL 10%  $\text{Na}_2\text{CO}_3$ . Samples were centrifuged 3 min at 4000 rpm, and the supernatants were extracted with 2 mL toluene. Toluene extracts were evaporated to 100  $\mu\text{L}$  under a nitrogen stream.

Solvolysis reaction products were separated on 60 Å silica gel plates (Merck)

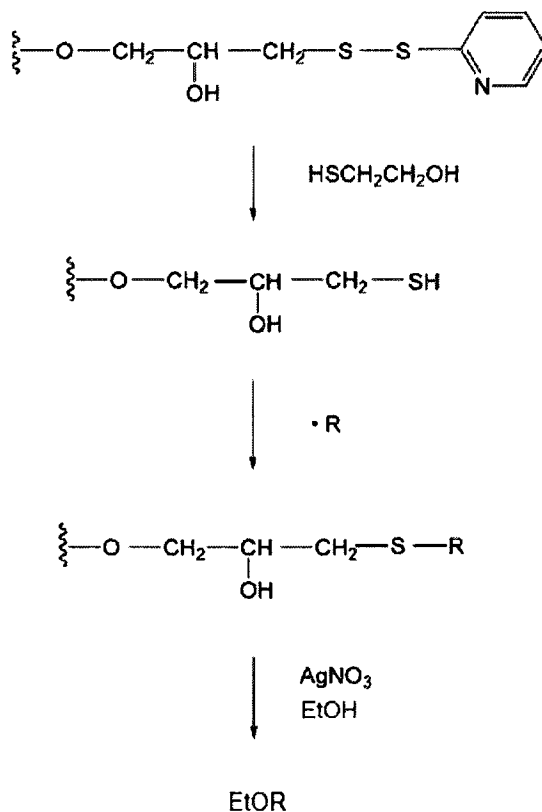


Fig. 8 - Overview of the reactions involved in thiopropyl sepharose 6B resin preparation, drug treatment, and derivative release.  $\beta$ -ME reduces the disulfide bond to a thiol that can react with carbon radicals. Adducts are cleaved in an ethanolic  $\text{AgNO}_3$  reaction to yield ethoxy derivatives.

using methods adapted from Beekman *et al.* and Gabriels and Plaizier-Vercammen [77, 78]. Toluene extracts (10-20  $\mu\text{L}$ ) were spotted on TLC plates and allowed to dry. Development was carried out with a hexane/diisopropyl ether/glacial acetic acid (130:85:8, v/v/v) mobile phase. Air-dried plates were sprayed with a glacial acetic acid/sulfuric acid (80%)/*p*-anisaldehyde (100:2:1,

v/v/v) derivatizing reagent and heated 6 min at 100°C in order to visualize ART products.

The reaction products of ART with iron alone were also run on TLC plates. Solutions of 125 mM Tris buffer, pH 6.8, contained 350  $\mu$ M ART and 0, 35, 100, or 350  $\mu$ M FeCl<sub>2</sub>. Following 24 h incubation, 25  $\mu$ L of the solutions were spotted directly on plates and developed and derivatized as described above.

### **Two-Dimensional Electrophoresis of Artemisinin-Treated Hexokinase**

Isoelectric focusing was employed to separate the HK isoforms, which are both 50 kD but share only 75% peptide sequence homology [53, 54], present in commercial HK preparations. Enzyme samples were incubated with drug and ferrous iron for 24 h at 28°C and assayed for activity. For the first set of 2DE gels, the HK solutions (each 150  $\mu$ g HK in 30 mL 125 mM Tris-HCl buffer, pH 6.8) were concentrated using 10 kD MWCO Vivaspin 15R centrifugal filtration units (Vivascience Sartorius Group) and then precipitated with acetone to remove Tris salts and to further concentrate the enzyme. A parallel experiment was conducted in order to establish amounts of protein present at each stage of sample concentration by Bradford assay along with SDS-PAGE. For the second set of 2DE gels, additional control samples were included. HK solutions (each 50  $\mu$ g HK in 10 mL 125 mM Tris-HCl buffer, pH 6.8) were again incubated 24 h at 28°C with 350  $\mu$ M ART and/or varying iron concentrations and assayed for activity. After 24 h, the solutions were centrifuged 25 min at 4°C and 4000 rpm to pellet any insoluble enzyme resulting from drug treatment. The supernatants

were then concentrated with 10 kD MWCO Amicon Ultra 15 centrifugal filtration units (Millipore) and precipitated with acetone. Bradford assay and SDS-PAGE were again used to quantify the amount of protein collected from each sample.

Kendrick Labs (Madison, WI) performed 2DE on the collected protein. HK samples were resolubilized in boiling buffer (5% SDS, 5%  $\beta$ ME, 10% glycerol, and 60 mM Tris) to a concentration of 2 mg/mL, and 5  $\mu$ g of each sample was loaded. Isoelectric focusing was carried out with 2% pH 3.5-10 ampholines for 9600 V•h, and a 10% acrylamide slab gel was used for electrophoresis. Gels were stained with Coomassie brilliant blue, and spots were excised for mass spectrometry. The most highly-separated spots were selected for excision; where possible, spots corresponding to the same location on multiple gels were excised.

### **Mass Spectrometry of Artemisinin-Treated Hexokinase**

Matrix-assisted laser desorption/ionization—time-of-flight mass spectrometry (MALDI-TOF) of trypsin-digested HK gel spots was performed on a Voyager DE Pro (Applied Biosystems) at the Columbia University Protein Core Facility (New York, NY). Peptide mass fingerprints were analyzed using Protein Prospector software (<http://prospector.ucsf.edu/>). Protein identification was made by comparing masses of the highest intensity (> 15%) MALDI-TOF ion peaks with the fragments predicted for HK-A and HK-B by the MS-Digest program. The following parameters were used for generating predicted fragment masses:



trypsin proteolysis, two missed cleavages at maximum, and variable modification of cysteines by acrylamide. Mass tolerance of monoisotopic ions was set to < 100 ppm in order to match resulting to predicted fragments.

## RESULTS

This study examined the molecular interactions between the established protein alkylator ART and HK, an enzyme well-suited to alkylation experiments. We hypothesized that enzyme inhibition occurred through covalent drug binding, which might explain the *in vivo* mechanism of action of ART. To characterize ART alkylation and its effects, a spectrophotometric assay of HK activity was combined with 2DE and mass spectrometry for identification of drug-modified peptides. ART-treated Sepharose 6B resin was used to demonstrate sulfur-bound adducts of ART in an *in vitro* system.

### Inhibition of Hexokinase Activity by Artemisinin

Because activity of HK in these coupled-enzyme assays cannot be assessed directly, a means of data interpretation is required. Provided that substrates are in excess, G6PD production of NADPH, as measured by absorbance readings, proceeds in a linear manner. Linear regression, therefore, was used to establish slope values that translate into residual HK activity rates, as HK function was the limiting factor in these assays. In Figure 9, linear regression of the plotted data points yielded lines with coefficient of determination ( $r^2$ ) values of 0.9980 (2 units of HK activity/mL), 0.9984 (1 U/mL), and 0.9961 (0.5 U/mL), demonstrating the appropriateness of this method of data-fitting. When the slope of the 1 U/mL line ( $m = 0.0004313$ ) is established as 100% residual activity, the 2 U/mL ( $m =$

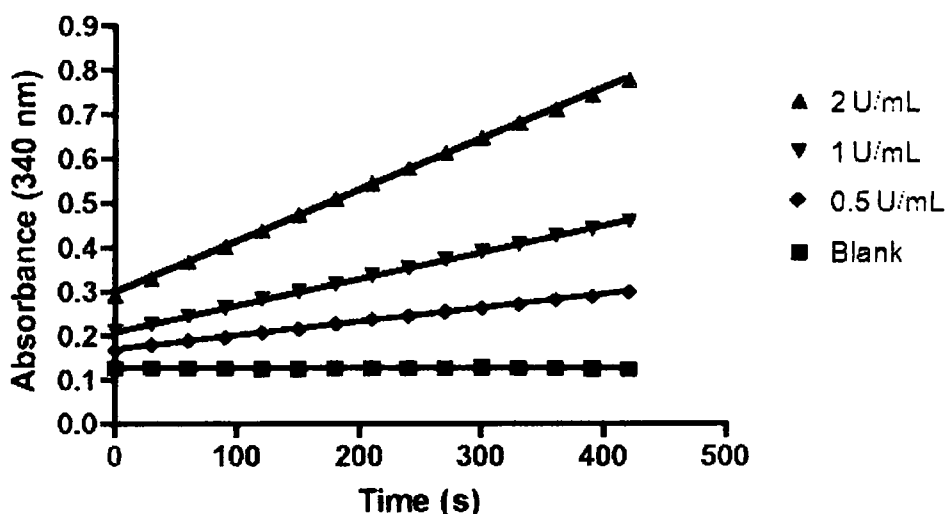


Fig. 9 - Plot of absorbance over time at varying HK concentrations. Data represent means of two replicate measurements.

0.0008920) and 0.5 U/mL ( $m = 0.0002167$ ) samples represent 206.8% and 50.2% activity of the control, respectively. Therefore, slope values are directly proportional to the amount of functional enzyme.

In order to demonstrate that the activity of the model enzyme in this system is susceptible to inhibition via alkylation, established inhibitors of HK, ninhydrin and iodoacetamide [71, 79], served as positive controls. Incubation of HK with the non-specific alkylating agent ninhydrin resulted in concentration-dependent inhibition of activity (Fig. 10). Iodoacetamide, which selectively alkylates thiols, also inhibited activity in a similar manner (Fig. 11). At 1 mM, ninhydrin and iodoacetamide produced comparable levels of inhibition, with  $78.0 \pm 5\%$  and  $81.7 \pm 0.7\%$  activity remaining, respectively. These results are in agreement

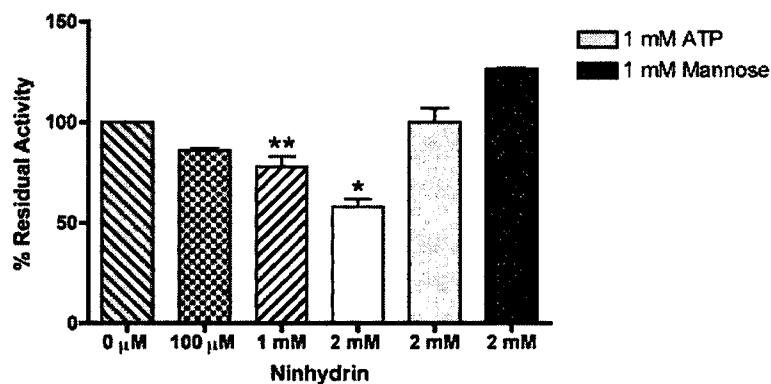


Fig. 10 - Dose-dependent inhibition of HK activity by ninhydrin. At 2 mM ninhydrin, HK was pre-incubated with no substrate, 1 mM ATP, or 1 mM mannose. Data represent means ( $\pm$  s.d.) of three independent experiments. \*Indicates that mean inhibition was significantly different than control ( $p < 0.001$ ). \*\*Indicates that mean inhibition was significantly different than control ( $p < 0.05$ ).

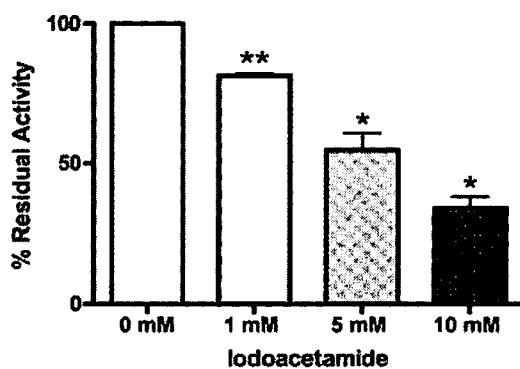


Fig. 11 - Dose-dependent inhibition of HK activity by iodoacetamide. Data represent means ( $\pm$  s.d.) of three independent experiments. \*Indicates that mean inhibition was significantly different than control ( $p < 0.001$ ). \*\*Indicates that mean inhibition was significantly different than control ( $p < 0.05$ ).

with published findings [71, 79] and validate use of this system for the study of inhibition via alkylation. Further, pre-incubation with a substrate such as mannose or ATP fully protected the HK active site against inhibitory effects of alkylators.

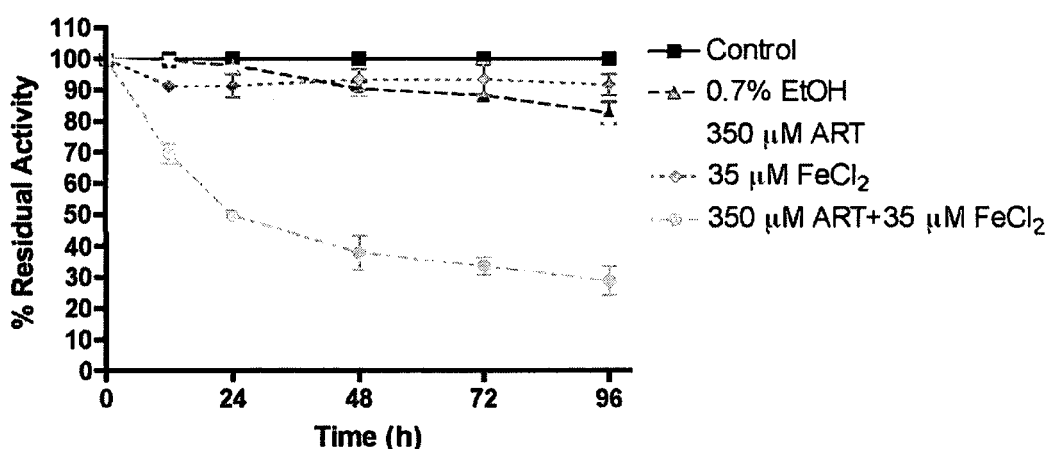


Fig. 12 - Time-dependent loss of HK activity in the presence of ART and/or ferrous iron. Data represent means ( $\pm$  s.d.) of three independent experiments.

For the incubation of HK with any reagents, pH 6.8 Tris buffer was used. In addition to preventing immediate autoxidation of ferrous iron [80], this pH preserves HK activity, as the enzyme becomes less active when buffer pH falls much below the optimal pH 7.0-9.5 range [81]. The phosphotransferase activity of HK was measured following 24 h incubation with reagents. This time point was established for maximal inhibition by ART in conjunction with iron as compared to no treatment or to treatment by ART or iron alone (Fig. 12). After 24 h, activity of

HK treated with both ART and iron was approximately 50% of the control, while ART and iron individually were responsible for less than 10% loss of activity.

ART significantly inhibited HK activity only in conjunction with iron. The rate of inhibition depended on the concentrations of both drug and iron. Even at 350  $\mu\text{M}$  (Fig. 13), ART showed no significant intrinsic inhibitory effect on enzyme activity, and, although ferrous iron can itself inhibit HK activity, its influence at 35  $\mu\text{M}$  was minimal (< 5% activity loss, Fig. 14). Inhibition by ART together with iron was

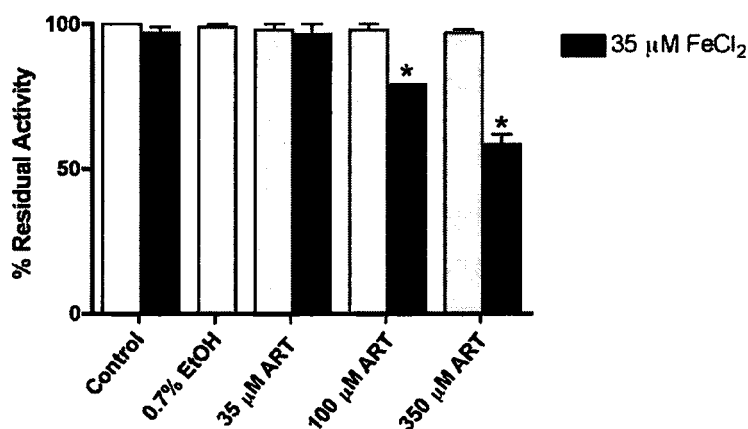


Fig. 13 - HK activity following incubation with ferrous iron and varying concentrations of ART. Measurements were taken after 24 h incubation. Data represent means of three independent experiments ( $\pm$  s.d.). \*Indicates that mean inhibition was significantly different than control ( $p < 0.001$ ).

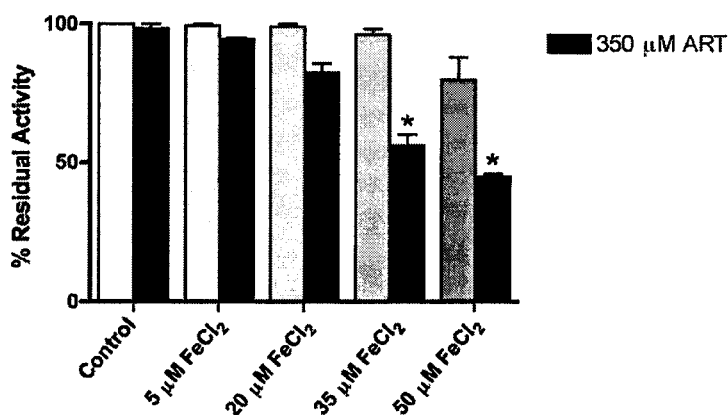


Fig. 14 - HK activity following incubation with ART and varying concentrations of ferrous iron. Measurements were taken after 24 h incubation. Data represent means of three independent experiments ( $\pm$  s.d.). \*Indicates that mean inhibition was significantly different than control ( $p < 0.001$ ).

more than additive and was highest (in comparison to drug and iron controls) at 350  $\mu$ M ART and 35  $\mu$ M FeCl<sub>2</sub>, with  $56.5 \pm 4.9\%$  activity remaining for the ART- and iron-treated sample versus  $98.0 \pm 1.4\%$  and  $97.3 \pm 2.8\%$  residual activity for samples treated with ART alone and iron alone, respectively (Fig. 13 and 14). Inhibition was concentration-dependent with both ART and iron. It was unlikely, however, that more moles of ART could interact with HK than were moles of iron present, as the drug is thought to react with ferrous non-heme iron in a 1:1 stoichiometric manner [82]. The approximate IC<sub>50</sub> for ART, 350  $\mu$ M, in the presence of 35  $\mu$ M Fe<sup>II</sup>, was lower than the estimated IC<sub>50</sub> of either

iodoacetamide or ninhydrin, signifying that the drug is a more potent inhibitor of HK activity under the assay conditions.

Unlike ART, deoxydihydroartemisinin (dDHA), which lacks an endoperoxide moiety, caused considerable activity loss (< 20%) when added alone to HK (Fig. 15). This finding indicates that structural alterations to the drug, in this case, replacement of the endoperoxide bridge with an epoxide and the C10 carbonyl group with a hydroxyl, modulate ART derivative interaction with the enzyme. However, inhibition by dDHA did not increase significantly, or to such a

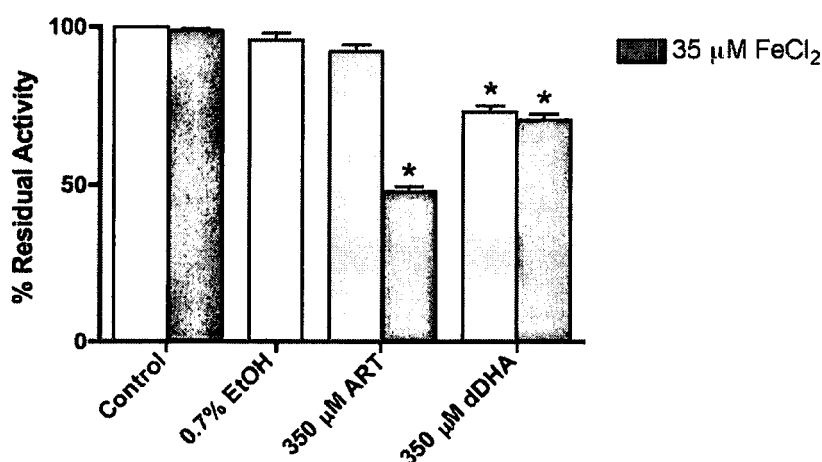


Fig. 15 - HK activity following incubation with ferrous iron and ART or dDHA. Measurements were taken after 24 h incubation. Data represent means of three independent experiments ( $\pm$  s.d.). \*Indicates that mean inhibition was significantly different than control ( $p < 0.001$ ).



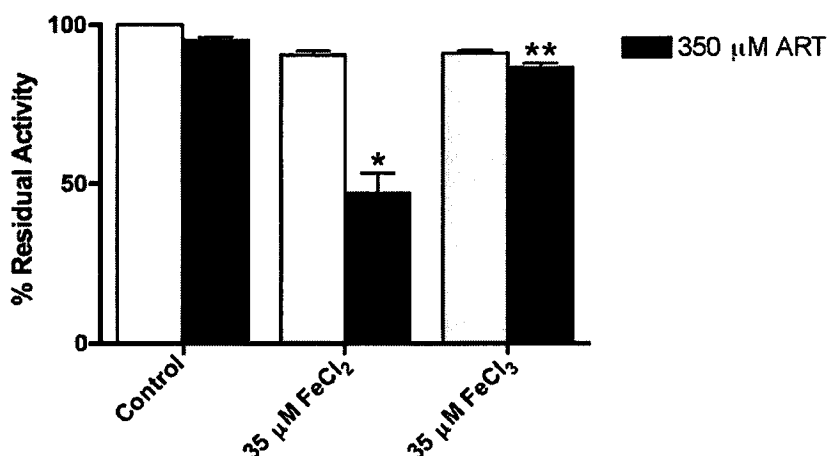


Fig. 16 - HK activity following incubation with ART and ferrous or ferric iron.

Measurements were taken after 24 h incubation. Data represent means of three independent experiments ( $\pm$  s.d.). \*Indicates that mean inhibition was significantly different than control ( $p < 0.001$ ). \*\*Indicates that mean inhibition was significantly different than control ( $p < 0.05$ ).

degree as by ART, when iron was available ( $p > 0.05$ ), suggesting that the peroxide is essential for ART action against HK.

The oxidative state of iron is also critical in these assays, as only the reduced form was able to induce significant inhibition together with the drug (Fig. 16). This observation is consistent with what is known about ART activation [14, 28]. When combined with ferric iron ( $\text{Fe}^{\text{III}}$ ), ART did not inhibit HK activity to the same extent as when combined with ferrous iron ( $86.7 \pm 2.1\%$  versus  $47.0 \pm 11.0\%$ ). Further, there was no significant difference in the activity of  $\text{FeCl}_3$ -treated samples in the

presence or absence of ART ( $p > 0.05$ ). Only the reduced form of iron appeared capable of activating the drug.

The requirements of reduced iron and an endoperoxide moiety, neither of which is significantly inhibitory on its own indicate that inhibition of HK was mediated through free radicals generated through attack by iron and opening of the trioxane ring of ART. Although activity loss may have been caused by unreactive ART metabolites, these results show that activation of the drug is necessary for significant inhibition. At 350  $\mu\text{M}$  ART and 35  $\mu\text{M}$   $\text{FeCl}_2$ , loss of activity was approximately five-fold greater than the combined independent activity loss caused by each reagent. This manner of  $\text{Fe}^{\text{II}}$ -dependent inhibition

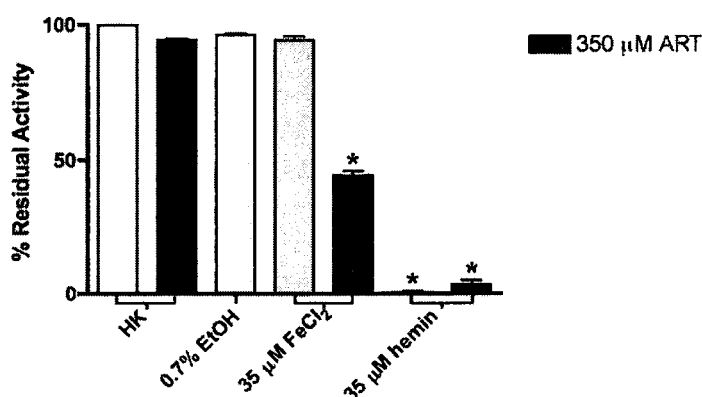


Fig. 17 - HK activity following incubation with ART and  $\text{FeCl}_2$  or hemin.

Measurements were taken after 24 h incubation. Data represent means of three independent experiments ( $\pm$  s.d.). \*Indicates that mean inhibition was significantly different than control ( $p < 0.001$ ).

is consistent with the wealth of literature showing the necessity of reduced metal ions for ART activation.

Heme iron was incorporated into the assays in order to test the effects of a biologically-relevant source of iron with ART on HK activity (Fig. 17). However, heme displayed strong inherent inhibition of the enzyme that precluded further investigation.

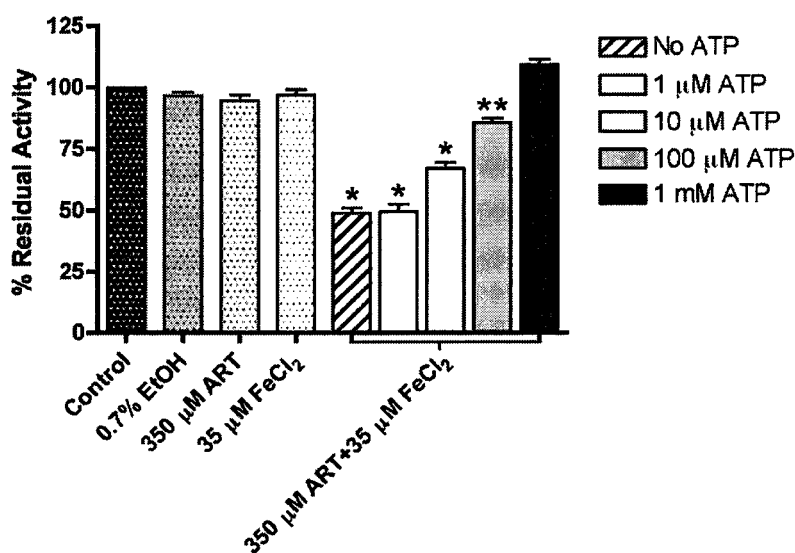


Fig. 18 - Protection of HK activity against inhibition by ART and iron by pre-treatment with ATP. ATP was added 20 min prior to other reagents.

Measurements were taken after 24 h incubation. Data represent means of three independent experiments ( $\pm$  s.d.). \*Indicates that mean inhibition was significantly different than control ( $p < 0.001$ ). \*\*Indicates that mean inhibition was significantly different than control ( $p < 0.05$ ).

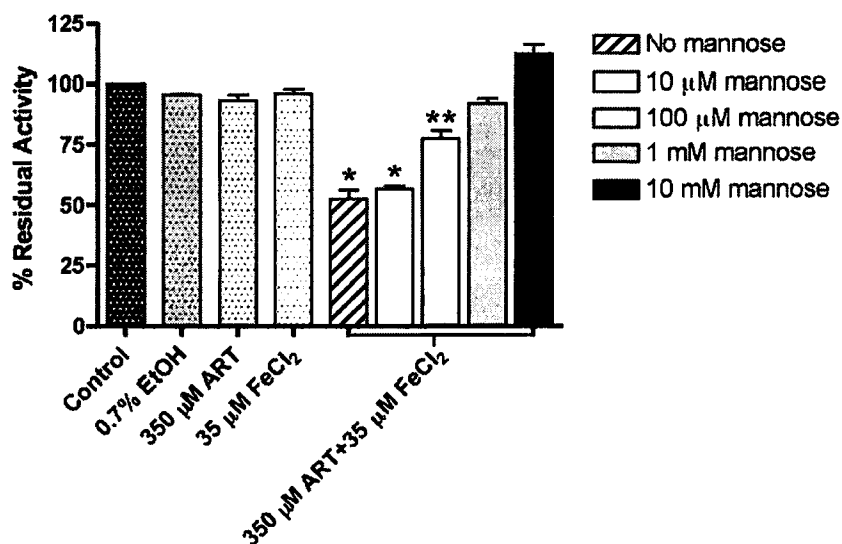


Fig. 19 - Protection of HK activity against inhibition by ART and iron by pre-treatment with mannose. Mannose was added 20 min prior to other reagents. Measurements were taken after 24 h incubation. Data represent means of three independent experiments ( $\pm$  s.d.). \*Indicates that mean inhibition was significantly different than control ( $p < 0.001$ ). \*\*Indicates that mean inhibition was significantly different than control ( $p < 0.05$ ).

Because occupation of the HK active site by substrates can protect against inactivation by agents that act at or near that region, mannose and ATP were incubated with HK prior to the addition of drug and iron. Pre-incubation with either substrate protected HK activity against inhibition by ART and iron together (Fig. 18 and 19). Equivalent activity rates were retained by HK with overall lower concentrations of ATP in relation to mannose. Full protection of activity was

reached with approximately 100  $\mu\text{M}$  ATP and 1 mM mannose. In general, concentrations of mannose one magnitude greater than those of ATP are needed for comparable protection levels.

When additional substrate was added to HK that had been incubated 24 h

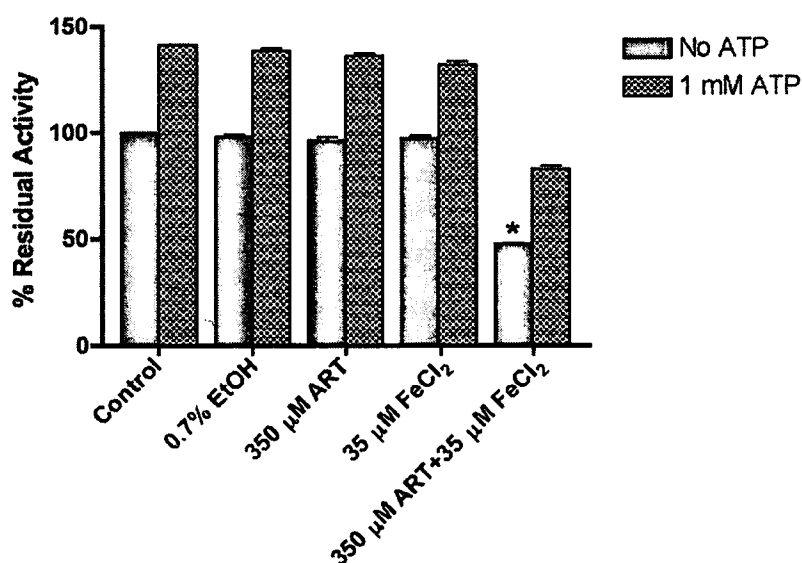


Fig. 20 - Inability of ATP to reverse inhibition of HK treated with ART and iron. First measurements (dark bars) were taken following 24 h incubation. Samples were then incubated 25 min with ATP before second measurements (patterned bars) were taken. Data represent means of three independent experiments ( $\pm$  s.d.). \*Indicates that mean inhibition was significantly different than control ( $p < 0.001$ ).

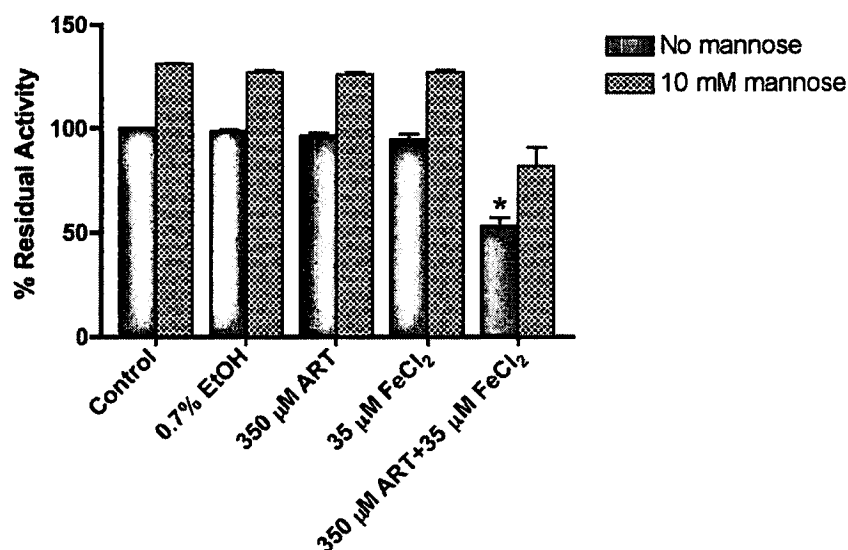


Fig. 21 - Inability of mannose to reverse inhibition of HK treated with ART and iron. First measurements (dark bars) were taken following 24 h incubation. Samples were then incubated 25 min with mannose before second measurements (patterned bars) were taken. Data represent means of three independent experiments ( $\pm$  s.d.). \*Indicates that mean inhibition was significantly different than control ( $p < 0.001$ ).

with ART and iron, HK exhibited an activity increase of approximately 30% (Fig. 20 and 21). This increase in activity was consistent among all the samples, regardless of drug treatment. Compared to other HK samples, the original activity loss of 50% remained in the ART- and iron-treated sample, indicating that relative residual activity rates are largely unchanged by the addition of substrate. Neither ATP nor mannose was able to reverse inhibition of drug-treated HK.

These results indicate a possible interaction between activated ART and the enzyme's active site. The precise mode by which ART inhibited HK was not revealed through protection assays, as the presence of substrates has been demonstrated to reduce activity inhibition from a variety of sources, including heat [83], pH [84], and free radicals [85], in addition to alkylation [86].

To further demonstrate that inhibition by ART and iron was irreversible, HK was dialyzed following incubation. Dialysis, which can separate noncovalently-

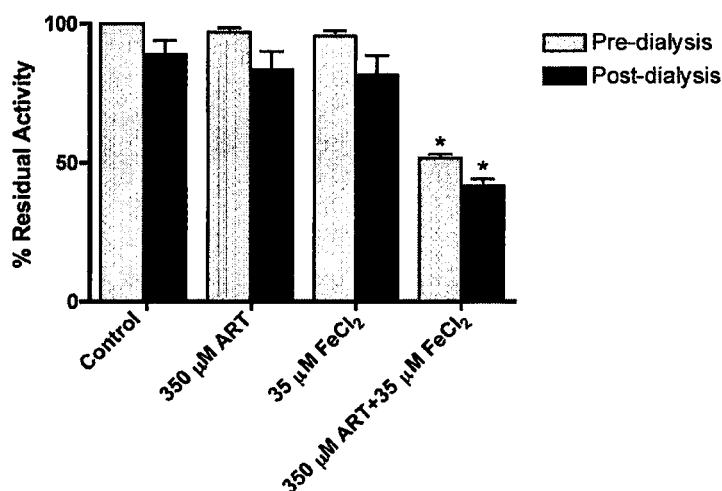


Fig. 22 - Inability of dialysis to restore activity to ART- and iron-treated HK. First measurements (grey bars) were taken after 24 h incubation. Samples were then dialyzed 3 h before second measurements (black bars) were taken. Data represent means of three independent experiments ( $\pm$  s.d.). \*Indicates that mean inhibition was significantly different than control ( $p < 0.001$ ).

interacting compounds from proteins, was unable to restore activity to HK that had been treated with drug and iron (Fig. 22), indicating that alkylation, or possibly another form of irreversible damage, had occurred.

### **Artemisinin Reaction with Thiopropyl Sepharose Resin**

The interaction of ART and ferrous iron with HK resulted in clear inhibition of enzymatic activity, indicating possible modification of HK. Detection of drug adducts would support the primary hypothesis of this research, that ART alkylation of proteins impairs their functions, and might provide a means of characterizing the drug activation pathway(s) involved in this system. Because alkylation likely targets HK cysteine residues, thiopropyl sepharose 6B resin, which possesses immobilized thiol groups, was used as a trap for alkylating ART metabolites. The substitution of thiopropyl sepharose resin for HK approximated the availability of sulfhydryl groups in the assayed quantities of enzyme. Following incubation with ART and iron, the resin was washed to remove unbound ART and then treated with ethanolic AgNO<sub>3</sub> in order to cleave drug adducts. ART products were extracted and then separated by TLC and visualized with *p*-anisaldehyde derivatization.

Figure 23 shows the results of solvolysis reaction products from ART-treated thiopropyl sepharose resin that had been resolved via TLC. In a mobile phase of hexane:diisopropyl ether:acetic acid, the unreacted ART control (lane 1) produced a band with an R<sub>f</sub> value of 0.36 and a bright pink color when



derivatized with a solution of *p*-anisaldehyde. This band also occurred when the resin sample did not undergo washing or solvolysis prior to extraction (lane 5). The presence of unreacted ART in the sample prior to washing was expected, given the excess of drug in relation to iron. Some self-quenched metabolites were also expected in this lane as indicators of drug activation, but none were visible. *P*-anisaldehyde has been demonstrated to detect the self-quenched ART product resulting from iron-catalyzed  $\beta$ -scission of the endoperoxide [76]. This compound, a ring-contracted ester, yields a green color upon derivitization. *P*-anisaldehyde also reacts with ART derivatives such as DHA and ARM [77] and could therefore be expected to permit visualization of various metabolites. Given a total availability of 12  $\mu\text{mol}$  sulfhydryl per resin sample and usage of excess  $\text{AgNO}_3$ , up to 12  $\mu\text{mol}$  ART product could have been released. Optimal yield should have produced 1.2  $\mu\text{mol}$  cleaved adduct per each 10  $\mu\text{L}$  TLC spot, presumably an amount more than sufficient for visual detection; for comparison, a total of 100 nmol ART was spotted as a highly-visible standard (lane 1).

No artifactual reaction products were detected in extracts from resin not incubated with ART or iron (lane 2). Additional negative controls, in which resin samples were treated with ART alone prior to extraction, were also run (lanes 3 and 4), since drug activation was believed to be iron-dependent. As expected, no novel bands that might indicate ART reaction products were visible (lanes 2-4). However, extractions of samples that had been treated with both ART and  $\text{FeCl}_2$ , did not display any unique bands, either (lanes 6-9). The lack of visible

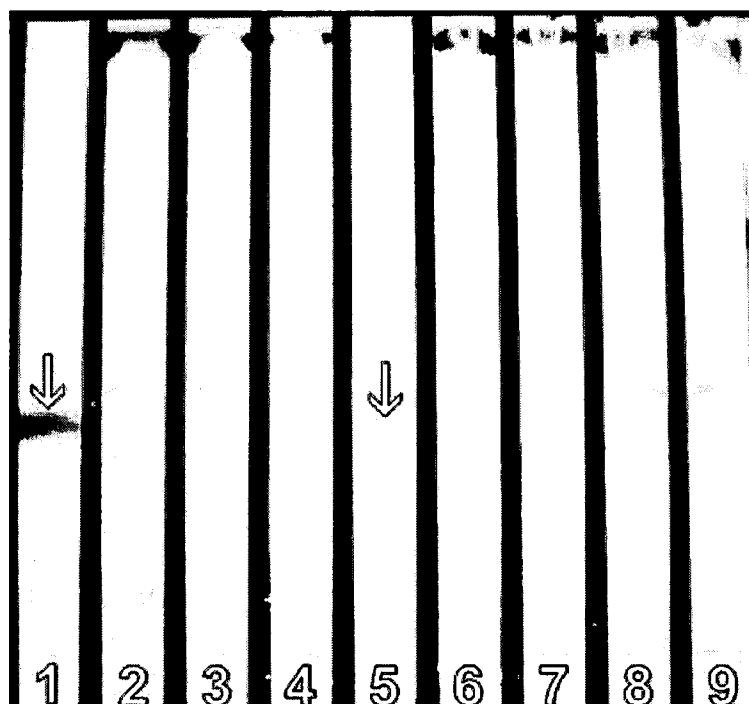


Fig. 23 - TLC of ART-thiopropyl sepharose resin solvolysis reaction products.

Resin samples were incubated 24 h with reagents prior to  $\text{AgNO}_3$  solvolysis and extraction. Solvolysis was performed on all samples except two (lanes 1 and 5). ART standard (lane 1). Resin unexposed to ART or iron (10  $\mu\text{L}$  extract spotted, lane 2). Resin treated with 350  $\mu\text{M}$  ART alone (10  $\mu\text{L}$  extract spotted, lane 2; 20  $\mu\text{L}$  extract spotted, lane 4). Resin treated with 350  $\mu\text{M}$  ART+35  $\mu\text{M}$   $\text{FeCl}_2$  without solvolysis (lane 5, 10  $\mu\text{L}$  spotted). Resin treated with 350  $\mu\text{M}$  ART+35  $\mu\text{M}$   $\text{FeCl}_2$  (10  $\mu\text{L}$  spotted, lane 6; 20  $\mu\text{L}$  spotted, lane 7). Resin treated with 350  $\mu\text{M}$  ART+350  $\mu\text{M}$   $\text{FeCl}_2$  (10  $\mu\text{L}$  spotted, lane 8; 20  $\mu\text{L}$  spotted, lane 9). Arrows indicate bands of unactivated ART.

metabolites in solvolysis extracts of ART- and  $\text{FeCl}_2$ -treated resin suggests that that drug adducts were not present in sufficient quantity for detection or at all. These results may indicate that  $\text{AgNO}_3$ -mediated thioether cleavage did not take place as theorized or because alkylation of resin thiols did not occur, possibly due to a failure to activate ART.

To assess whether the drug was, in fact, reactive under the assay conditions, ART was incubated with varying amounts of ferrous iron, and the aqueous solution was spotted directly on plates for TLC. Figure 24 clearly shows that ART was consumed as the amount of iron increased, as seen in the disappearance of the characteristic pink spot of unreacted derivatized drug. However, again, no metabolites were visible, which indicates that the derivatizing agent may have been unsuitable for visualizing the ART reaction products of this system.

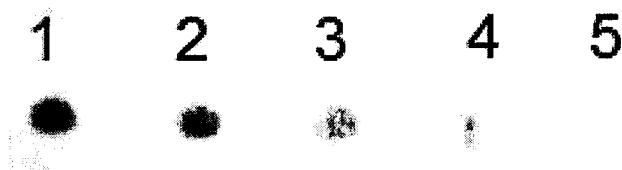


Fig. 24 - TLC of ART following 24 h incubation with varying concentrations of  $\text{FeCl}_2$ . ART standard (1). 350  $\mu\text{M}$  ART without iron (2). 350  $\mu\text{M}$  ART+35  $\mu\text{M}$  iron (3). 350  $\mu\text{M}$  ART+100  $\mu\text{M}$  iron (4). 350  $\mu\text{M}$  ART+350  $\mu\text{M}$  iron (5).

### Alkylation of Artemisinin-Treated Hexokinase

Because we hypothesized that ART inhibited HK through alkylation, a proteomic approach was used to investigate this interaction. Two-dimensional electrophoresis was employed prior to mass spectrometry in order to separate predicted HK isoforms A and B, which share sequence 75% homology. We anticipated that performing MALDI-TOF separately on each HK isoform would facilitate interpretation of the resulting spectra and provide direct evidence of covalent binding of ART to inhibited HK.

In the first set of gels (Fig. 25), the untreated HK control sample (gel A) did

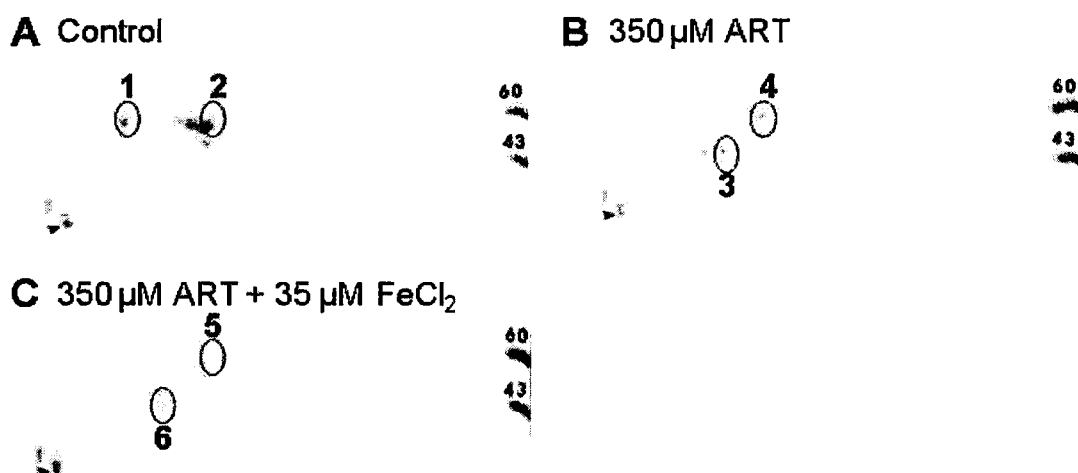


Fig. 25 - Two-dimensional electrophoresis of drug-treated HK (first gel set).

Soluble enzyme fractions were used for all gels. Spots excised for MALDI-TOF are circled. Trypsin standards (pI 5.2) in bottom left corners are indicated by arrows.

not separate into two discrete spots—one for each isoform—as expected. Instead, seven spots were visible at 55 kD between pH 5.5 and 7, and four spots at 50 kD, all below the most intense 55 kD spots. The other two samples, one treated with ART (gel B) and the other with ART and  $\text{FeCl}_2$  (gel C) also showed multiple spots at 55 kD in the same pI range of 5.5-7. These samples exposed to ART both produced a number of spots at 43 kD. Approximately 30% less protein was recovered from the drug- and iron-treated HK sample, as confirmed by Bradford assay and fainter 2DE gel spots, which may be due to degradation or precipitation of modified HK. Where possible, spots sharing the same molecular weight and pI were excised for MALDI-TOF to increase accuracy of comparisons between treatments.

The second set of gels (D-K) included additional control samples (Fig. 26). The HK control (gel D) yielded a number of closely-grouped spots at 55 kD and two faint spots at 43 kD. The EtOH-treated sample (gel E) separated into three spots at 55 kD and six spots at 43 kD; approximately half of the total protein in the sample appeared to migrate to the lower molecular weight. Separation of the ART-treated sample (gel F) was much the same as in its counterpart in the first set of 2DE gels, with 43 kD spots occurring at lower pIs than do 55 kD spots. For this 2DE set, iron concentrations were increased to 50  $\mu\text{M}$  and 100  $\mu\text{M}$  in order to facilitate ART activation and activation and alkylation of HK. To determine possible drug modification to insoluble HK, the enzyme fraction that had precipitated during incubation with 100  $\mu\text{M}$   $\text{FeCl}_2$  was also used (gels J and K). Both of the HK samples exposed to iron alone (gels G and J) showed spots only

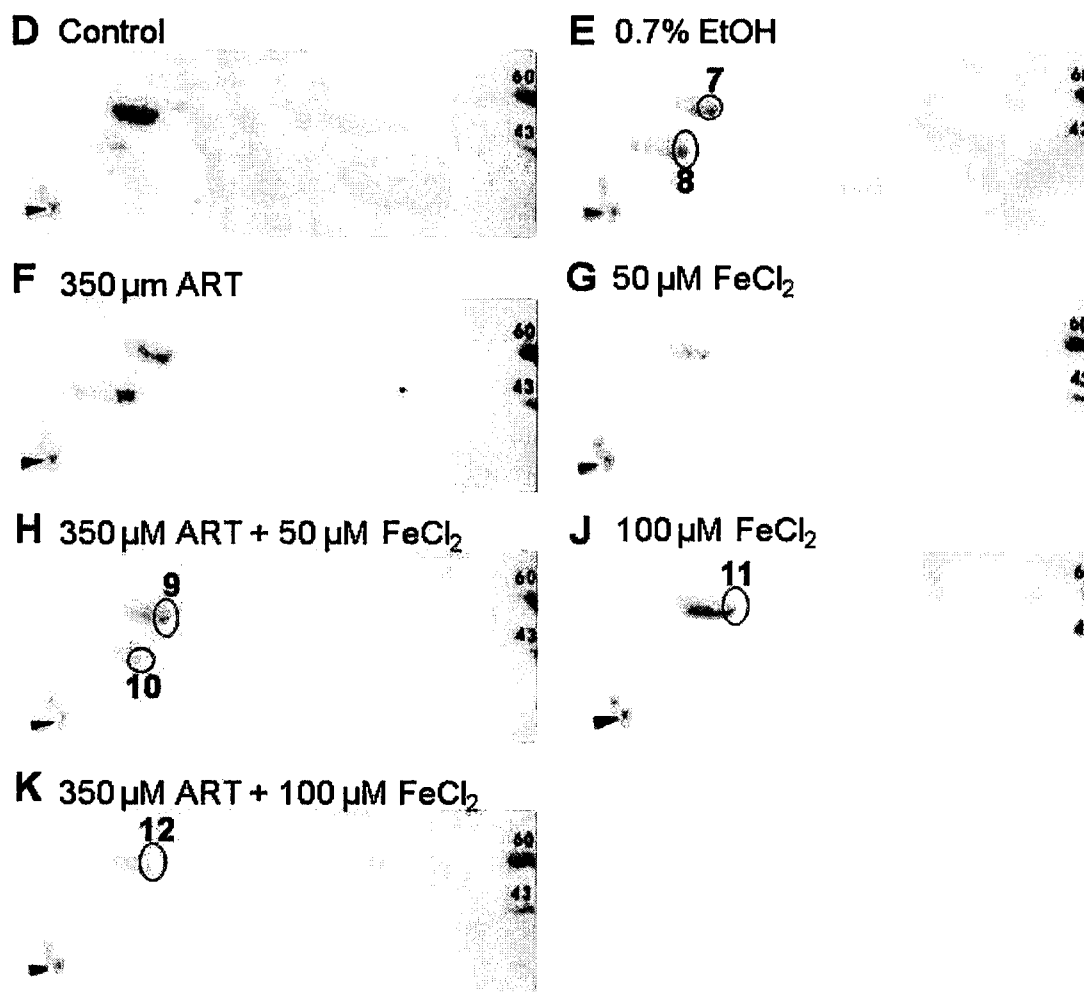


Fig. 26 - Two-dimensional electrophoresis of drug-treated HK (second gel set). Soluble enzyme fractions were used for all gels except two (J and K). Spots excised for MALDI-TOF are circled. Trypsin standards (pI 5.2) in bottom left corners are indicated by arrows.

at 55 kD. The insoluble HK sample incubated with ART and 100  $\mu$ M FeCl<sub>2</sub> (gel K) also resolved only as spots visible at 55 kD, but the lack of overall intensity may indicate that too little protein was loaded onto the gel. Little difference was evident between the samples treated with ART and the EtOH control, but 2DE was intended primarily as a preparatory step, and alkylation of an uncharged residue such as cysteine would not likely affect pI. Notably, the gel spots at 43 kD were observed almost exclusively in enzyme samples exposed to EtOH, either alone or as a drug vehicle. Another unexpected result of 2DE was that the pI for every gel spot was more basic than the 4.25-5 range previously reported for HK isoforms through affinity chromatography and chromatofocusing [87].

### **Mass Spectrometry of Drug-Treated Hexokinase**

Following separation of ART-treated HK isoforms by 2DE, MALDI-TOF was used to identify possible alkylated residues. Mass spectrometry is able to demonstrate covalent modification of proteins by a variety of agents [88-90]. Peptide “fingerprints” of treated enzyme samples were generated by MALDI-TOF (Fig. 27 and 28; Appendix II), and Protein Prospector was used to predict peaks for both HK isoforms for comparison.

In the first set of gels, spot 1 was revealed to be a combination of isoforms HK-A and HK-B. Considerably more fragments resulted from this spot than from the other spots, and peaks at  $m/z$  1022, 1548, 1916, 2067, 2254, 2410, 2483, 3259, and 3459, all of which are unique to HK-B, were present, as well (Appendix

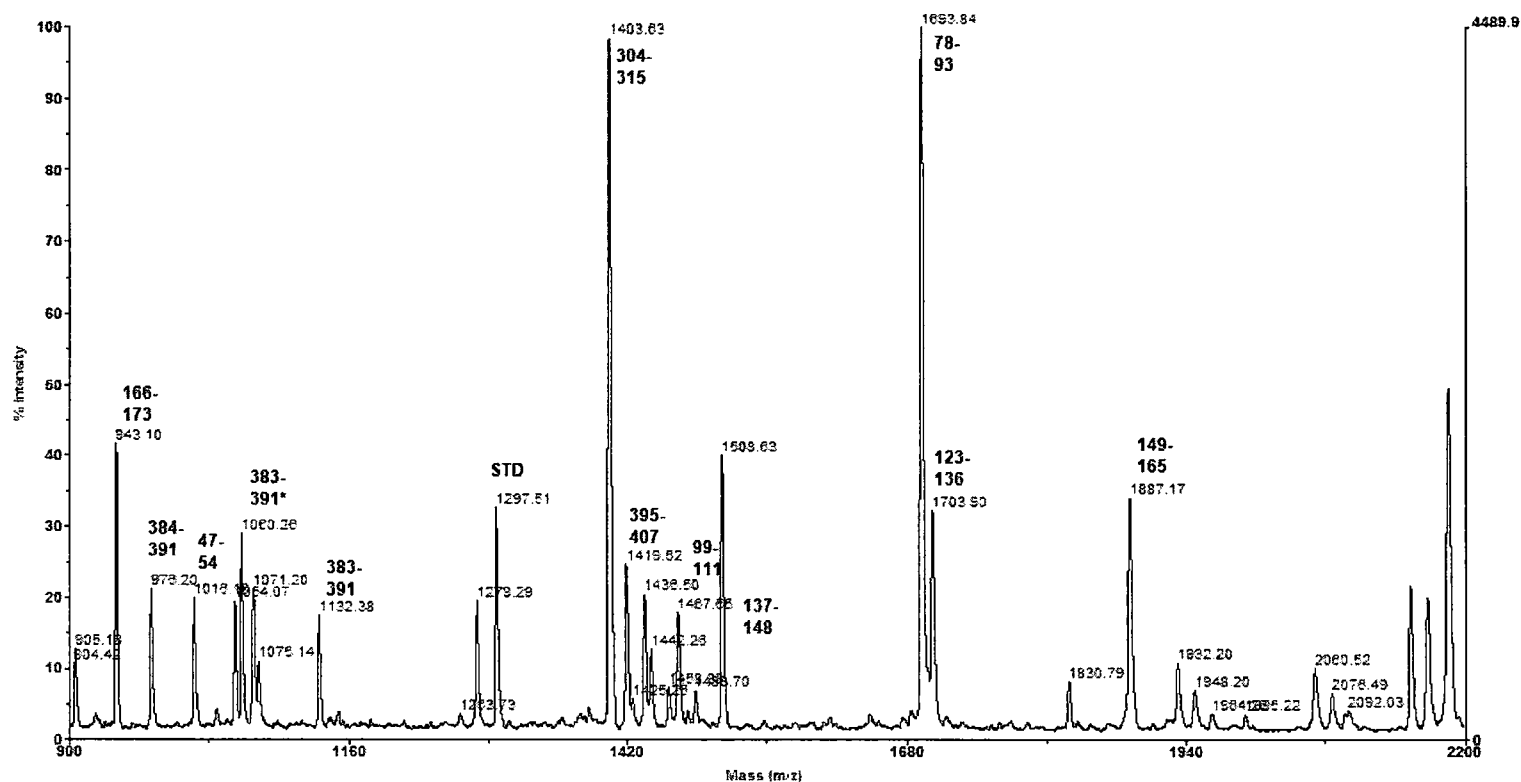


Fig. 27 - MALDI-TOF spectrum of untreated HK-A, fragment mass 900-2200. The enzyme sample was taken from 2DE spot 2. Peaks are labeled with corresponding predicted amino acid fragments. Asterisks mark fragments possessing an acrylamide-modified cysteine. Autolyzed trypsin standards are noted.



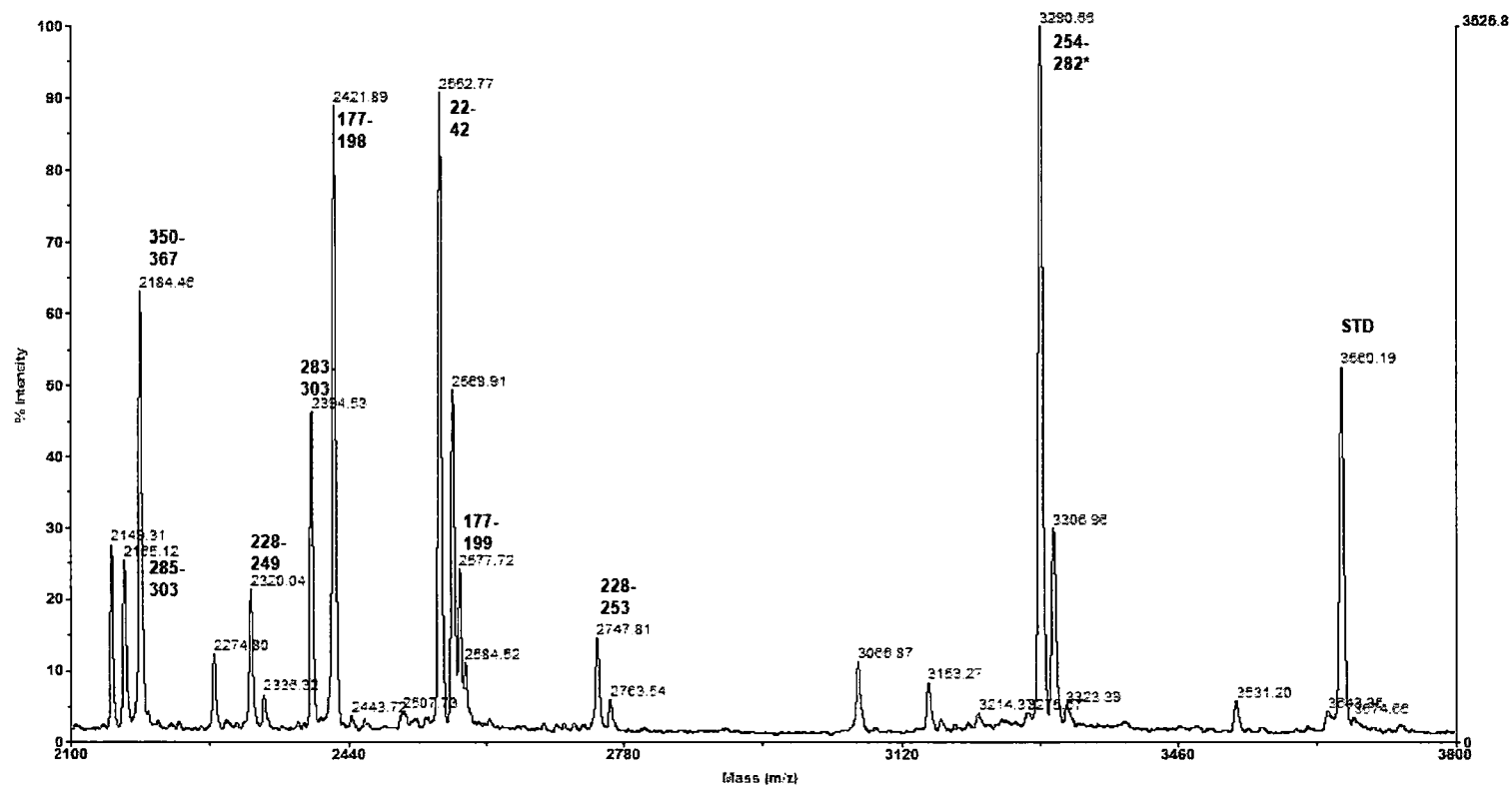


Fig. 28 - MALDI-TOF spectrum of untreated HK-A, fragment mass 2200-3800. The enzyme sample was taken from 2DE spot 2. Peaks are labeled with corresponding predicted amino acid fragments. Asterisks mark fragments possessing an acrylamide-modified cysteine. Autolyzed trypsin standards are noted.

Table1 - 2DE gel spots used for MALDI-TOF.

Spot	Treatment	Mass (kD)	pI
1	Control	55	5.5
2	Control	55	7.0
3	350 $\mu$ M ART	43	6.2
4	350 $\mu$ M ART	55	7.0
5	350 $\mu$ M ART+35 $\mu$ M FeCl <sub>2</sub>	55	7.0
6	350 $\mu$ M ART+35 $\mu$ M FeCl <sub>2</sub>	43	6.2
7	0.7% EtOH	55	7.0
8	0.7% EtOH	43	6.2
9	350 $\mu$ M ART+50 $\mu$ M FeCl <sub>2</sub>	55	7.0
10	350 $\mu$ M ART+50 $\mu$ M FeCl <sub>2</sub>	43	6.2
11	100 $\mu$ M FeCl <sub>2</sub>	55	7.0
12	350 $\mu$ M ART+100 $\mu$ M FeCl <sub>2</sub>	55	7.0

II). Spots 2-6 (Table 1) contained primarily isoform HK-A; possible trace presence of HK-B cannot be excluded. Coverage of 61.7% of the HK-A peptide sequence was established for 55 kD spots 2, 4, and 5 (Fig. 29). For spots 3 and 6, both migrating to 43 kD, peaks at  $m/z$  1332, corresponding to peptide fragments 395-406 or 411-423, and  $m/z$  1926, corresponding to fragment 411-428, were not detected. The absence of these peaks likely indicates loss of the C-terminus of the enzyme.

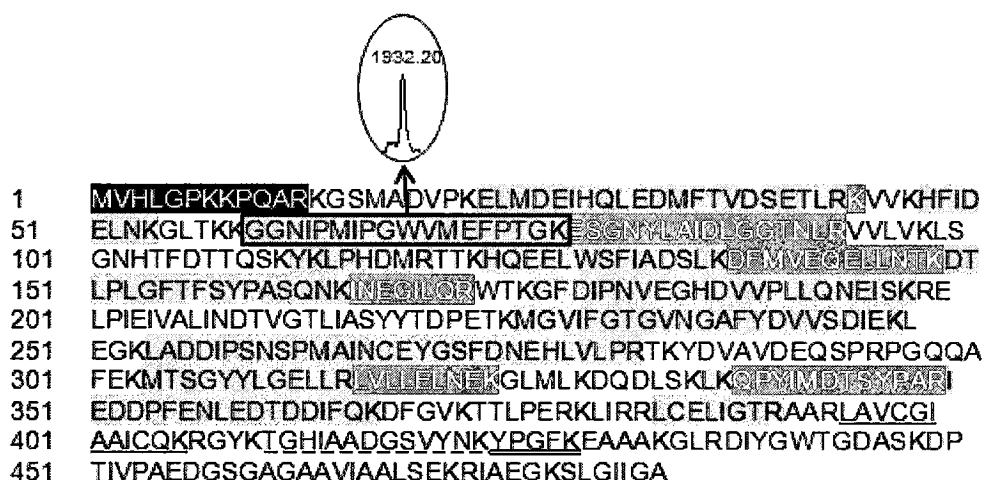


Fig. 29 - MALDI-TOF peptide matches to the amino acid sequence of HK-A.

Gray-shaded regions represent fragments (0-2 missed cleavages) corresponding to peaks identified in all 12 spots. Underlined regions represent fragments corresponding to peaks identified only in spots 2, 4, 5, 7, 9, 11, and 12 (all 55 kD). The black region represents a fragment corresponding to a peak identified in spots 6-12. The inset shows the peak at  $m/z$  1932 matched with the peptide fragment it represents, as an example.

The second set of MALDI-TOF spectra indicated that HK-A comprised spots 6-12. Again, no peaks which might have represented peptide fragments 395-406, 411-423 or 411-428 were present in the 43 kD spots, even though they were detected in all of the 55 kD spots. Because the 43 kD spots were prominent only in the HK samples exposed to EtOH, which was used as a drug vehicle, EtOH-induced C-terminus degradation appeared to be responsible for the lower mass. A low-intensity peak at  $m/z$  1490 common to all six spots, representing amino

acids (AA) 1-12, suggested that the N-terminus of the enzyme remains fully intact, regardless of treatment. Several peaks prominent in all of the samples were unable to be matched with any predicted fragments for either isoform.

With respect to various drug treatments, no novel or mass-shifted peaks were observed. A mass shift reflecting an increase of 282, the approximate size of an ART radical, would have indicated covalent drug binding to a given fragment. Additionally, no variant patterns in peak intensity were evident, suggesting consistent handling of all of the enzyme samples throughout the MS process. Such similarity between spectra indicates that the MALDI-TOF instrumentation was unable to detect hypothesized ART-bound fragments or that those fragments were not present in sufficient quantity for detection or at all.

## DISCUSSION

ART derivatives are currently in global use against malaria, but knowledge of their mechanism of action remains limited. Although it is accepted that the drug's potency hinges on its endoperoxide moiety, every other aspect of its action is uncertain. Exactly how ART is activated, the structure of its reactive intermediate(s), and its target(s) within *Plasmodium* are topics of considerable debate in the malaria community. Previous work on the interaction of ART with proteins has demonstrated either alkylation (hemoglobin [27, 41], albumin [27], TCTP [49]) or activity inhibition (ATPases [46, 91], hepatitis C virus polymerase [64]). To date, no published study has provided evidence for enzyme inhibition due to alkylation beyond what is circumstantial. This void cannot not preclude inhibition due to nonalkylating drug intermediates or protein alkylation that is not significantly deleterious to the parasite. Because we hypothesized a causal relationship between alkylation and activity inhibition, the investigation centered on a model enzyme, HK, which was treated with ART and assayed for phosphotransferase activity. An inactive ART derivative, various iron sources, and enzyme substrates were used to help characterize the interaction of ART and HK and to place these experiments in the context of previous work. Mass spectrometry was used to test for alkylation of inhibited HK by activated ART. The reaction between ART and resin-bound thiols was intended to elucidate the interaction between the drug and its possible targets in HK. We aimed to provide a cohesive examination of the effects of covalent modification by ART on HK function and structure, so as to shed light on the *in vivo* action of ART.

### **Inhibition of Hexokinase Activity by Artemisinin**

Under the conditions of the assays, phosphotransferase activity of HK clearly was inhibited by ART, but only in the presence of ferrous iron, as shown in Figures 13 and 14. Unlike a number of other sesquiterpene lactones [92], ART had very little intrinsic ability to inhibit HK, even at just under the limits of drug solubility [93]. ART and iron inhibited HK activity in a concentration-dependent manner. At a ferrous iron concentration of 35  $\mu\text{M}$ , raising the ART concentration in approximate threefold increments (35  $\mu\text{M}$ , 100  $\mu\text{M}$ , 350  $\mu\text{M}$ ) yielded a linear relationship ( $r^2 = 0.9549$ ) in the resulting amounts of inhibition. That is, each threefold increase in ART concentration resulted in an additional activity loss of approximately 25%.

Drug potency against the enzyme was noteworthy; assuming that all of the ferrous iron in the assays reacted with ART (i.e., 35  $\mu\text{M}$  activated ART if 35  $\mu\text{M}$  iron was available), the approximate  $\text{IC}_{50}$  for ART in the assays is nearly 100-fold lower than experimental  $\text{IC}_{50}$  values for the established, widely-used alkylating agents ninhydrin and iodoacetamide against HK (Fig. 10 and 11). The results also indicate that the drug is more potent than hydrogen peroxide and other ROS [94]. Because the buffer pH was not acidic enough to prevent gradual autoxidation of ferrous iron [80], it is likely that the inhibitory effects of ART were caused by even fewer moles of drug radicals than were moles of iron added, if iron is consumed in a 1:1 stoichiometric ratio to ART in drug activation [82]. The potency of ART may reflect an especially strong affinity of activated drug for HK or more extensive modification of the enzyme than seen with other inhibitors.

As shown in Figure 15, the ART endoperoxide bridge is essential for significant inhibition of HK in conjunction with ferrous iron. This finding is consistent with virtually every study published on its mechanism of action. Likewise, the necessity of a reduced metal source for drug activity is strongly supported in the literature [28, 32, 33]. Ferric iron (Fig. 16) did not induce HK activity loss to nearly the same extent as did ferrous iron, in the presence of ART. Taken together, the requirements of reduced iron and an endoperoxide moiety, neither of which is significantly inhibitory on its own, indicate that drug effects on HK are mediated through free radicals. Reduced iron catalyzes scission, whether homolytic or heterolytic, of the endoperoxide bridge that leads to decomposition of ART to radical intermediates. It can be inferred that, in the enzyme assays, ferrous iron activates ART by peroxide cleavage to metabolites that inhibit HK. Because no  $\text{FeCl}_2$  plus EtOH control was used, we cannot rule out possible, if unlikely, synergy between the drug vehicle and iron. Although ferrous iron has been demonstrated to induce oxygen free radicals with EtOH, no radicals are detected via NMR when the reaction is carried out in Tris buffer [80].

While ferrous iron had little inherent inhibitory effect on HK activity at 35  $\mu\text{M}$ , the same concentration of hemin nearly eliminated enzyme activity (Fig. 17). This finding may be due to hemin's peroxidative capacity or to hydrophobic interactions between HK and the heme porphyrin ring. Although hemin possesses a central  $\text{Fe}^{\text{III}}$  atom, when ferric iron is complexed within a metalloporphyrin, it retains peroxidative capacity [95, 96], similar to free ferrous iron cations.

Substrate assays are useful in demonstrating the irreversibility of inhibition by ART and probing possible drug binding sites on the enzyme. HK was incubated with ATP or mannose prior to the addition of ART and iron in order to investigate whether substrate occupation of the enzyme's active site could preserve activity against inhibition. Full protection of activity was achieved with ATP and mannose (Fig. 18 and 19), possibly indicating that ART acts at or near the HK active site. The greater protection afforded by ATP may be artifactual, due to its propensity for forming complexes with divalent cations [97], thereby chelating iron that could otherwise activate ART. Drug-inactivated HK was also incubated with substrate, which could displace ART from the active site if a competitive, noncovalent interaction were involved between drug and enzyme. Presence of excess substrate is also known to protect HK activity from the effects of oxidants [85], so alkylation may not be the only means by which drug radicals inhibit catalysis. The observation that mannose and ATP could not restore activity to inhibited HK (Fig. 20 and 21) may refute ionic interaction and conformation-driven docking as possible noncovalent modes of drug action. ART may associate with the HK active site to decrease capacity for hexose phosphorylation, but an allosteric mechanism is also possible. Allosteric inhibition may be especially important, as HK exhibits model cooperativity [98]. The HK monomer possesses a bilobed shape, and the binding of hexose in a cleft between the lobes induces conformational change, in which the lobes are brought closer together to create a binding site for ATP [99]. Any secondary or tertiary structural modification may interfere with the enzyme's ability to transition between conformational states.



Dialysis of inhibited enzyme was also used to investigate possible covalent drug-ART interactions (Fig. 22). During the course of dialysis, the concentration of ART in the enzyme samples was diluted approximately one thousand-fold, which likely would have washed away much or all of the drug from HK, provided that it were not covalently-bound. No restoration of activity was observed in dialyzed ART- and iron-treated samples, suggesting that inhibition was irreversible. Dialysis, however, does not exclude the possibility of oxidative damage to the enzyme, as the procedure would also be unable to restore activity in such a situation.

### **Alkylation of Hexokinase by Artemisinin**

As a preparatory step for mass spectrometry, 2DE was performed on ART- and iron-treated HK as well as on control samples (Fig. 25 and 26). Because sequence homology varies between HK isoforms, 2DE was meant to simplify MALDI-TOF spectra interpretation by separating the isoforms prior to mass spectrometry. HK-A and HK-B were expected to resolve as two discrete 55 kD spots, the former at pI 4 and the latter at pI 5.25. Instead, numerous spots in the pI 5-7 range were observed. Because these spots were present in the Tris buffer-incubated HK control sample, the likeliest explanation is differential post-translational modification. Addition of methyl and phosphoryl groups, for example, has been invoked to account for variations in predicted and observed pI in HK [100, 101]. Other alterations such as esterification could account for multiple spots as well as basic pI shifts [102]. Low-level hydrolysis of the enzyme

stock by contaminants might also result in pI shifts without causing an observable change in mass [103].

Another unexpected finding was evidence of EtOH-induced truncation of HK, as shown by 43 kD 2DE gel spots and supported by mass spectrometry results. This observation may stem from partial HK denaturation during exposure to EtOH and peptide degradation or fragment loss in a subsequent experimental step, such as resolubilization in 2DE boiling buffer. Although it does not directly relate to thesis aims, there appears to be no published data for this manner of HK truncation. The HK C-terminus peptide fragment comprising AA 392-485 has an estimated mass of 9.65 kD, and its absence would account for much, if not all, of the mass differential between the expected 55 kD 2DE gel spots and the 43 kD spots observed in the samples exposed to EtOH, whether alone or as a vehicle for ART. The loss of the 392-485 AA fragment might be anticipated to cause decreased activity in the EtOH-treated samples due to hampered nucleotide binding: in HK-A, AA 422-424 are binding sites for the adenine ring of ATP, and regions 425-439 and 453-473 are associated with the overall ATP-binding motif [101]. However, no significant reduction of HK activity was found, indicating that fragment loss likely occurred after, rather than during, drug treatment.

Apart from gel spot intensity, no significant difference was observed in the spots treated with ART alone or with ART and iron. Even though activated drug caused some HK precipitation, the difference in intensity was probably due to underestimation of the amount of protein present. The resolution of the 2DE gel

would not allow detection of one or multiple covalent ART groups added to HK, but the procedure was not intended to provide information in that regard.

### **Detection of Covalent Hexokinase-Artemisinin Adducts**

HK displayed significant loss of activity following incubation with ART and ferrous iron, the enzyme is typically inhibited by alkylators via thiol binding, and ART has been demonstrated to alkylate thiols. In light of these observations, thiopropyl sepharose 6B resin was incubated with ART and iron to serve as a model for the integral cysteine-ART interaction that may inhibit HK activity. An ethanolic silver nitrate solvolysis reaction was performed to cleave drug adducts from the resin and convert them to more lipophilic ethoxy derivatives prior to analysis by TLC. We theorized that any adducts recovered could be structurally identified by GC-MS due to the increased volatility imparted by the ethoxy group.

No adducts released through solvolysis were detected through TLC (Fig. 23). Although the ethanolic silver nitrate solvolysis reaction has been demonstrated to cleave thioether-linked adducts of other alkylating drugs to produce ethoxy derivatives [76], it may not have been compatible with or efficient in this *in vitro* system. Alternatively, adduct yield may have been below the limits of detection. Further, the derivatization procedure may have been inappropriate for visualizing any adducts recovered. Although *p*-anisaldehyde has been used to detect an ART metabolite, the ring-contracted ester resulting from  $\beta$ -scission and self-quenching of ART [77], this metabolite was not observed by TLC. *P*-anisaldehyde reacts with a variety of ART derivatives to produce colored spots

when heated [78] and would likely enable detection of additional metabolites or cleaved adducts. It is also possible that the lack of evidence for adducts reflects a non-alkylating interaction between HK and ART.

Evidence of ferrous iron-mediated decomposition, thus activation, of ART was demonstrated by TLC of reaction solutions of drug and iron in buffer (Fig. 24). Disappearance of the pink ART spot, indicating unreacted drug, was dependent on the iron concentration present in the reaction, however, increases in  $\text{FeCl}_2$  may have caused some precipitation of ART rather than activation. Because the reaction solutions were spotted directly onto silica plates, every stable end metabolite of the pathway(s) involved in drug activation in the *in vitro* model was present on the plates. No spots other than those of the parent compound were visible by derivatization, indicating that the end product of the homolytic O2 pathway was absent and that *p*-anisaldehyde cannot detect other ART metabolites. A nonspecific positive control, such as iodine staining, might have been useful in visualizing drug metabolites that did not react with *p*-anisaldehyde.

### **Mass Spectrometric Studies of Covalent Artemisinin Binding**

Even though released ART-thiol adducts, particularly those of the O2 pathway, were not detected by TLC, a possibility of adducts due to homolytic O1 pathway carbon radicals or heterolytic scheme carbocations still existed. Therefore, MALDI-TOF was used as an additional strategy to provide evidence of alkylation as well as the identities of any modified HK peptide fragments (Fig. 27 and 28; Appendix II). No differences, however, were observed in the spectra of

ART- and iron-treated HK versus control enzyme samples. We hypothesized mass shifts of approximately 282 (or a multiple thereof) to reflect the covalent addition of a single (or more) drug radical to HK fragments, particularly those containing cysteine residues.

Although MALDI-TOF is a powerful tool for characterizing covalent protein modification, several theories may account for the observations made with HK: ART-bound enzyme may have been present below the limits of detection in the 2DE spots selected; fragments bearing adducts may not ionize well under the laser or may have a poor fit with the matrix material; alkylated fragments may exceed the 3600-3800 upper mass limit imposed by the detector; finally, HK may not be alkylated by ART under assay conditions.

### **Oxidative Damage to Hexokinase by Artemisinin Radicals**

Given the irreversible inhibition of HK by ART and iron, along with the lack of evidence of alkylation, oxidative damage may provide an answer for the drug's mechanism of action, at least in these assays. Oxidation by free radicals can modify a wealth of molecules, such as lipids and metal complexes, but comparatively few studies have investigated effects on proteins [104]. Oxygen radicals have been demonstrated to inactivate enzymes through side-chain cleavage, fragmentation, denaturation, and cross-linking, especially through disulfide bridges. Such modifications might account not only for the loss of HK activity and absence of adducts but for the precipitation of ART- and iron-treated enzyme, as well. Disulfide cross-linking and hydrogen abstraction due to ROS

can cause increased surface hydrophobicity, leading to protein aggregation [104]. Studies on various forms of HK have shown the enzyme to be particularly sensitive to oxidation. Rabbit erythrocyte HK is one of the first cellular enzymes to lose activity in oxygen radical-generating systems [97], and rat lens HK is likewise inhibited in the presence of peroxides [86]. Because homology between the yeast and mammalian forms of the enzyme is high [105, 106], similar damage might be expected when yeast HK is exposed to a known alkoxy radical-generating drug such as ART.

### **Pathways in Artemisinin-Induced Oxidative Damage**

Closer examination of ART activation may reveal a more specific mechanism in its action against HK. Reductive cleavage of the endoperoxide bridge in ART results in an alkoxy radical, with either of the peroxidic oxygens bearing an additional electron [107] (Fig. 4). Attack by ferrous iron on a given oxygen results in a radical at the other oxygen. If O2 is attacked, the additional electron associates with O1 to mark entrance into the O1 pathway. In the next step, provided that the alkoxy radical does not react with another molecule, a hydrogen atom shifts from C4 to O1 to yield a carbon radical at C4. If O1 is attacked, however, the electron associates with O2 (the O2 path); this arrangement leads to scission of the bond between C3 and C4 to create a C4 carbon radical that is structurally-distinct from that of the O1 pathway.

Whether drug activation proceeds down the O1 or O2 path depends on reaction conditions, and the solvent present appears to be an important factor.

Products of the O1 pathway predominate in purely aqueous solution; as the percentage of organic solvent in the reaction solution increases, O2 pathway products increase proportionally [108, 109]. The O1 path, therefore, would be more likely to occur in the Tris incubation buffer used for the HK activity assays and may favor oxidation over alkylation, as well.

Quantum chemical calculations on ART compounds performed by Tonmuphean *et al.* [33] found that, although the O1 alkoxyl radical has a lower energy of activation (EA) than does its O2 counterpart, the O2 carbon radical has a significantly lower EA than does the O1 carbon radical. Thus, completion of the O2 pathway is energetically favored, overall. The lower EA of O1 versus O2 alkoxyl radicals may mean that ART enters into the O1 pathway more readily, which appears to hold especially true for aqueous solutions. However, of the alkoxyl radicals that do form, the O2 species is more likely to rearrange to the alkylating carbon radical. The high  $\Delta$ EA between the O1 alkoxyl and carbon radicals may contribute to stabilization of the former, even though the half-lives of alkoxyl radicals tend to be particularly short, owing to their high reactivity. Provided that suitable labile hydrogens are available for intramolecular transfer, rapid H-shifts ( $k \approx 10^6$ - $10^7$  s<sup>-1</sup>) occur with a primary or secondary alkoxyl radical [104] such as that in the O1 pathway, but even a slight delay in rearrangement to the carbon radical could greatly increase the likelihood of alkoxyl radical interaction with a target.

Support for O1 radical-mediated damage to HK may be seen in the TLC results of ART reaction products (Fig. 23 and 24). If the O2 pathway, which is

favored to result in alkylation, were the primary mode of ART activation, then the ring-contracted ester metabolite should have been detectable. This product can only arise through self-quenching of the O2 carbon radical. Self-quenching will occur, to some extent, in every scenario, since ART is thought to exist only for nanoseconds in radical form [41], and not every free radical will interact with a target. A fairly high amount of self-quenched products could be expected, then, in a dilute solution of HK. Clear consumption of ART by ferrous iron, along with lack of published confirmation of self-quenched O1 carbon radical detection by *p*-anisaldehyde derivatization, further supports the O1 pathway at work in this system. However, oxygen radicals generated by iron complexation and heterolytic endoperoxide bond opening cannot be excluded, even though there is a paucity of published data for this activation scheme. Figure 30 depicts the scheme proposed by this thesis for the activation of ART to oxygen radicals capable of inhibiting HK activity.

### **Significance of Artemisinin Alkoxy Radicals *in vivo***

At present, inhibition of HK activity by O1 alkoxy radicals is speculative, but there is evidence that this species may be important to the cytotoxicity of ART. Three of the aforementioned trioxane alcohol ART derivatives (Appendix I) synthesized by Posner *et al.* [37] as a stereochemical probe yielded significant results: of the compounds (which were all differently substituted at C4), only the compound which was able to complete the O1 pathway demonstrated efficacy against *Plasmodium* on par with ART. Because the O2 pathway was not



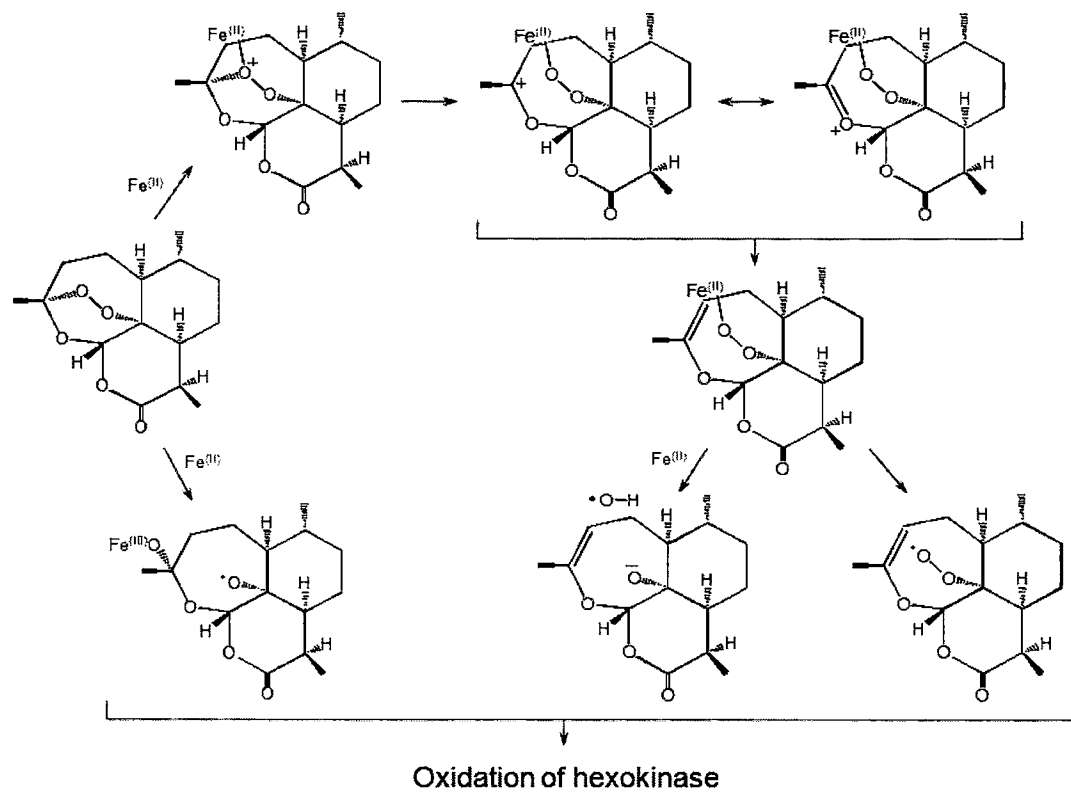


Fig. 30 - Proposed pathways in the ferrous iron-mediated activation of ART to oxygen radicals capable of HK activity inhibition. Endoperoxide bridge opening occurs by iron attack at O2 (the O1 pathway) and homolytic cleavage or by iron complexation and heterolytic cleavage.

hindered by the substitutions, it was proposed that O1 carbon radicals, which could not be formed by the less active compounds, held some significance in parasite death. Any evidence of *in vivo* O1 radical alkylation, however, has yet to be found, and it is unknown whether substitution affected the stability of the O1 alkoxy radicals. In a separate study, Opsenica *et al.* [110] synthesized several tetraoxanes that had antimalarial activity comparable to or better than ART. Spin trapping experiments with these compounds detected the generation of only alkoxy radicals. Although synthetic analogues may not necessarily be metabolized exactly as ART within the parasite, the experiment demonstrates that structurally similar peroxides can exert cytotoxic effects through oxygen free radicals.

The structural studies performed on ART adducts have confirmed that only the O2 carbon radical binds to heme, whether *in vivo* or *in vitro* [42, 111], and of those performed on cysteine, only one has indicated binding of an O1 carbon radical. Wu *et al.* detected an adduct resulting from the O1 path in low yield under aqueous experimental conditions [54]. The lack of evidence for O1 alkylation may be due to second-step energetics in the activation of ART or to steric hindrance. The C4 O1 radical, unlike the C4 O2 radical, is still a part of an intact seven-membered ring structure, and, as such, may experience difficulty in interacting with targets, particularly those that are not highly exposed. A secondary radical, the O1 carbon radical is more stable than the primary O2 carbon radical, due to increased substitution. As such, it might be expected to play a larger part in alkylation, but this does not appear to be the case.

Interestingly, ART compounds that are calculated to move most easily through the O1 pathway have the highest antimalarial activity [33].

### ***In vivo* Correlations of the *in vitro* Hexokinase Assay**

Some difficulty always exists in drawing parallels between *in vitro* and *in vivo* systems, but the yeast HK assays may allow a glimpse of representative ART interactions with cytosolic parasite proteins. The cytosolic milieu is considerably more complex than the *in vitro* environment, and there are no lipids or lipophilic molecules in the incubation buffer with which ART might preferentially associate. Additionally, the assays necessitate a dilute (5 µg/mL) HK solution that, therefore, presents few, homogenous protein targets. Tris buffer, however, more accurately replicates the aqueous environment of the cell than organic solvents such as DMSO and acetonitrile used experimentally by a majority of researchers, owing partly to the drug's poor water-solubility.

The concentration of ART in the assays, while substantially higher than the nanomolar quantities needed to kill *Plasmodium*, remains pharmacologically-relevant. During treatment regimens, plasma levels of ART derivatives can reach 0.5-2.5 µM [112], and parasitized erythrocytes are known to accumulate the drug to greater concentrations than uninfected cells. Vyas *et al.* [22] reported that 55-60% of available ART was partitioned by parasitized cells through passive diffusion versus 35-40% by nonparasitized erythrocytes. Higher accumulation—a 150-fold increase in relation to uninfected cells—was demonstrated using [<sup>3</sup>H]DHA in an earlier study [113]. Ostensibly, drug levels within the parasite

could approach the millimolar range due to active uptake by the parasite.

Drug concentration in these experiments was high in order to facilitate interaction between ART and iron and between activated ART and HK. Relative molar concentrations of high ART and low iron in the assays necessarily create the converse of the situation in the parasite DV, assuming that is the actual site of ART activation and action. The heme concentration within the DV is 350–400 mM [114], as an erythrocyte contains 10–16 mM hemoglobin [115], approximately 80% of which is digested within 24 h [116]. The amount of iron in the assays could not exceed low millimolar levels due to the enzyme's sensitivity to inactivation by metal ions [117].

Ferrous chloride was originally intended to serve as a biomimetic source of iron, as heme, commonly presumed to be the activator of ART within the parasite, inhibits HK activity to a high extent on its own. It has been recently proposed, though, that the site of drug action is the cytosol, not the DV. Uhlemann *et al.* reported diffuse cytosolic localization of a synthetic trioxolane that antagonizes ART action [118]. The same research group also proposes PfATP6, an endoplasmic reticulum analogue of the mammalian SERCA, as the definitive drug target [46]. If the drug does exert its actions in the parasite cytosol, then HK assay conditions of high drug concentration in relation to iron concentration might act as a reasonably good mimic of biological conditions. Iron concentrations and oxidative states within a cell must be strictly controlled so as to prevent excessive damage from oxidation [119].

Further contention is growing over whether heme plays a significant role in

parasite killing by ART. Although *in vitro* alkylation of heme by ART is well-documented, the association constants of the two molecules indicate a low-affinity interaction [53]. The reaction of ART and heme in aqueous environments is also questionable. Hemoglobin reacts with the drug to cause decreased intensity of the Soret band, the characteristic peak of porphyrins occurring near 400 nm, indicating drug coordination or reaction with heme. Approximately equimolar concentrations of ART and heme in buffer with 4% DMSO (v/v) yield a Soret band decrease of 80% after 20 h as well as a heme-ART adduct [111]. The reaction causes only a 25% decrease in the absence of DMSO. Additionally, the amount of heme-ART adducts recovered from the spleens of infected mice is estimated to correspond to 0.4-1.1% of the administered drug dosage, while urine adducts are thought to account for another 0.4-0.9% [42]. The recovery of such small amounts of drug adducts may indicate that only moderate alkylation of heme is required to exert cytotoxic effects or that alkylation plays a minor role in ART action. There are conflicting reports on whether the drug adversely affects hemozoin formation [47, 48]. ART is effective against a broad range of blood-stage forms of the parasite, from newly-formed rings that have little hemozoin, to schizonts, and it impedes gametocyte growth, as well [120, 121]. The development of synthetic alternatives to ART that retain its key feature of an endoperoxide bridge within a 1,2,4-trioxane ring may aid provide more information about the drug's need for interaction with heme. A trioxane able to generate carbon radicals but lacking the ability to alkylate heme exhibits no toxicity against *Plasmodium* [122]. This suggests that either heme alkylation has

biological importance or that carbon radicals are not necessary for drug activity.

What appears as conflicting theories on the action of ART may, in fact, point toward a multifaceted mechanism. It is possible that protein oxidation is only one way in which ART exerts its effects on *Plasmodium*. Multiple mechanisms of action, rather than a single mechanism with perhaps multiple targets, could account for the lack of clinical resistance seen in the malarial parasite, as well for the drug's effectiveness against viruses [63-65], cancer cells [30, 31], other protozoans [57, 58, 62], and helminths [59, 61].

## CONCLUSIONS

Currently, the single most effective drug against malaria also happens to be the most puzzling. A number of mechanisms and targets involved in the action of ART have been proposed, but none have been thoroughly substantiated. Although widely accepted, the link between the ability of ART to alkylate proteins and its mode of action is tenuous. The experiments described herein were originally intended to provide evidence of activity inhibition of an ART-alkylated enzyme, which could indicate an important cytotoxic mechanism.

ART is considered a pro-drug that is activated at its endoperoxide bridge by ferrous iron, and the results of this research support that view. ART significantly inhibited HK activity only in the presence of ferrous iron. Because neither ART nor ferrous iron alone was significantly inhibitory against HK, and because ferric iron was unable to induce inhibition to the same extent as ferric iron, opening of the drug's endoperoxide bridge was implicated in inhibition. The importance of this structural feature was further borne out by the inability of dDHA, an ART derivative lacking an endoperoxide moiety, and iron to effect HK activity inhibition that was more than simply additive.

Inhibition of HK by activated ART was irreversible. Activity could not be restored to ART- and iron-treated enzyme by addition of excess substrate or by dialysis, although it could be protected by pre-incubation with substrate before treatment with drug and iron, indicating a possible interaction between ART and the HK active site.

Possible alkylation of HK by ART was not detected through MALDI-TOF. No visible difference was observed between the spectra of control and drug- and iron-treated enzyme. Further, no covalent drug adducts were detected through solvolysis of ART- and iron-treated Thiopropyl Sepharose 6B resin, which mimicked possible HK alkylation sites. The absence of adducts suggests that alkylation may not be a strong component of ART action against HK. Taken together, the lack of covalent binding by ART in this *in vitro* system and the irreversible inhibition of HK activity strongly suggest a drug activation pathway leading to enzymatic damage by oxygen radicals. Further supporting this theory is the lack of metabolites resulting from the O<sub>2</sub> pathway, essentially the only pathway of activation demonstrated to produce alkylating radicals, observed via TLC of ART reaction solutions. We propose that generation of inhibitory ART oxygen radicals occurs via homolytic endoperoxide cleavage in the O<sub>1</sub> pathway or heterolytic cleavage by iron complexation.

The research presented herein may provide the first evidence of oxidative damage by ART to a soluble protein. Although direct extrapolation of *in vitro* findings is difficult, we propose that enzymatic inhibition due to oxygen free radicals of ART may be a significant component of the drug's mechanism of action. Future research with ART might incorporate additional activity assays using purified parasite proteins, kinetic analysis of drug-induced protein conformational change, or detection and localization of oxidized proteins within ART-treated parasites. Ultimately, elucidating the mechanism or mechanisms of action of ART may provide important information about drug bioactivation in



*Plasmodium*, preclude possible resistance development, and aid in the rational design of inexpensive and more potent drugs.

## REFERENCES

- [1] Roll Back Malaria, World Health Organization and Unicef. World Malaria Report 2005; 2005.
- [2] Roberts LS, Janovy J. Foundations of parasitology. Sixth edition. Boston: McGraw Hill, 2001.
- [3] Jearnpipatkul A, Govitrapong P, Yuthavong Y, Wilairat P, Panijpan B. Binding of antimalarial drugs to hemozoin from *Plasmodium berghei*. *Experientia* 1980;36:1063-4.
- [4] Kessl JJ, Lange BB, Merbitz-Zahradnik T, Zwicker K, Meunier B, Palsdottir H, Hunte C, Meshnick S, Trumppower BL. Molecular basis for atovaquone binding to the cytochrome bc1 complex. *J Biol Chem* 2003;278:31312-8
- [5] Most H, Herman R, Schoenfeld C. Chemotherapy of sporozoite- and blood-induced *Plasmodium berghei* infections with selected antimalarial agents. *Am J Trop Med Hyg* 1967;5:572-5.
- [6] Clyde DF, Miller RM, DuPont HL, Hornick RB. Antimalarial effects of tetracyclines in man. *Am J Trop Med Hyg* 1971;74:238-42.
- [7] Rosenthal PJ. Antimalarial drug discovery: old and new approaches. *J Exp Biol* 2003; 206:3735-44.
- [8] Sharma S, Pathak S. Malaria vaccine: A current perspective. *J Vector Borne Dis* 2008;45:1-20.
- [9] Fidock DA, Nomura T, Talley AK, Cooper RA, Dzekunov SM, Ferdig MT, Ursos LM, Sidhu AB, Naude B, Deitsche KW, Su XZ, Wootton JC, Roepe PD, Wellems TE. Mutations in the *P. falciparum* digestive vacuole transmembrane protein PfCRT and evidence for their role in chloroquine resistance. *Mol Cell* 2000;6:861-71.
- [10] Reed MB, Saliba KJ, Caruana SR, Kirk K, Cowman AF. Pgh1 modulates sensitivity and resistance to multiple antimalarials in *Plasmodium falciparum*. *Nature* 2000;403:906-9.
- [11] Looareesuwan S, Vivaran C, Webster HK, Kyle DE, Hutchinson DB, Canfield CJ. Clinical studies of atovaquone, alone or in combination with other antimalarial drugs, for treatment of acute uncomplicated malaria in Thailand. *Am J Trop Med Hyg* 1996;54:62-6.

- [12] Trape JF. The public health impact of chloroquine resistance in Africa. *Am J Trop Med Hyg* 2001;64:12-7.
- [13] Bruce-Chawitt LJ. Qinghausu: a new antimalarial. *Br Med J* 1982;284:767-8.
- [14] Bray PG, Ward SA, O'Neill PM. Quinolines and artemisinin: Chemistry, biology, and history. *Curr Top Microbiol Immunol* 2005;295:3-38.
- [15] Wongsrichanalai C, Pickard AL, Wernsdorfer WH, Meshnick SR. Epidemiology of drug-resistant malaria. *Lancet Infect Dis* 2002;2:209-18.
- [16] Noedl H, Se Y, Schaecher K, Smith BL, Socheat D, Fukuda MM. Evidence of artemisinin-resistant malaria in western Cambodia. *N Engl J Med* 2008;359:2619-20.
- [17] Wongsrichanalai C, Meshnick SR. Declining artesunate-mefloquine efficacy against falciparum malaria on the Cambodia-Thailand border. *Emerg Infect Dis* 2008;14:716-9.
- [18] Davis TM, Karunajeewa HA, Ilett KF. Artemisinin-based combination therapies for uncomplicated malaria. *Med J Aust* 2005;182:181-5.
- [19] Skinner TS, Manning LS, Johnston WA, Davis TM. In vitro stage-specific sensitivity of *Plasmodium falciparum* to quinine and artemisinin drugs. *Int J Parasitol* 1996;26:519-25.
- [20] Oliaro PL, Nair NK, Sathasivam K, Mansor SM, Navaratnam V. Pharmacokinetics of artesunate after single oral administration to rats. *BMC Pharmacol* 2001;1:1-12.
- [21] Silamut K, Newton PN, Teja-Isavadharm P, Suputtamongkol Y, Siriyanonda D, Rasameesoraj M, Pukrittayakamee S, White NJ. Artemether bioavailability after oral or intramuscular administration in uncomplicated falciparum malaria. *Antimicrob Agents Chemother* 2003;47:3795-8.
- [22] Vyas N, Avery BA, Avery MA, Wyandt CM. Carrier-mediated partitioning of artemisinin into *Plasmodium falciparum*-infected erythrocytes. *Antimicrob Agents Chemother* 2002;46:105-9.
- [23] Akompong T, VanWye J, Ghorri N, Haldar K. Artemisinin and its derivatives are transported by a vacuolar-network of *Plasmodium falciparum* and their antimalarial activities are additive with toxic sphingolipid analogues that block the network. *Mol Biochem Parasit* 1999;101:71-9.
- [24] Park BK, O'Neill PM, Maggs JL, Pirmohamed M. Safety assessment of

peroxide antimalarials: clinical and chemical perspectives. *Br J Clin Pharmacol* 1998;46:521-9.

- [25] Klayman, DL. Qinghaosu (artemisinin): an antimalarial drug from China. *Science* 1985;228:1049-55.
- [26] Sadrzadeh SM, Graf E, Panter SS, Hallaway PE, Eaton JW. Hemoglobin: A biologic fenton reagent. *J Biol Chem* 1984;10:14354-6.
- [27] Yang YZ, Little B, Meshnick SR. Alkylation of proteins by artemisinin. Effects of heme,pH, and drug structure. *Biochem Pharmacol* 1994;48:569-73.
- [28] Meshnick SR, Yang YZ, Lima V, Kuypers F, Kamchonwongpaisan S, Yuthavong Y. Iron-dependent free radical generation from the antimalarial agent artemisinin (qinghaosu). *Antimicrob Agents Chemother* 1993;37:1108-14.
- [29] Gatter KC, Brown G, Trowbridge IS, Woolston RE, Mason DY. Transferrin receptors in human tissues: their distribution and possible clinical relevance. *J Clin Pathol* 1983;36:539-45.
- [30] Moore JC, Lai H, Li JR, Ren RL, McDougall JA, Singh NP, Chou CK. Oral administration of dihydroartemisinin and ferrous sulfate retarded implanted fibrosarcoma growth in the rat. *Cancer Lett* 1995;98:83-7.
- [31] Singh NP, Lai H. Selective toxicity of dihydroartemisinin and holotransferrin toward human breast cancer cells. *Life Sci* 2001;70:49-56.
- [32] Olliaro P, Haynes RK, Meunier B, Yuthavoth Y. Possible modes of action of the artemisinin-type compounds. *Trends Parasitol* 2001;17:122-6.
- [33] Tonmuphean S, Parasuk V, Kokpol S. Effective discrimination of antimalarial potency of artemisinin compounds based on quantum chemical calculations of their reaction mechanism. *Bioorg Med Chem* 2006;14:2082-8.
- [34] Scott MD, Meshnick SR, Williams RA, Chiu DT, Pan HC, Lubin BH, Kuypers FA. Qinghaosu-mediated oxidation in normal and abnormal erythrocytes. *J Lab Clin Med* 1989;114:401-6.
- [35] Berman PA, Adams PA. Artemisinin enhances heme-catalyzed oxidation of lipid membranes. *Free Radic Biol Med* 1997;22:1283-8.
- [36] Taranto AG, Carneiro JW de M, de Oliveira FG, de Araujo MT, Correa CR. The role of C-centered radicals on the mechanism of artemisinin. *J Mol*

Struct 2002;580:207-15.

- [37] Posner GH, Oh CH, Wang D, Gerena L, Milhous WK, Meshnick SR, Asawamahasakda W. Mechanism-based design, synthesis, and in vitro antimalarial testing of new 4-methylated trioxanes structurally-related to artemisinin: The importance of a carbon-centered radical for antimalarial activity. *J Med Chem* 1994;37:1256-8.
- [38] LoPachin RM, DeCaprio AP. Protein adduct formation as a molecular mechanism in neurotoxicity. *Tox Sci* 2005;86:214-25.
- [39] Friedman J, Huberman E. Postreplication repair and the susceptibility of Chinese hamster cells to cytotoxic and mutagenic effects of alkylating agents. *Proc Nat Acad Sci* 1980;77:6072-6.
- [40] Frankfort OS. Flow cytometry analysis of DNA damage and the evaluation of cytotoxicity of alkylating agents. *Cancer Res* 1987;47:5537-41.
- [41] Cazalles J, Robert A, Meunier B. Alkylating capacity and reaction products of antimalarial trioxanes after activation by a heme model. *J Org Chem* 2002;67:609-19.
- [42] Robert A, Benoit-Vical F, Claparols C, Meunier B. The antimalarial drug artemisinin alkylates heme in infected mice. *Proc Natl Acad Sci USA* 2005;102:13676-80.
- [43] Maeno Y, Toyoshima T, Fujioka H, Ito Y, Meshnick SR, Benakis A, Milhous WK, Aiwaka M. Morphologic effects of artemisinin in *Plasmodium falciparum*. *Am J Trop Med Hyg* 1993;49:485-91.
- [44] Bousejra-El Garah F, Claparols C, Benoit-Vical F, Meunier B, Robert A. The antimalarial trioxaquine DU1301 alkylates heme in malaria-infected mice. *Antimicrob Agents Chemother* 2008;52:2966-9.
- [45] Asawamahasakda W, Ittarat I, Pu YM, Ziffer H, Meshnick SR. Reaction of antimalarial endoperoxides with specific parasite proteins. *Antimicrob Agents Chemother* 1994;38:1854-8.
- [46] Eckstein-Ludwig U, Webb RJ, van Goethem IDA, East JM, Lee AG, Kimura M, O'Neill PM, Bray PG, Ward SA, Krishna S. Artemisinins target the SERCA of *Plasmodium falciparum*. *Nature* 2003;424:957-61.
- [47] Hong YL, Yang YZ, Meshnick SR. The interaction of artemisinin with malarial hemozoin. *Mol Biochem Parasitol* 1994;63:121-8.
- [48] Haynes RK, Monti D, Taramelli D, Basilico N, Parapini S, Oliaro P.

- Artemisinin antimalarials do not inhibit hemozoin formation. *Antimicrob Agents Chemother* 2003;47:1175.
- [49] Bhisutthibhan J, Pan XQ, Hossler PA, Walker DJ, Yowell CA, Carlton J, Dame JB, Meshnick SR. The *Plasmodium falciparum* translationally controlled tumor protein homologue and its reaction with the antimalarial drug artemisinin. *J Bio Chem* 1998; 273:16192-8.
  - [50] Bhisutthibhan J, Philbert MA, Fujioka H, Aikawa M, Meshnick SR. The *Plasmodium falciparum* translationally controlled tumor protein: subcellular localization and calcium binding. *Eur J Cell Biol* 1999;78:665-70.
  - [51] Uhlemann AC, Cameron A, Eckstein-Ludwig U, Fischbarg J, Iserovich P, Zuniga FA, East M, Lee A, Brady L, Haynes RK, Krishna S. A single amino acid residue can determine the sensitivity of SERCAs to artemisinins. *Nat Struct Mol Bio* 2005;12:628-9.
  - [52] Accarro A, Laurent SA, Mazarguil H, Meyer M, Robert A, Meunier B. Interaction of iron(II)-heme and artemisinin with a peptide mimic of *Plasmodium falciparum* HRP-II. *J Inorg Biochem* 2007;101:1739-47.
  - [53] Pandey AV, Tekwani BL, Singh RL, Chauhan VS. Artemisinin, an endoperoxide antimalarial, disrupts the hemoglobin catabolism and heme detoxification systems in malarial parasites. *J Biol Chem* 1999;274:19383-8.
  - [54] Wu Y, Yue ZY, Wu YL. Interaction of qinghaosu (artemisinin) with cysteine sulfhydryl mediated by traces of non-heme iron. *Agnew Chem Int Ed Engl* 1999;38:2580-2.
  - [55] Wang D, Wu Y. A possible antimalarial action of qinghaosu (artemisinin) series compounds. Alkylation of reduced glutathione by C-centered primary radicals produced from antimalarial compounds qinghaosu and 12-(2,4-dimethoxyphenyl)-12-deoxoqinghaosu. *Chem Commun* 2000;2193-2194.
  - [56] O'Neill PM, Rawe SL, Borstnik K, Miller A, Ward SA, Bray PG, Davies J, Oh CH, Posner GH. Enantiomeric 1,2,4-trioxanes display equivalent in vitro antimalarial activity versus *Plasmodium falciparum* malaria parasites: implications for the molecular mechanism of action of the artemisinins. *Chembiochem* 2005;6:2048-54.
  - [57] Mishina YV, Krishna S, Haynes RK, Meade JC. Artemisinins inhibit *Trypanosoma cruzi* and *Trypanosoma brucei rhodesiense* in vitro growth. *Antimicrob Agents Chemother* 2007;41:1852-54.
  - [58] Nagamune K, Beatty WL, Sibley LD. Artemisinin induces calcium-

- dependent protein secretion in the protozoan parasite *Toxoplasma gondii*. *Eukaryot Cell* 2007;6:2147-56.
- [59] Abdel Aziz SS, el-Badawy NM. Experimental trials of an artemisinin derivative in treatment of *Schistosoma mansoni*-infected mice. *J Egypt Soc Parasitol* 2000;30:295-303.
  - [60] Chen MM, Shi L, Sullivan DJ Jr. *Haemoproteus* and *Schistosoma* synthesize heme polymers similar to *Plasmodium* hemozoin and beta-hematin. *Mol Biochem Parasitol* 2001;113:1-8.
  - [61] Xiao S, Shen BG, Utzinger J, Chollet J, Tanner M. Transmission electron microscopic observations on ultrastructural damage in juvenile *Schistosoma mansoni* caused by artemether. *Acta Trop* 2002;81:53-61.
  - [62] Yang DM, Liew FY. Effects of qinghaosu (artemisinin) and its derivatives on experimental cutaneous leishmaniasis. *Parasitology* 1993;106:7-11.
  - [63] Romero MR, Efferth T, Serrano MA, Castano B, Macias RI, Briz O, Marin JJ. Effect of artemisinin/artesunate as inhibitors of hepatitis B virus production in an "in vitro" replicative system. *Antiviral Res* 2005;68:75-83.
  - [64] Paeshuyse J, Coelmont L, Vliegen I, Van hemel J, Vandenkerckhove J, Peys E, Sas B, De Clercq E, Neyts J. Hemin potentiates the anti-hepatitis C virus activity of the antimalarial drug artemisinin. *Biochem Biophys Res Comm* 2006;348:139-44.
  - [65] Romero MR, Serrano MA, Vallejo M, Efferth T, Alvarez M, Marin JJ. Antiviral effect of artemisinin from *Artemisia annua* against a model member of the Flaviviridae family, the bovine viral diarrhea virus (BVDV). *Planta Med* 2006;72:1169-74.
  - [66] Lazarus NR, Derechin M, Barnard EA. Yeast hexokinase. 3. Sulfhydryl groups and protein dissociation. *Biochemistry* 1968;7:2390-400.
  - [67] Jones JG. Active-site thiol groups of yeast hexokinase. *Biochem J* 1969;115:41.
  - [68] Thor H, Hartzell P, Svensson SA, Orrenius S, Mirabelli F, Marinoni V, Bellomo G. On the role of thiol groups in the inhibition of liver microsomal  $\text{Ca}^{2+}$  sequestration by toxic agents. *Biochem Pharmacol* 1985;34:3717-23.
  - [69] Ashida H, Kanazawa K, Minamoto S, Danno G, Natake M. Effect of orally administered secondary autoxidation products of linoleic acid on carbohydrate metabolism in rat liver. *Arch Biochem Biophys* 1987;259:114-23.

- [70] Lash LH, Tokarz JJ. Isolation of two distinct populations of cells from rat kidney cortex and their use in the study of chemical-induced toxicity. *Anal Biochem* 1989;182:271-9.
- [71] Lenzen S, Freytag S, Panten U, Flatt PR, Bailey CJ. Alloxan and ninhydrin inhibition of hexokinase from the pancreatic islets and tumoral insulin-secreting cells. *Pharmacol Toxicol* 1990;66:157-62.
- [72] Chambers JW, Fowler ML, Morris MT, Morris JC. The anti-trypanosomal agent lonidamine inhibits *Trypanosoma brucei* hexokinase I. *Mol Biochem Parasitol* 2008;158:202-7.
- [73] Frölich KU, Entian KD, Mecke D. The primary structure of the yeast hexokinase PII gene (HXK2) which is responsible for glucose respiration. *Gene* 1985;36:105-11.
- [74] Kopetzki E, Entian KD, Mecke D. Complete nucleotide sequence of the hexokinase PI gene (HXK1) of *Saccharomyces cerevisiae*. *Gene* 1985;39:95-101.
- [75] Mulcahy P, O'Flaherty M, Jennings L, Griffin T. Application of kinetic-based biospecific affinity chromatographic systems to ATP-dependent enzymes: studies with yeast hexokinase. *Anal Biochem* 2002;309:279-92.
- [76] Mattocks AR, Jukes R. Recovery of the pyrrolic nucleus of pyrrolizidine alkaloid metabolites from sulphur conjugates in tissues and body fluids. *Chem Biol Interact* 1990;75:225-39.
- [77] Beekman AC, Woerdenbag HJ, Van Uden W, Pras N, Konings AW, Wikstrom HV. Stability of artemisinin in aqueous environments: impact on its cytotoxic action to Ehrlich ascites tumour cells. *J Pharm Pharmacol* 1997;49:1254-8.
- [78] Gabriels M, Plaizier-Vercammen JA. Densitometric thin-layer chromatographic determination of artemisinin and its lipophilic derivatives, artemether and arteether. *J Chromatogr Sci* 2003;41:359-66.
- [79] Jones JG, Otieno S, Barnard C, Bhargava AK. Essential and nonessential thiols of yeast hexokinase. Reactions with iodoacetate and iodoacetamide. *Biochemistry* 1975;14:2396-403.
- [80] Welch KD, Davis TZ, Aust SD. Iron autoxidation and free radical generation: effects of buffers, ligands, and chelators. *Arch Biochem Biophys* 2002;397:360-9.
- [81] Kumar DP, Tiwari A, Bhat R. Effect of pH on the stability and structure of



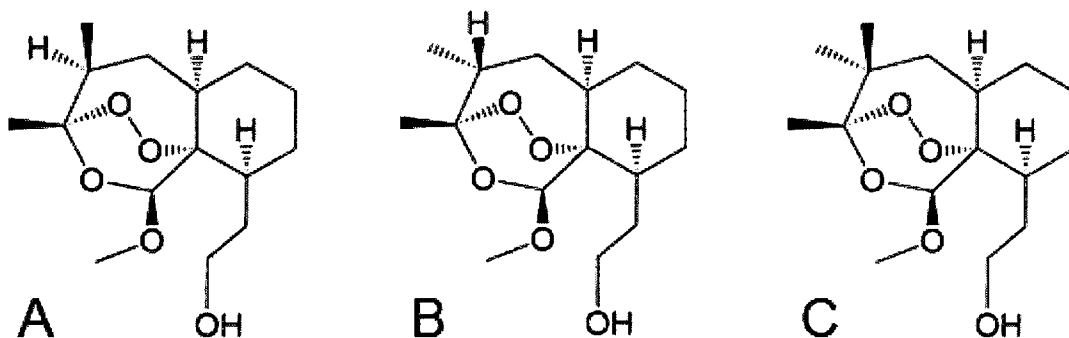
- yeast hexokinase A. *J Biol Chem* 2004;279:32093-9.
- [82] Sibmooh N, Udomsangpetch R, Kijjoa A, Chantharaksri U, Mankhetkorn S. Redox reaction of artemisinin with ferrous and ferric ions in aqueous buffer. *Chem Pharm Bull* 2001;49:1541-6.
- [83] Grossman SH. A note on the dual role of glucose in the protection of glucokinase against inactivation. *Biochim Biophys Acta* 1976;452:392-7.
- [84] Williams DC, Jones JG. Dissociation and catalysis in yeast hexokinase. *Biochem J* 1976;155:661-7.
- [85] Kletzkly DL, Tung WH, Chylack LT Jr. The protective effect of glucose on soluble rat lens hexokinase in the presence of oxidative stress. *Curr Eye Res* 1986;5:433-9.
- [86] Clonis YD, Goldfinch MJ, Lowe CR. The interaction of yeast hexokinase with Procion Green H-4G. *Biochem J* 1981;197:203-11.
- [87] Kopetzky E, Entian KD. Purification of yeast hexokinase isoenzymes using affinity chromatography and chromatofocusing. *Anal Biochem* 1982;121:181-5.
- [88] Bailey E, Farmer PB, Shuker DE. Estimation of exposure to alkylating carcinogens by the GC-MS determination of adducts to hemoglobin and nucleic acid bases in urine. *Arch Toxicol* 1987;60:187-91.
- [89] Slaughter DE, Hanzlik RP. Identification of epoxide- and quinone-derived bromobenzene adducts to protein sulfur nucleotides. *Chem Res Toxicol* 1991;4:349-59.
- [90] Krusemark CJ, Ferguson JT, Wenger CD, Kelleher NL, Belshaw PJ. Global amine and acid functional group modification of proteins. *Anal Chem* 2008;80:713-20.
- [91] Wei N, Sadrzadeh SM. Enhancement of hemin-induced membrane damage by artemisinin. *Biochem Pharmacol* 1994;48:737-41.
- [92] Gaspar AR, Potgieter DJ, Vermeulen NM. The effect of the sesquiterpene lactones from *Geigeria* on glycolytic enzymes. *Biochem Pharmacol* 1986;35:493-7.
- [93] Augustijns P, D'Hulst A, Van Daele J, Kinget R. Transport of artemisinin and sodium artesunate in Caco-2 intestinal epithelial cells. *J Pharm Sci* 1996;85:577-9.

- [94] Stocchi V, Biagiarelli B, Fiorani M, Palma F, Piccoli G, Cucchiarin L, Dacha M. Inactivation of rabbit red blood hexokinase activity promoted in vitro by an oxygen-radical-generating system. *Arch Biochem Biophys* 1994;311:160-7.
- [95] Chiu D, Lubin B. Oxidative hemoglobin denaturation and RBC destruction: the effect of heme on red cell membranes. *Semin Hematol* 1989;26:128-35.
- [96] Usha Devi S, Ramasarma T. Hemin-mediated oxidative inactivation of 3-hydroxy-3-methylglutaryl CoA reductase. *Mol Cell Biochem* 1987;77:103-10.
- [97] Pecoraro VL, Hermes JD, Cleland WW. Stability constants of  $Mg^{2+}$  and Cd complexes of adenine nucleotides and thionucleotides and rate constants for formation and dissociation of MgATP and MgADP. *Biochemistry* 1984;23:5262-71.
- [98] Ainslie GR Jr, Shill JP, Neet KE. Transients and cooperativity. *J. Biol Chem* 1972;247:7088-96.
- [99] Kopetzky E, Entian KD. Glucose repression and hexokinase isoenzymes in yeast. Isolation and characterization of a modified hexokinase PII isoenzyme. *Eur J Biochem* 1985;146:657-62.
- [100] Bianchi M, Serafini G, Bartolucci E, Palma F, Magnani M. Expression, purification, and characterization of a recombinant erythroid-specific hexokinase isozyme. *Blood Cells Mol Dis* 1998;24:401-11.
- [101] Wilson JE, Schwab DA. Functional interaction of hexokinase with ATP requires participation by both small and large lobes of the enzyme: implications for other proteins using the actin fold as a nucleotide binding motif. *FASEB J* 1996;10:799-801.
- [102] Halpin MI, Richardson T. Selected functionality changes of beta-lactoglobulin upon esterification of side-chain carboxyl groups. *J Dairy Sci* 1985;68:3189-98.
- [103] Ross PE, Helgerson SL, Miercke LJ, Dratz EA. Isoelectric focusing studies of bacteriorhodopsin. *Biochim Biophys Acta* 1989;991:134-40.
- [104] Davies MJ, Dean RT. Radical-mediated protein oxidation. Oxford University Press, 1997.
- [105] Schirch DM, Wilson JE. Rat brain hexokinase: Amino acid sequence at the substrate hexose binding site is homologous to that of yeast hexokinase. *Arch Biochem Biophys* 1987;257:1-12.

- [106] Marcus F, Ureta T. Amino acid sequence homology between yeast hexokinases and rat hexokinase C. *Biochem Biophys Res Commun* 1986;139:714-9.
- [107] Cumming JN, Ploypradith P, Posner GH. Antimalarial activity of artemisinin (qinghaosu) and related trioxanes: Mechanism(s) of action. *Adv Pharm* 1997;37:253-97.
- [108] Creek DJ, Chiu FCK, Prankerd RJ, Charman SA, Charman WN. Kinetics of iron-mediated artemisinin degradation: Effects of solvent composition and iron salt. *J Pharm Sci* 2005;94:1820-9.
- [109] Wu Y, Liu H. Probing the possible molecular origin of the highly selective toxicity of the antimalarial peroxide qinghaosu (artemisinin). *Chem Res Toxicol* 2003;16:1202-6.
- [110] Opsenica I, Terzic N, Opsenica D, Angelovski G, Lehnig M, Eilbracht P, Tinant B, Juranic Z, Smith KS, Yang YS, Diaz DS, Smith PL, Milhous WK, Dokovic D, Solaja BA. Tetraoxane antimalarials and their reaction with Fe(II). *J Med Chem* 2006;49:3790-9.
- [111] Messori L, Gabbiani C, Casini A, Siragusa M, Vincieri FF, Bilia AR. The reaction of artemisinin with hemoglobin: A unified picture. *Bioorg Med Chem* 2006;14:2972-7.
- [112] Smith SL, Maggs JL, Edwards G, Ward SA, Park BK, McLean WG. The role of iron in neurotoxicity: A study of novel antimalarial drugs. *Neurotoxicology* 1998;19:557-9.
- [113] Gu HM, Warhurst DC, Peters W. Uptake of [3H]dihydroartemisinin by erythrocytes infected with *Plasmodium falciparum* in vitro. *Trans R Soc Trop Med Hyg* 1984;78:265-70.
- [114] Francis SE, Sullivan DJ Jr, Goldberg DE. Hemoglobin metabolism in the malaria parasite *Plasmodium falciparum*. *Annu Rev Microbiol* 1997;51:97-123.
- [115] Kumar S, Bandyopadhyay U. Free heme toxicity and its detoxification systems in humans. *Toxicol Lett* 2005;157:175-88.
- [116] Becker K, Tilley L, Vennerstrom JL, Roberts D, Rogerson S, Ginsburg H. Oxidative stress in malaria parasite-infected erythrocytes: host-parasite interactions. *Int J Parasitol* 2004;34:163-89.
- [117] Zewe V, Fromm HJ, Fabiano R. The effect of manganous iron on the kinetics and mechanism of the yeast hexokinase reaction. *J Biol Chem*

1964;239:1625-34

- [118] Uhlemann, AC, Wittlin S, Matile H, Bustamante LY, Krishna S. Mechanism of antimalarial action of the synthetic trioxolane RBX11160 (OZ277). *Antimicrob Agents Chemother* 2007;51:667-72.
- [119] MacKenzie EL, Iwasaki K, Tsuji Y. Intracellular iron transport and storage: From molecular mechanisms to health implications. *Antioxid Redox Signal* 2008;10:997-1030.
- [120] ter Kuile FO, White NJ, Holloway PA, Pasvol G, Krishna S. *Plasmodium falciparum*: in vitro studies of the pharmacodynamic properties of antimalarials used for the treatment of severe malaria. *Exp Parasitol* 1993;76:85-95.
- [121] Angus BJ, Chotivanich K, Udomsangpetch R, White NJ. In vivo removal of malaria parasites from red blood cells without their destruction in acute falciparum malaria. *Blood* 1997;90:2037-40.
- [122] Cazelles J, Camuzat-Dedenis B, Provot O, Robert A, Mayrargue J, Meunier B. Alkylating properties of synthetic trioxanes related to artemisinin. *J Chem Soc Perkin Trans* 2000;1:1265-70.

**APPENDIX I: ADDITIONAL DRUG STRUCTURES**

Structures of three synthetic trioxane derivatives of ART [37]. Only compound A is able to complete the O1 pathway.

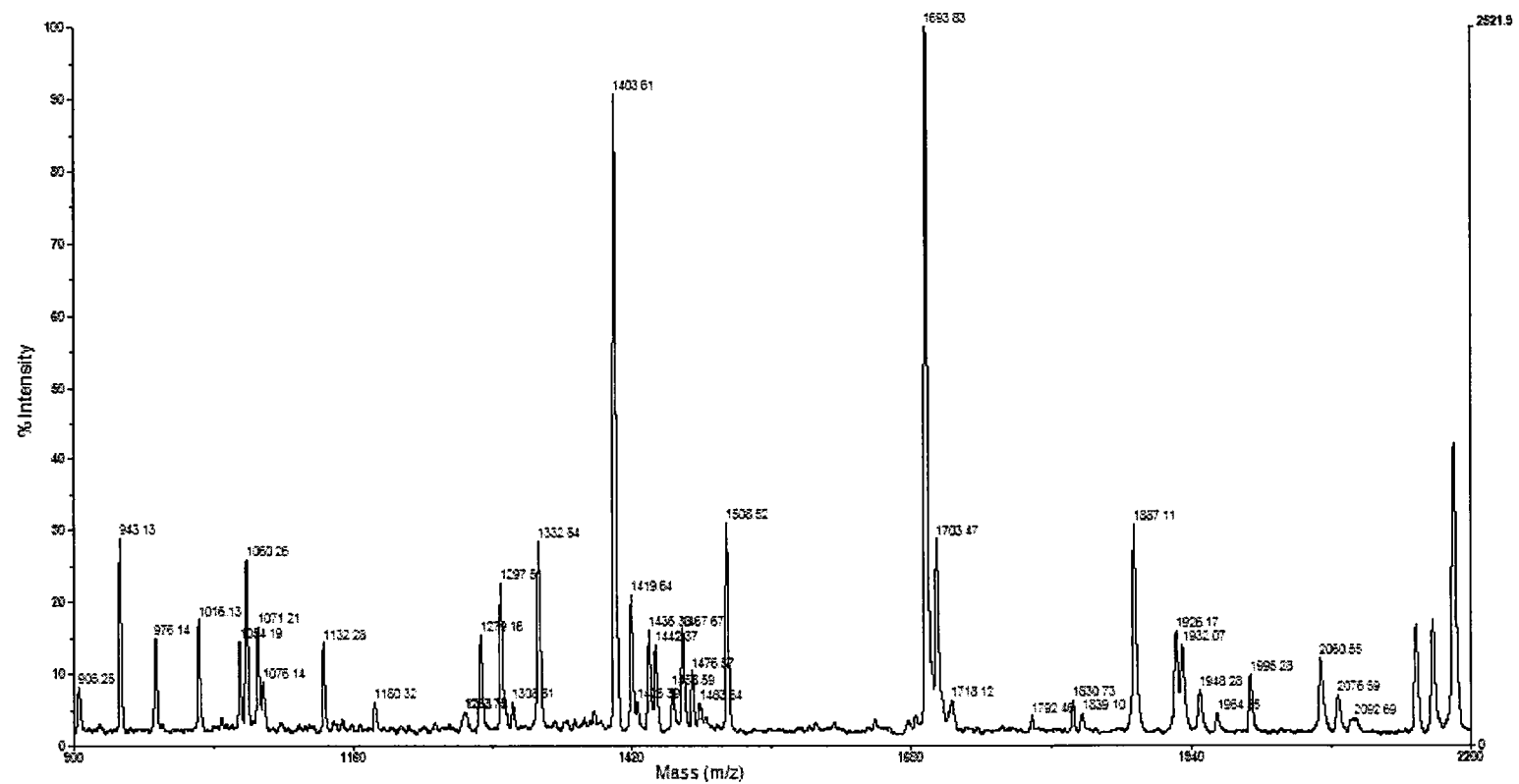


Fig. 31- MALDI-TOF spectrum of spot 1, fragment mass 900-2200. Spot 1 was an untreated HK control migrating to 55 kD and pI 5.5.

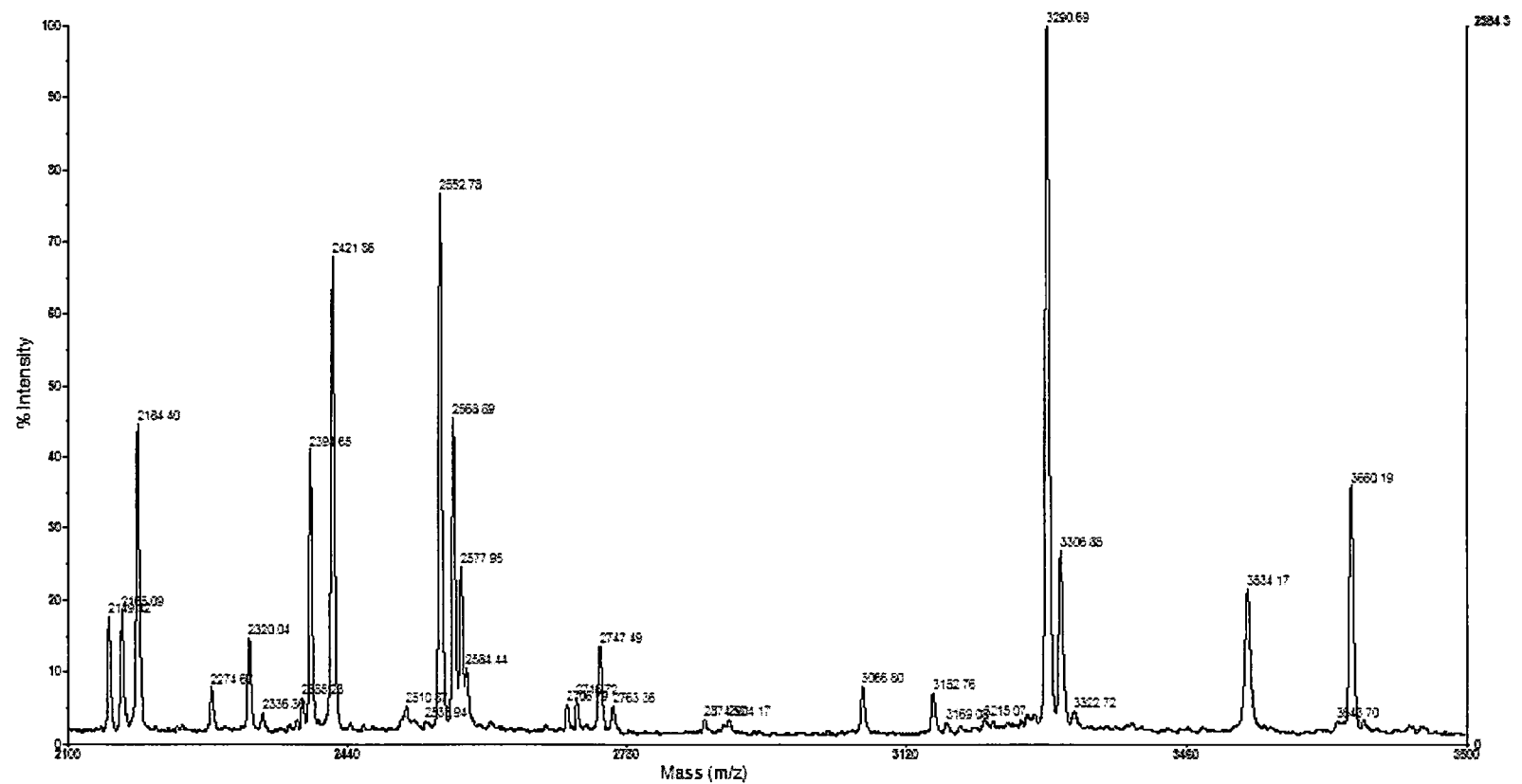


Fig. 32 - MALDI-TOF spectrum of spot 1, fragment mass 2200-3800. Spot 1 was an untreated HK control migrating to 55 kD and pI 5.5.

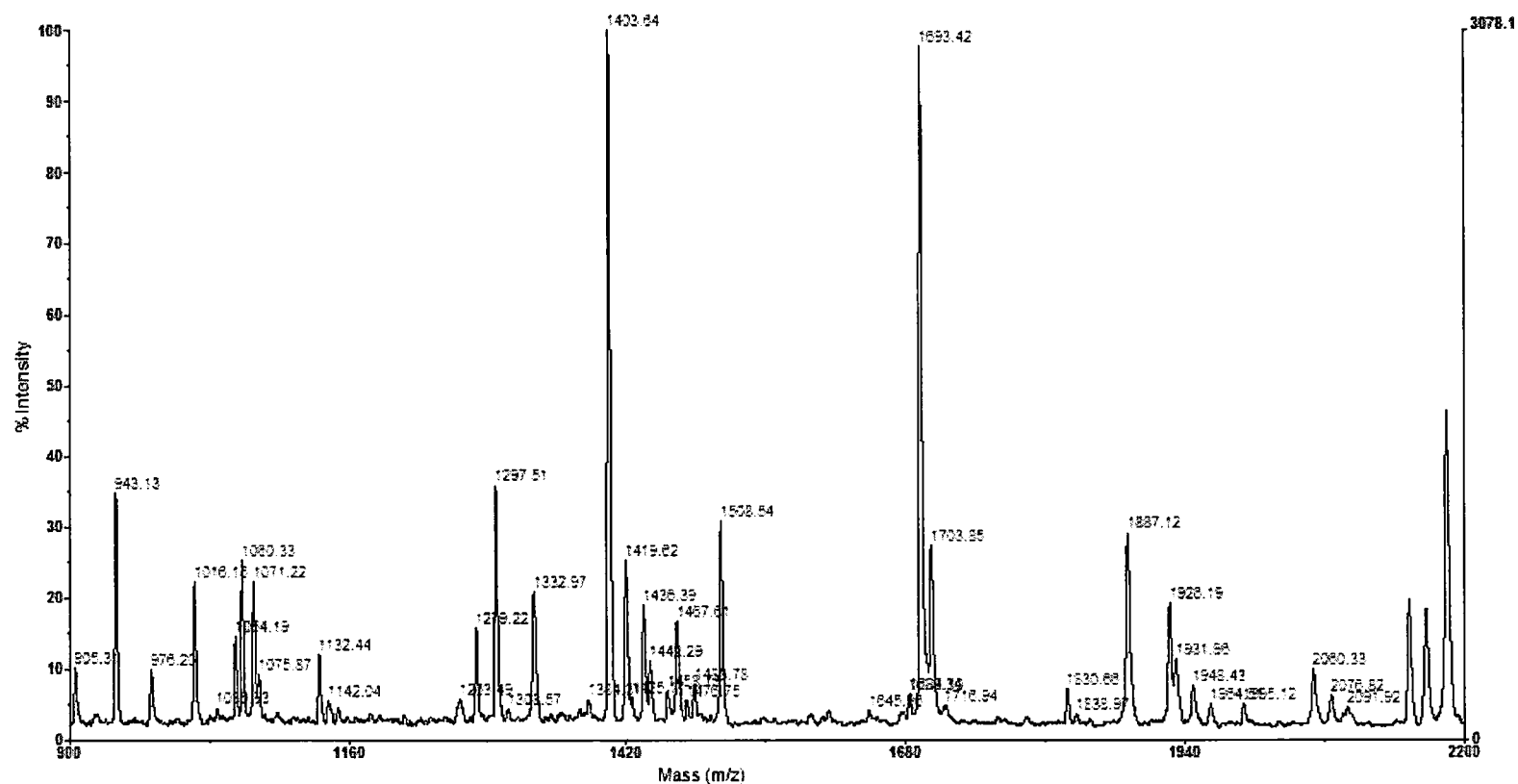


Fig. 33 - MALDI-TOF spectrum of spot 3, fragment mass 900-2200. Spot 3 was HK treated with 350  $\mu$ M ART, migrating to 43 kD and pI 6.2.



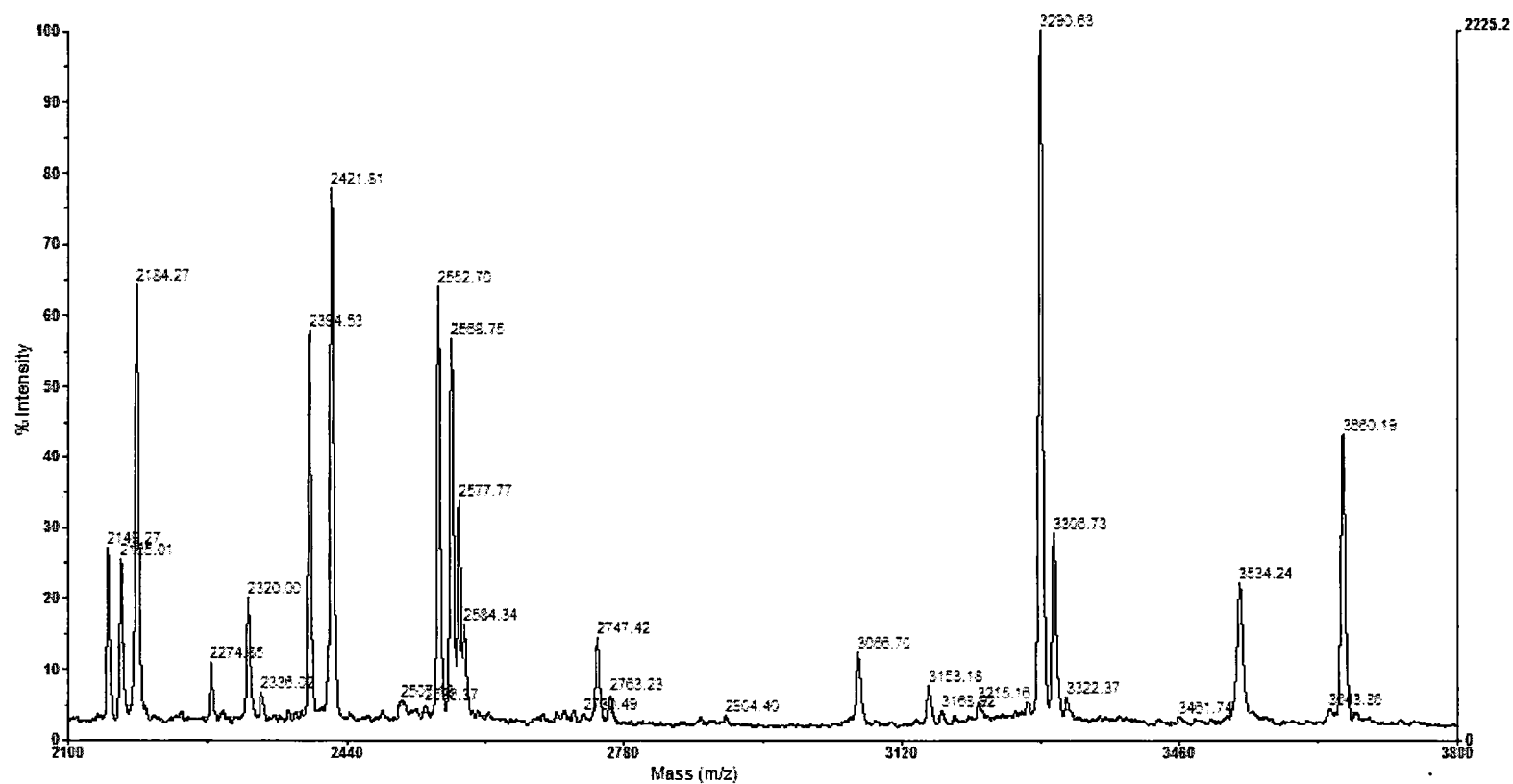


Fig. 34 - MALDI-TOF spectrum of spot 3, fragment mass 2200-3800. Spot 3 was HK treated with 350  $\mu$ M ART, migrating to 43 kD and pI 6.2.

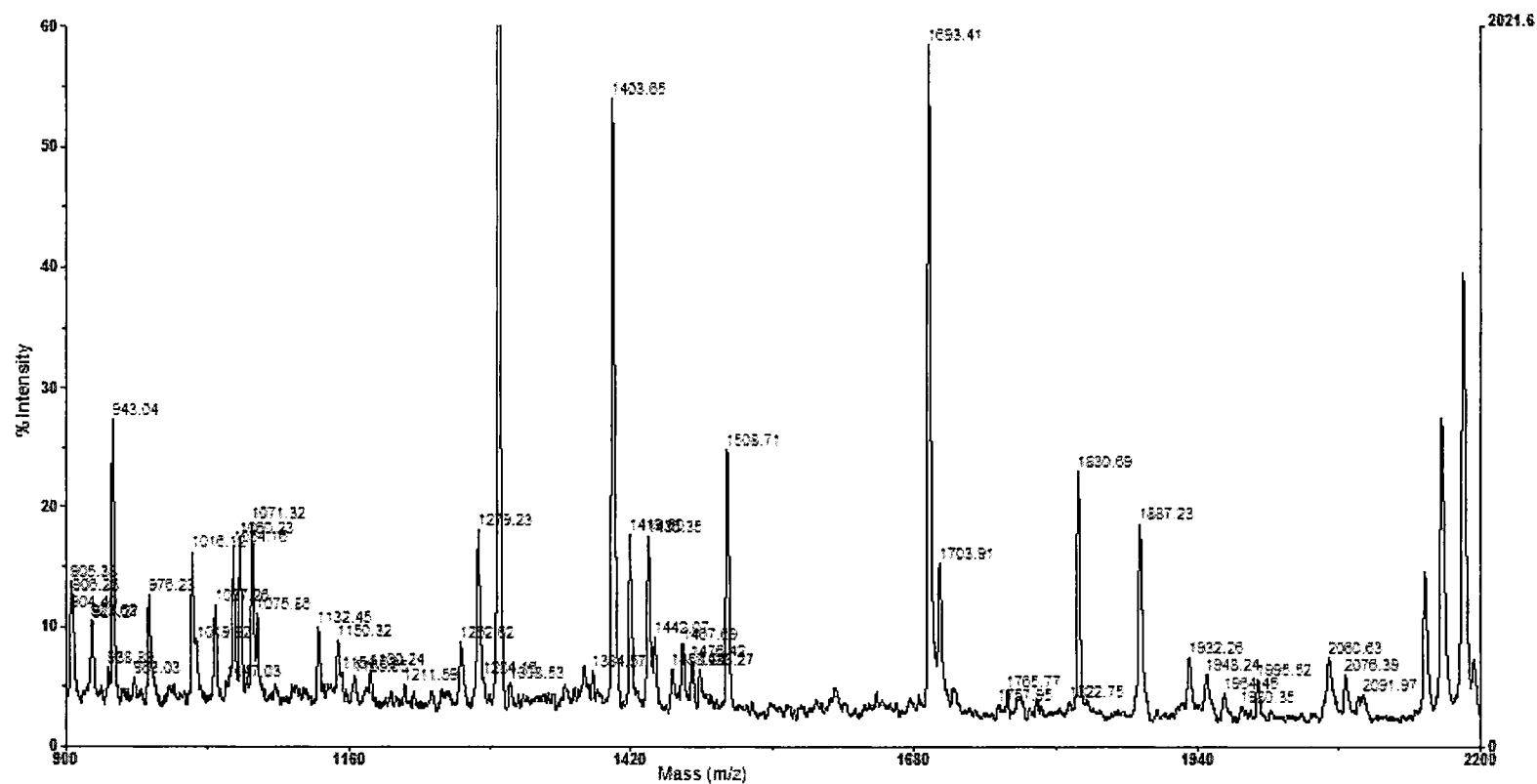


Fig. 35 - MALDI-TOF spectrum of spot 4, fragment mass 900-2200. Spot 4 was HK treated with 350  $\mu$ M ART, migrating to 55 kD and pI 7.0.

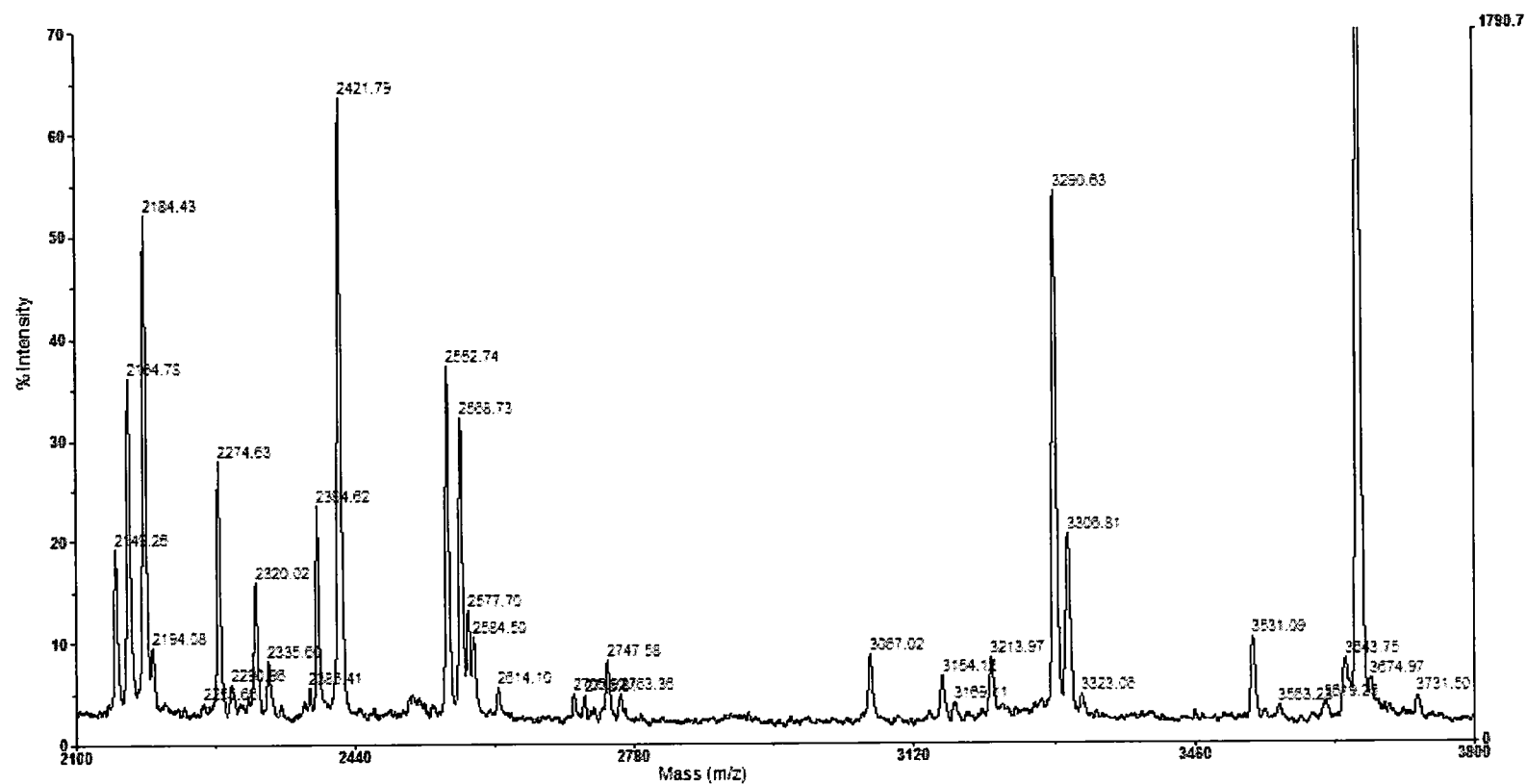


Fig. 36- -MALDI-TOF spectrum of spot 4, fragment mass 2200-3800. Spot 4 was HK treated with 350  $\mu$ M ART, migrating to 55 kD and pI 7.0.

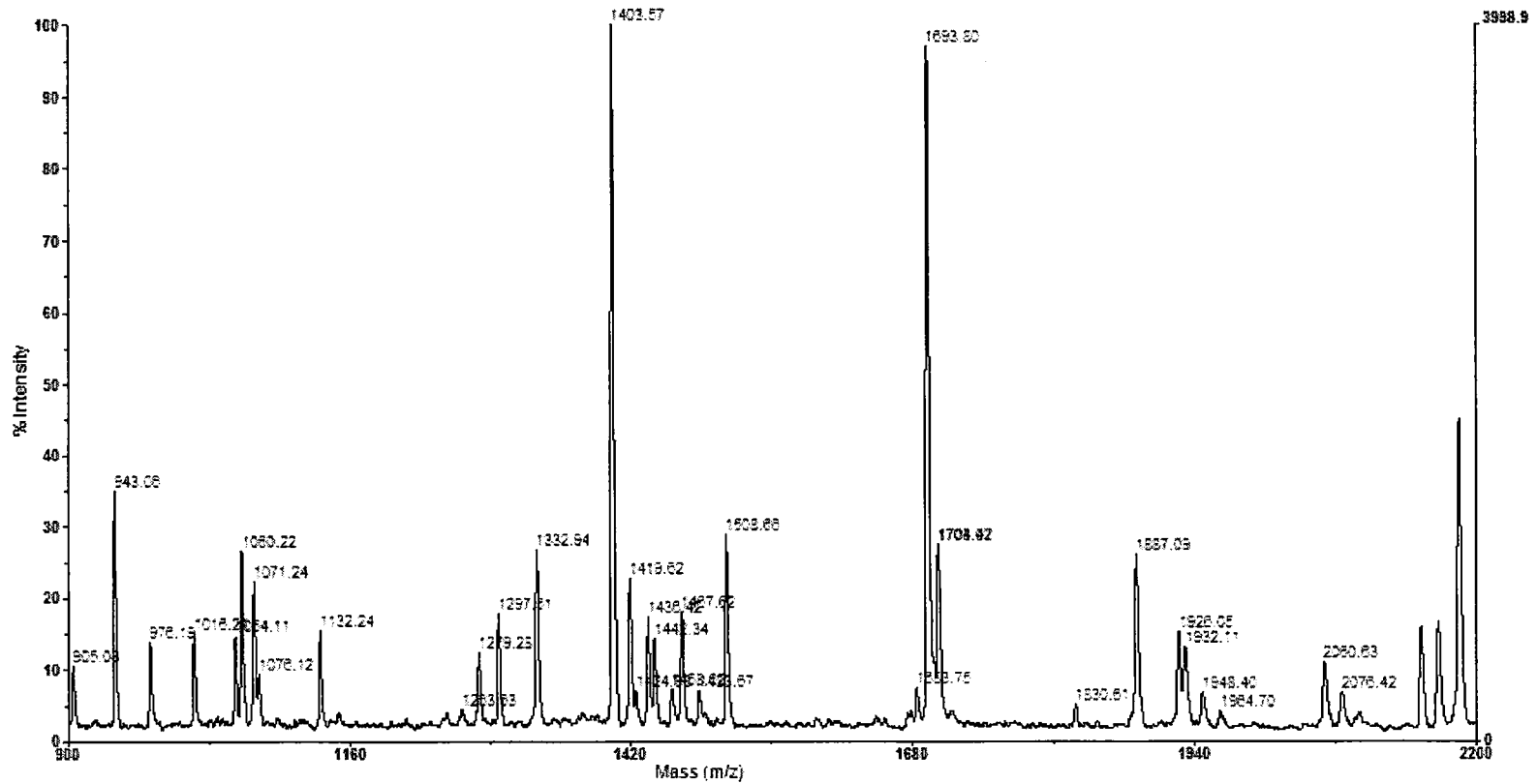


Fig. 37 - MALDI-TOF spectrum of spot 5, fragment mass 900-2200. Spot 5 was HK treated with 350  $\mu\text{M}$  ART and 35  $\mu\text{M}$   $\text{FeCl}_2$ , migrating to 55 kD and pI 7.0.

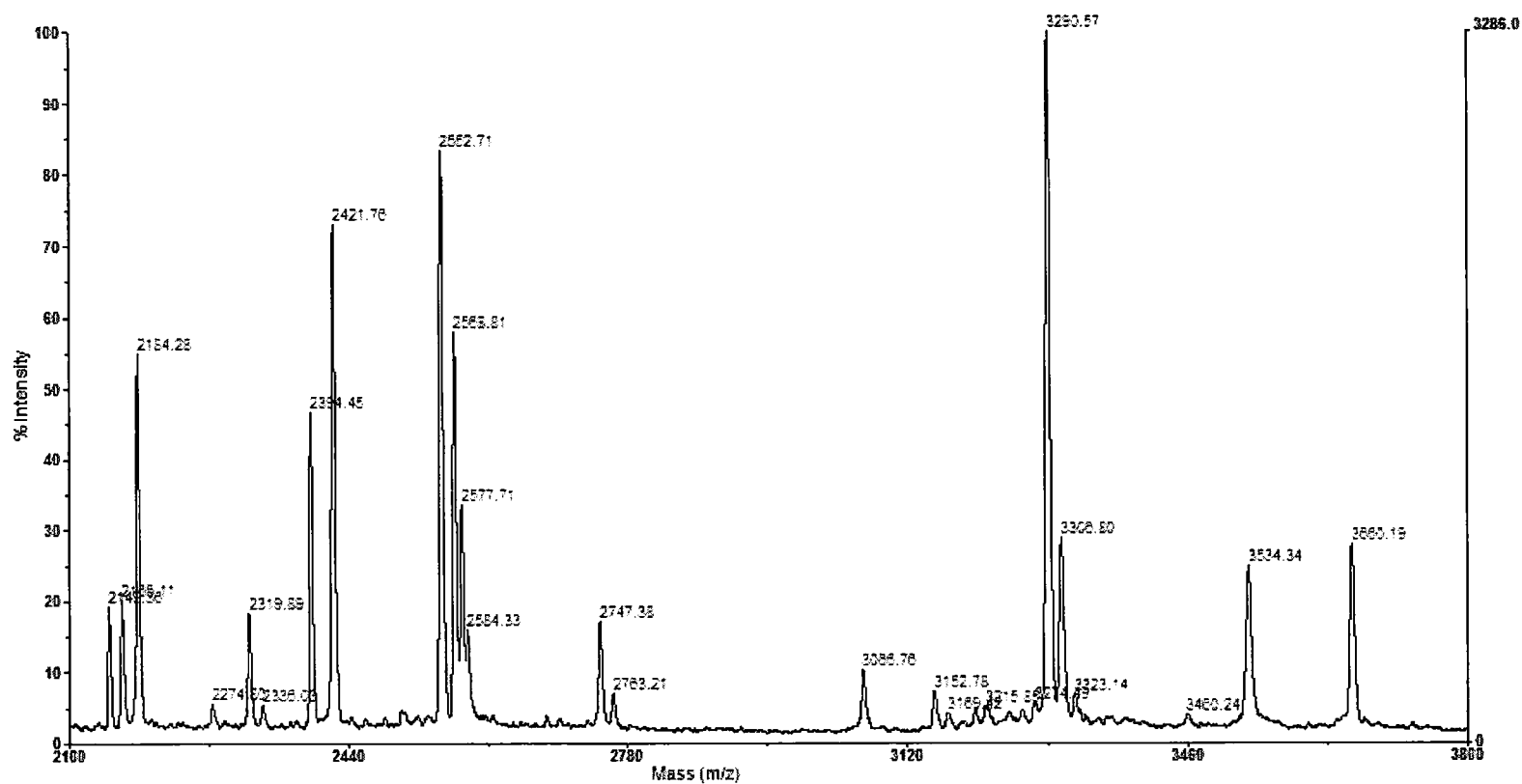


Fig. 38 - MALDI-TOF spectrum of spot 5, fragment mass 2200-3800. Spot 5 was HK treated with 350  $\mu$ M ART and 35  $\mu$ M FeCl<sub>2</sub>, migrating to 55 kD and pI 7.0.

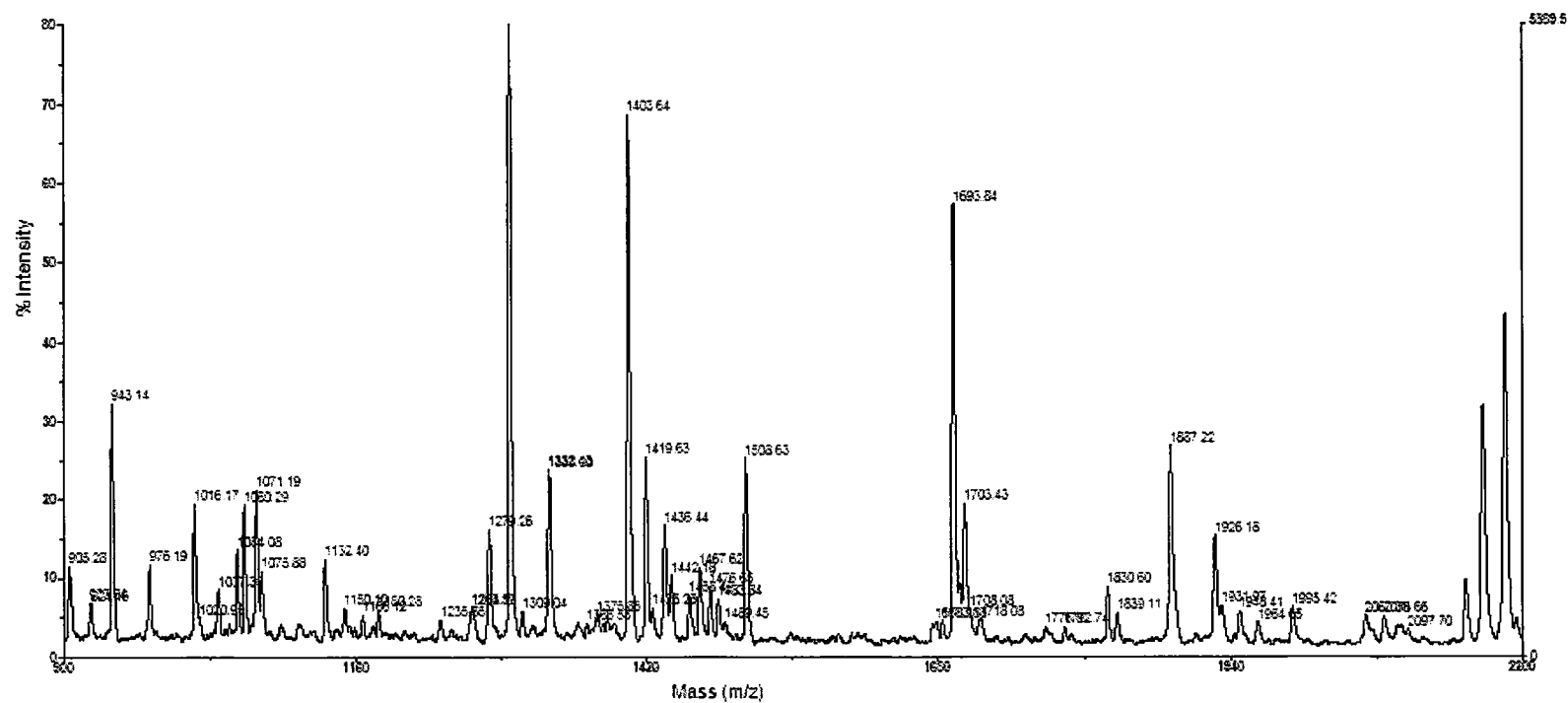


Fig. 39- MALDI-TOF spectrum of spot 6, fragment mass 900-2200. Spot 6 was an untreated HK control migrating to 43 kD and pI 6.2.

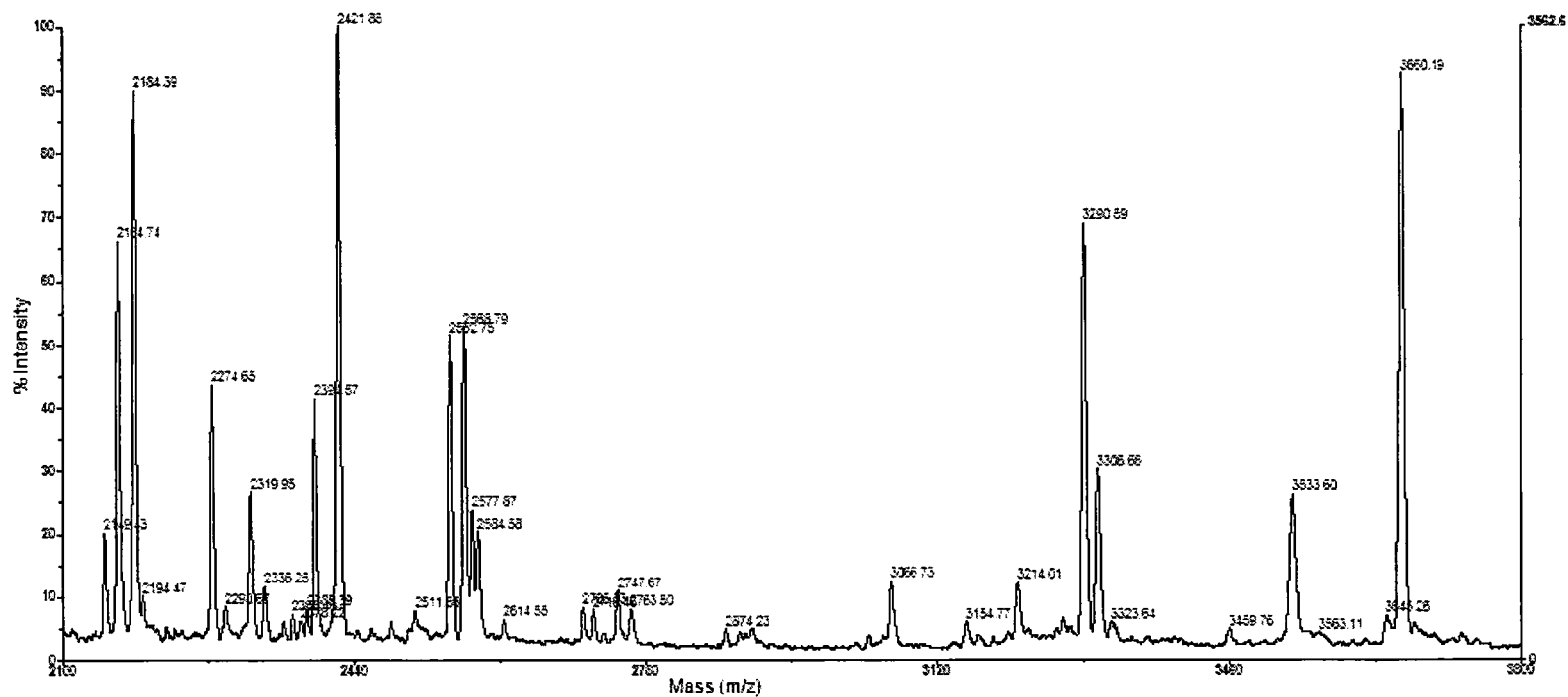


Fig. 40 - MALDI-TOF spectrum of spot 6, fragment mass 2200-3800. Spot 6 was an untreated HK control migrating to 43 kD and pI 6.2.

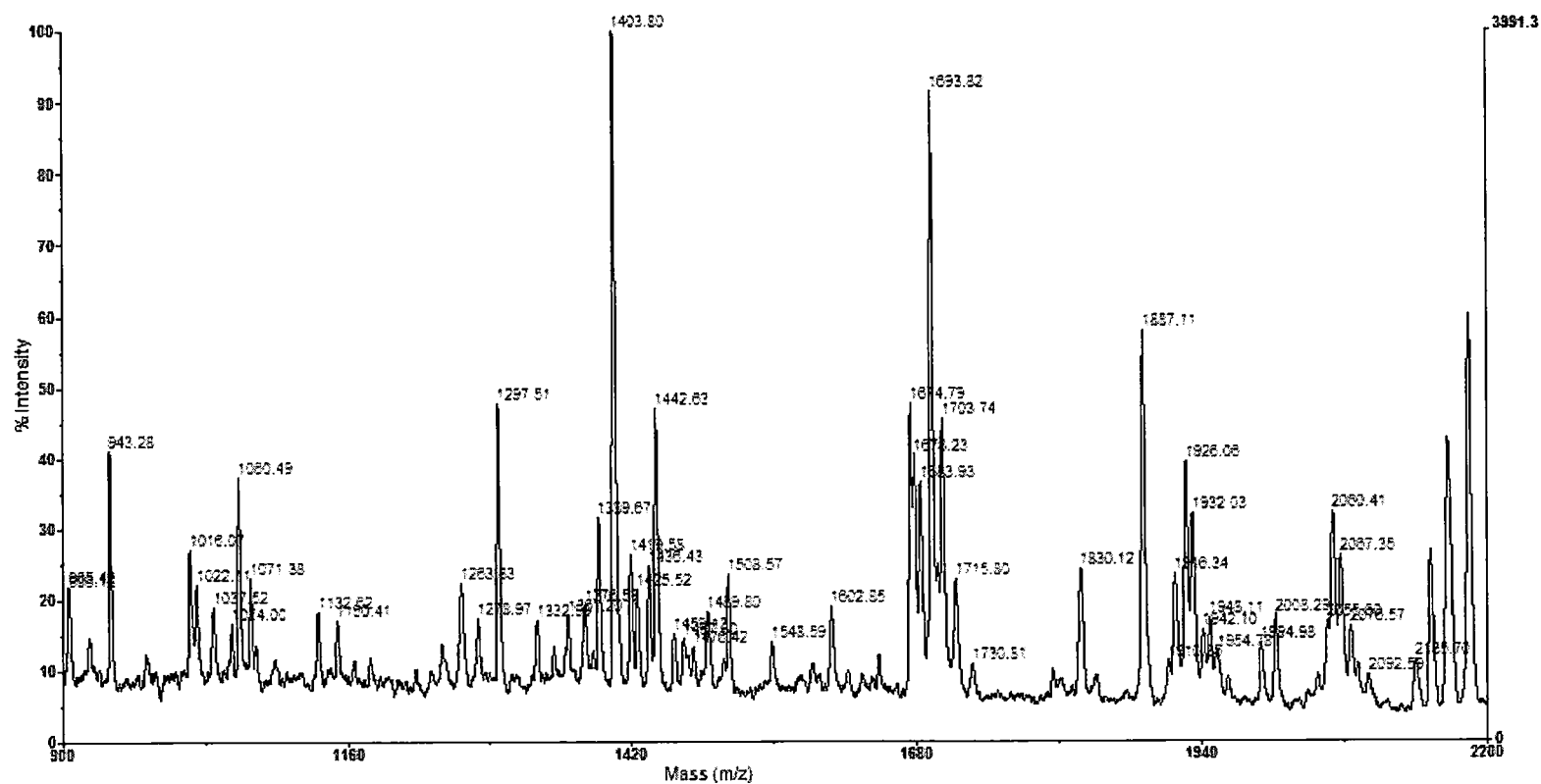


Fig. 41 - MALDI-TOF spectrum of spot 7, fragment mass 900-2200. Spot 7 was HK treated with 0.7% EtOH, migrating to 55 kD and pI 7.0.



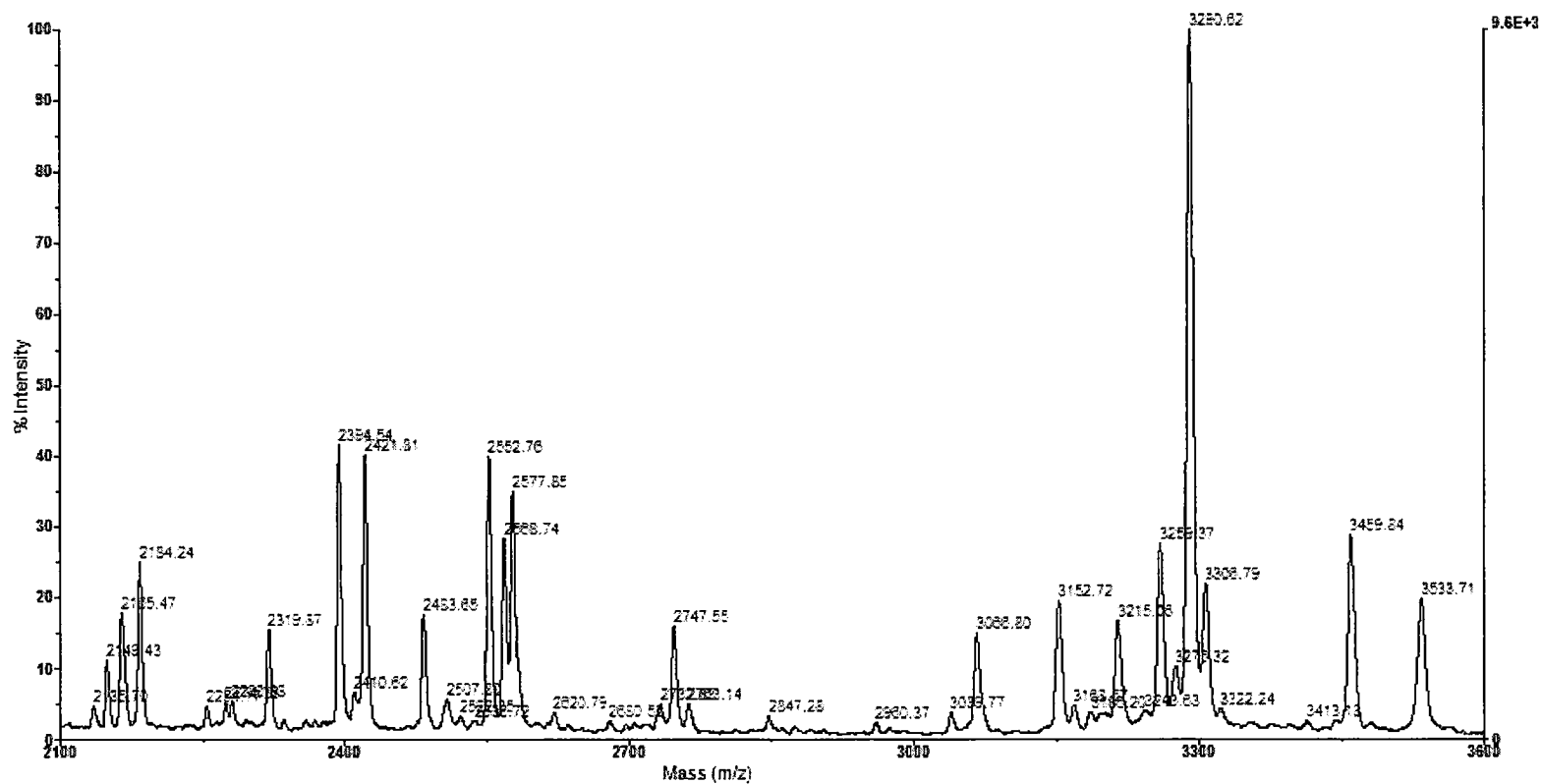


Fig. 42 - MALDI-TOF spectrum of spot 7, fragment mass 2200-3600. Spot 7 was HK treated with 0.7% EtOH, migrating to 55 kD and pI 7.0.

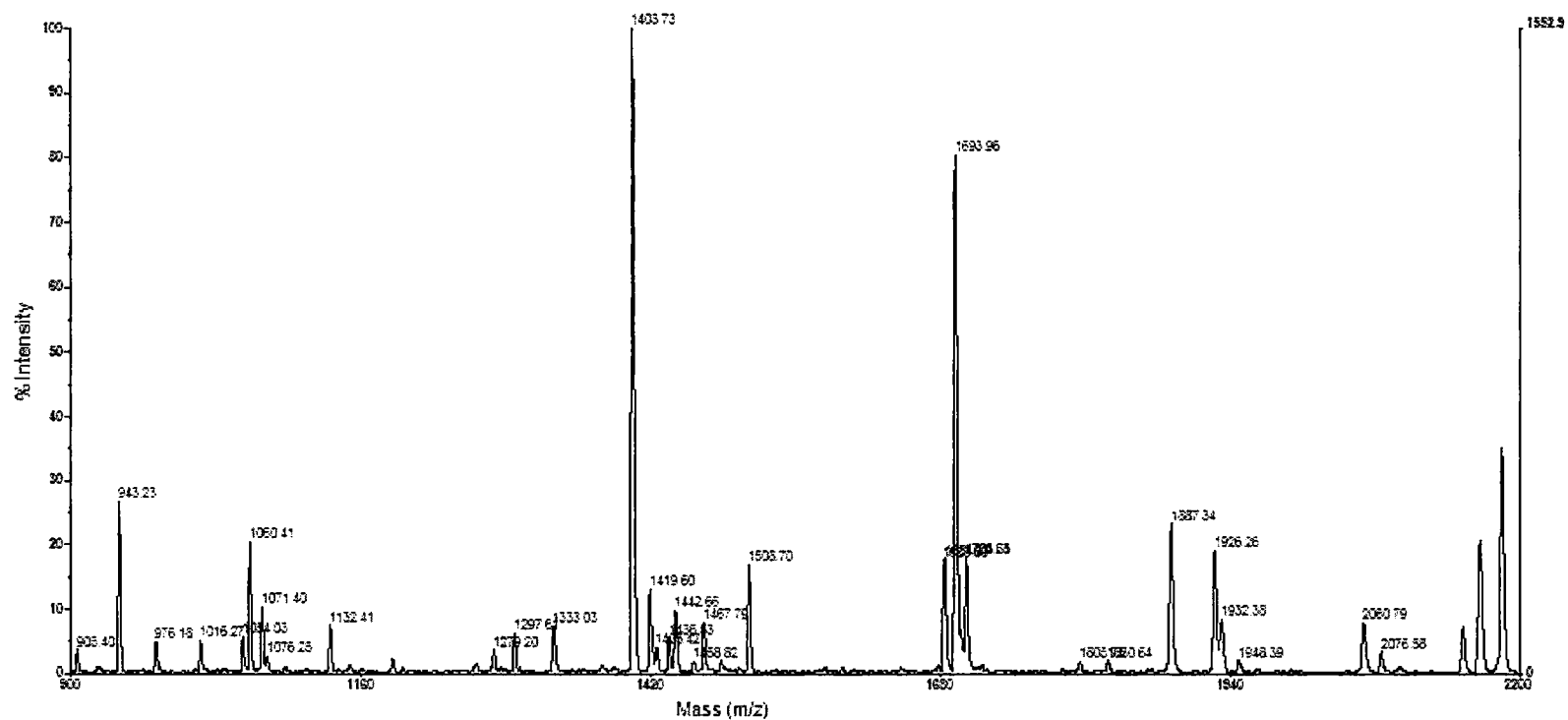


Fig. 43 - MALDI-TOF spectrum of spot 8, fragment mass 900-2200. Spot 8 was HK treated with 0.7% EtOH, migrating to 43 kD and pI 6.2.

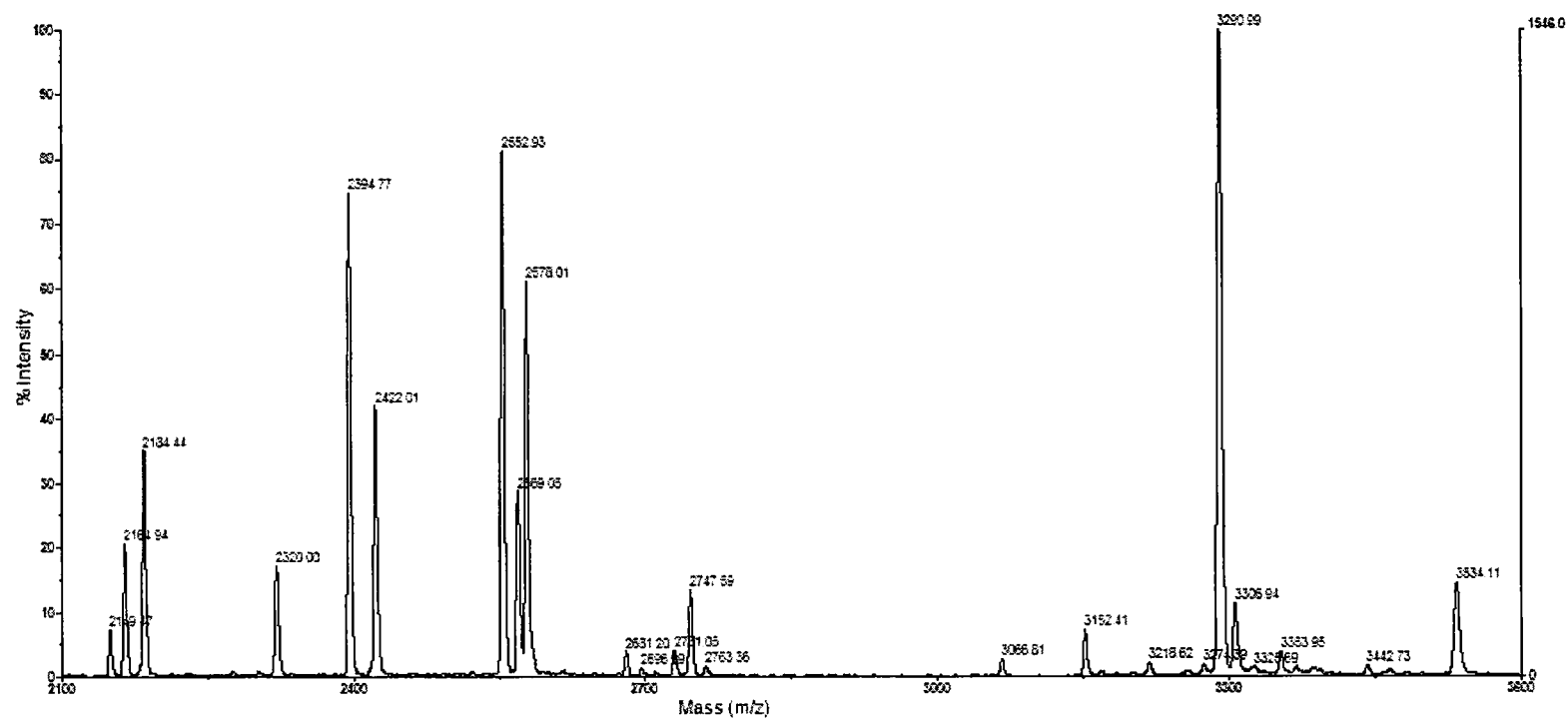


Fig. 44 - MALDI-TOF spectrum of spot 8, fragment mass 2200-3600. Spot 8 was HK treated with 0.7% EtOH, migrating to 43 kD and pI 6.2.

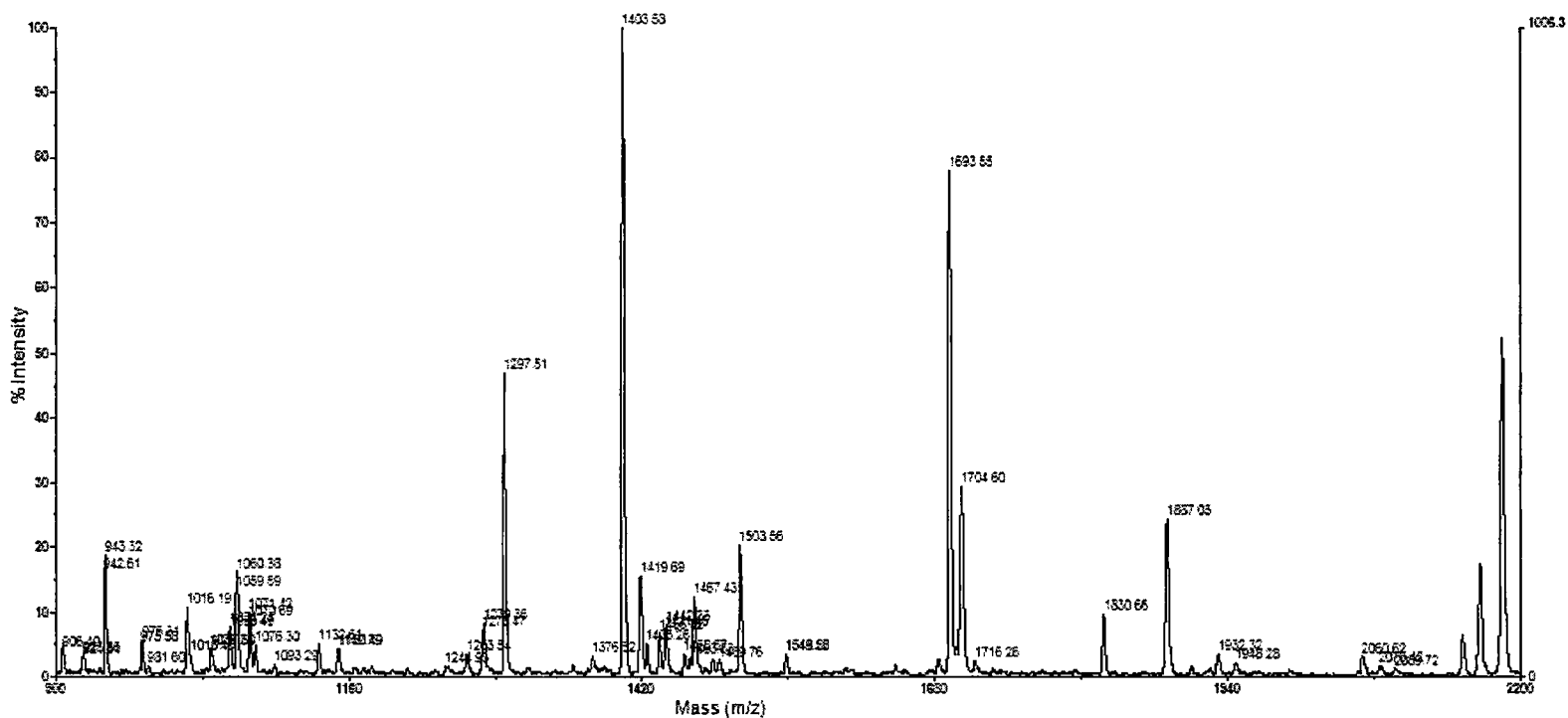


Fig. 45 - MALDI-TOF spectrum of spot 9, fragment mass 900-2200. Spot 9 was HK treated with 350  $\mu\text{M}$  ART and 50  $\mu\text{M}$   $\text{FeCl}_2$ , migrating to 55 kD and pI 7.0.

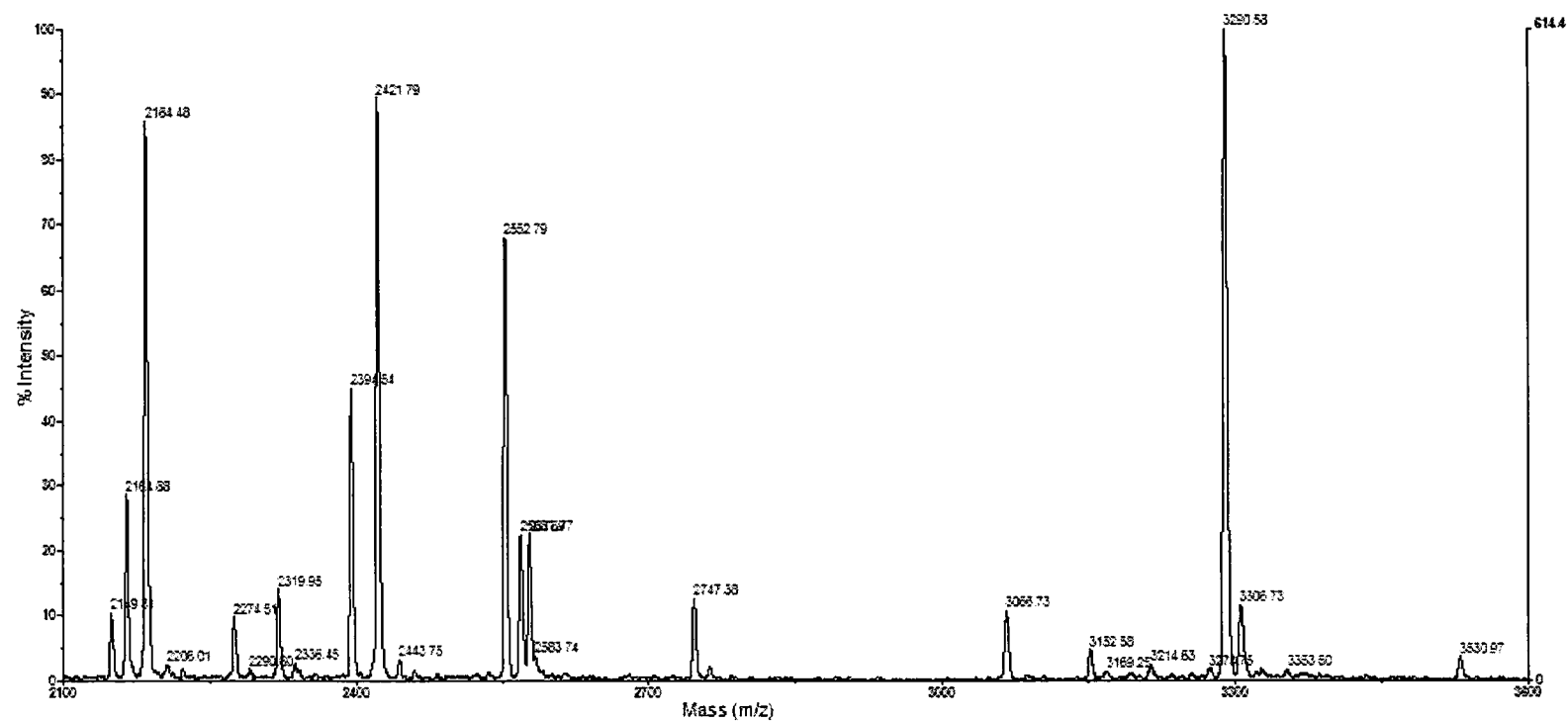


Fig. 46 - MALDI-TOF spectrum of spot 9, fragment mass 2200-3600. Spot 9 was HK treated with 350  $\mu$ M ART and 50  $\mu$ M  $\text{FeCl}_2$ , migrating to 55 kD and pI 7.0.

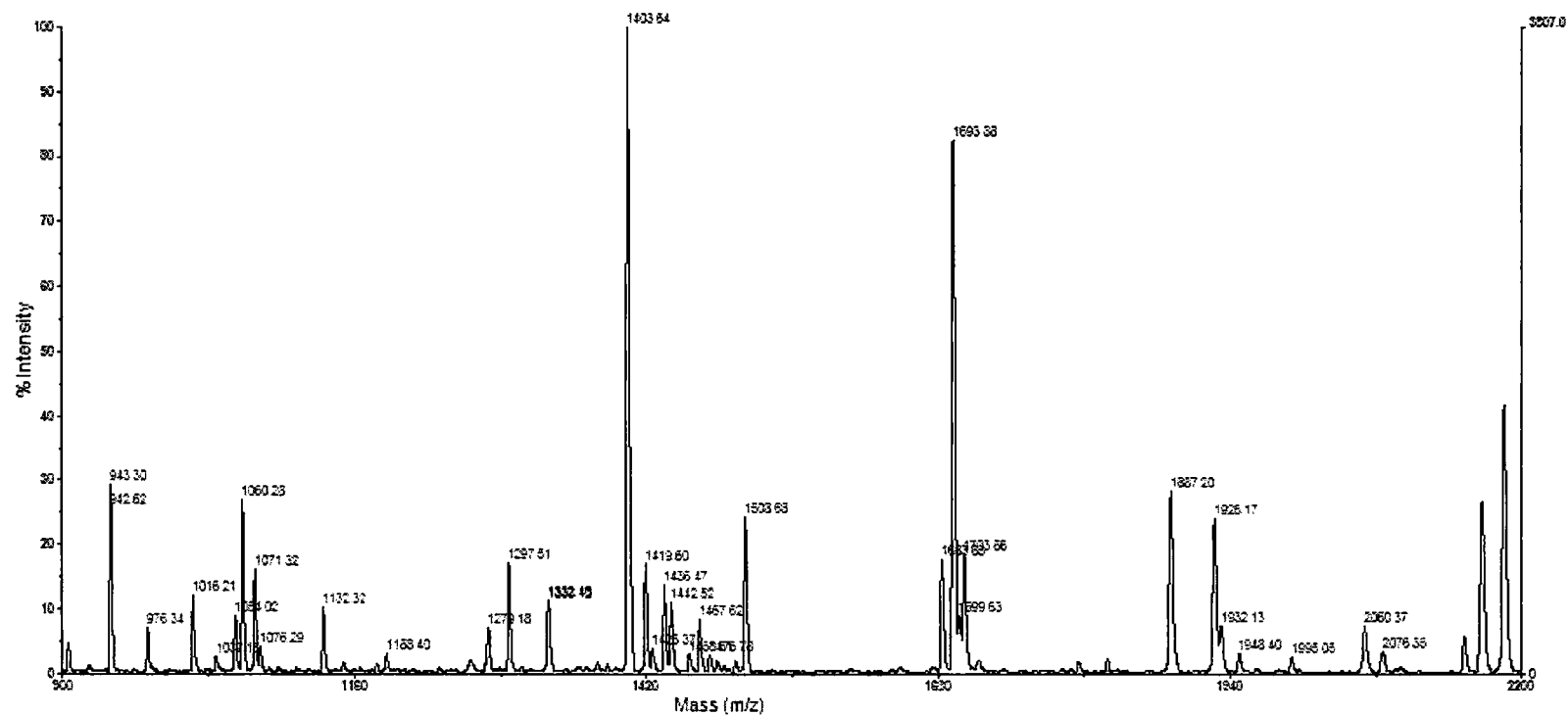


Fig. 47 - MALDI-TOF spectrum of spot 10, fragment mass 900-2200. Spot 10 was HK treated with 350  $\mu$ M ART and 50  $\mu$ M FeCl<sub>2</sub>, migrating to 43 kD and pI 6.2.

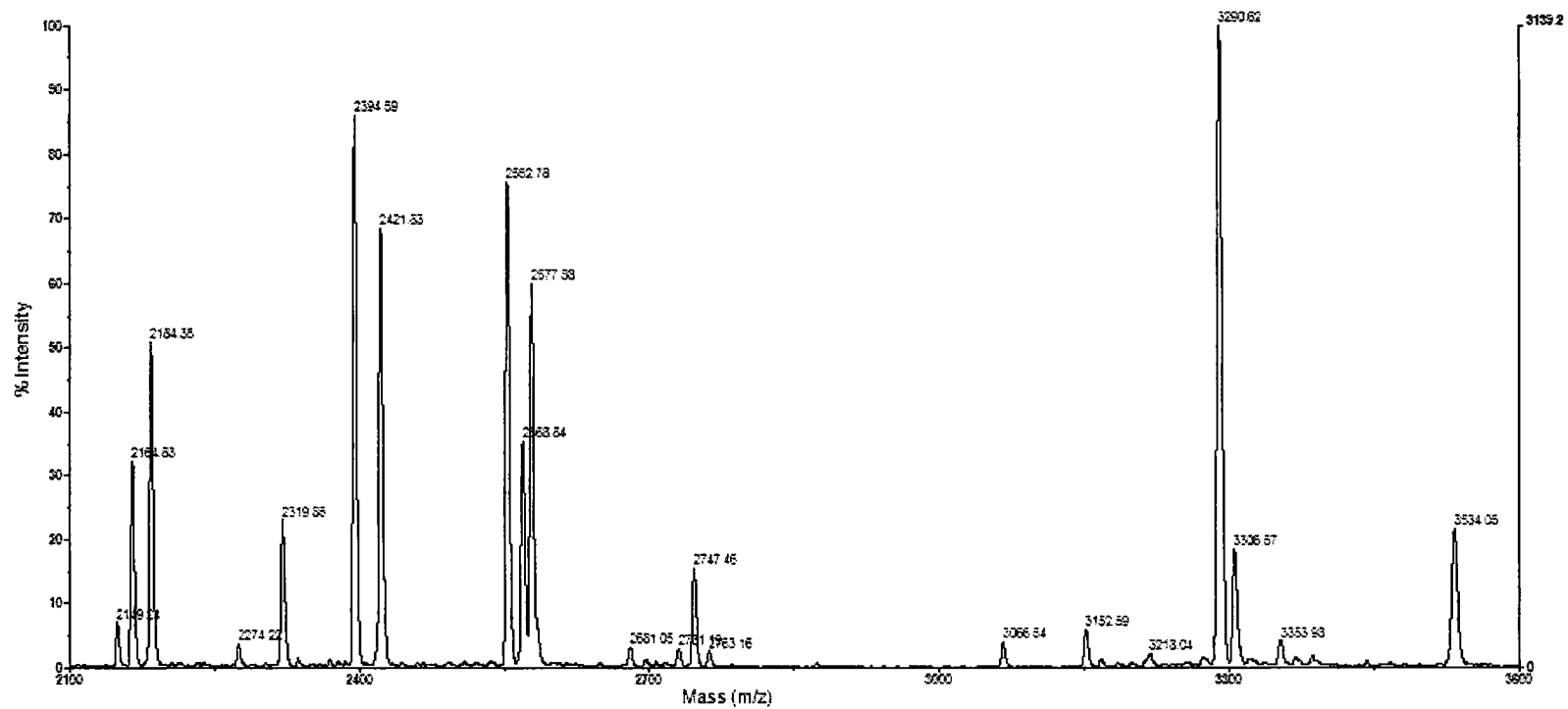


Fig. 48 - MALDI-TOF spectrum of spot 10, fragment mass 2200-3600. Spot 10 was HK treated with 350  $\mu$ M ART and 50  $\mu$ M  $\text{FeCl}_2$ , migrating to 43 kD and pI 6.2.

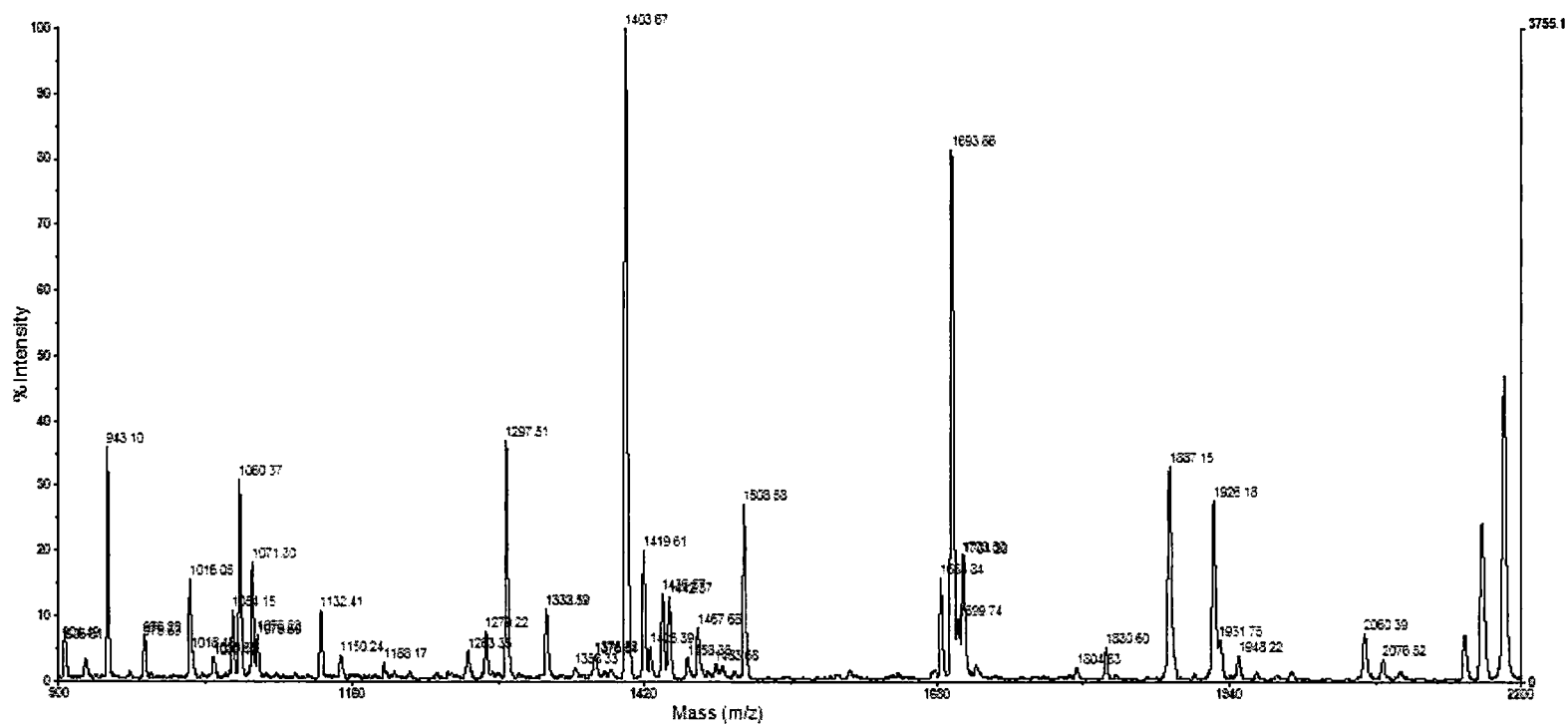


Fig. 49 - MALDI-TOF spectrum of spot 11, fragment mass 900-2200. Spot 11 was HK treated with 100  $\mu$ M FeCl<sub>2</sub>, migrating to 55 kD and pI 7.0.



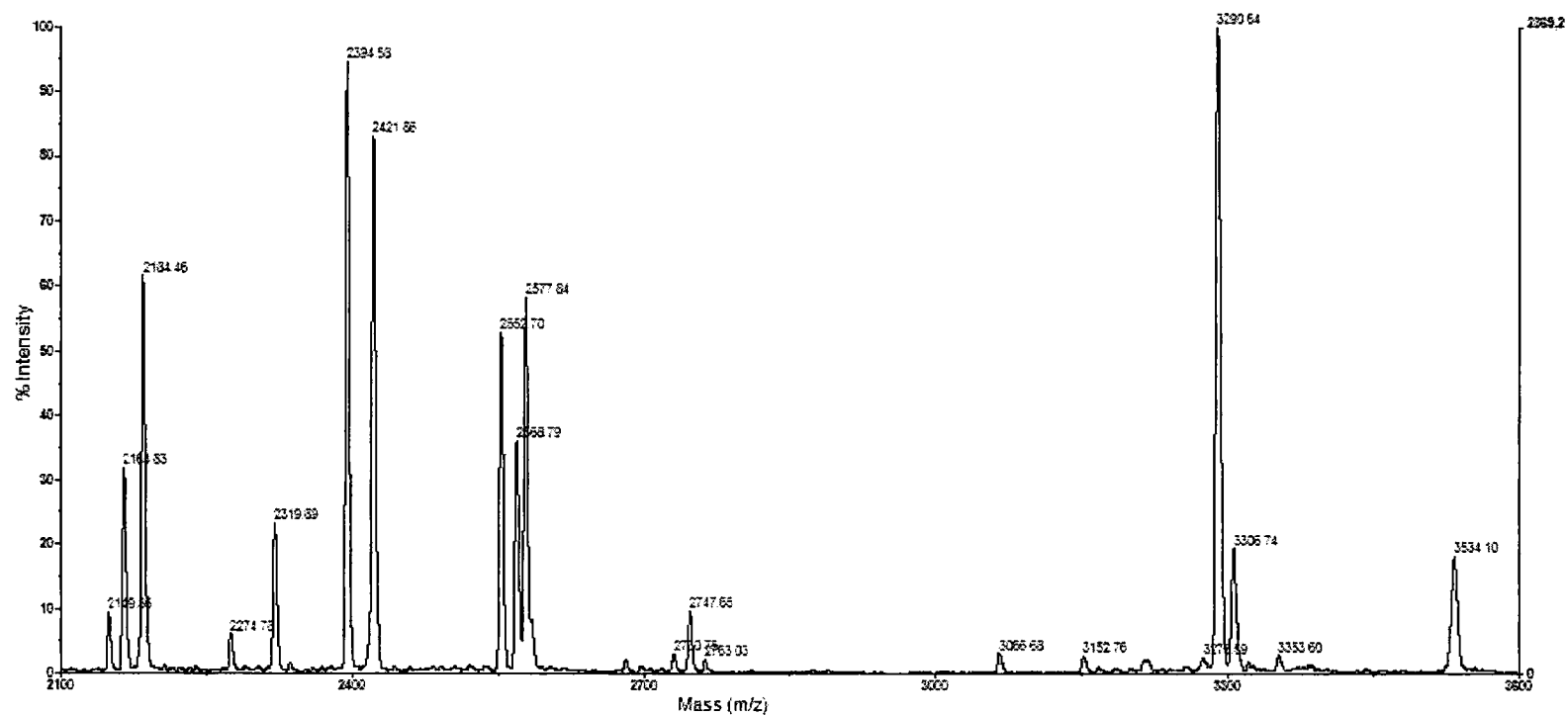


Fig. 50 - MALDI-TOF spectrum of spot 11, fragment mass 2200-3600. Spot 11 was HK treated with 100  $\mu$ M FeCl<sub>2</sub>, migrating to 55 kD and pI 7.0.

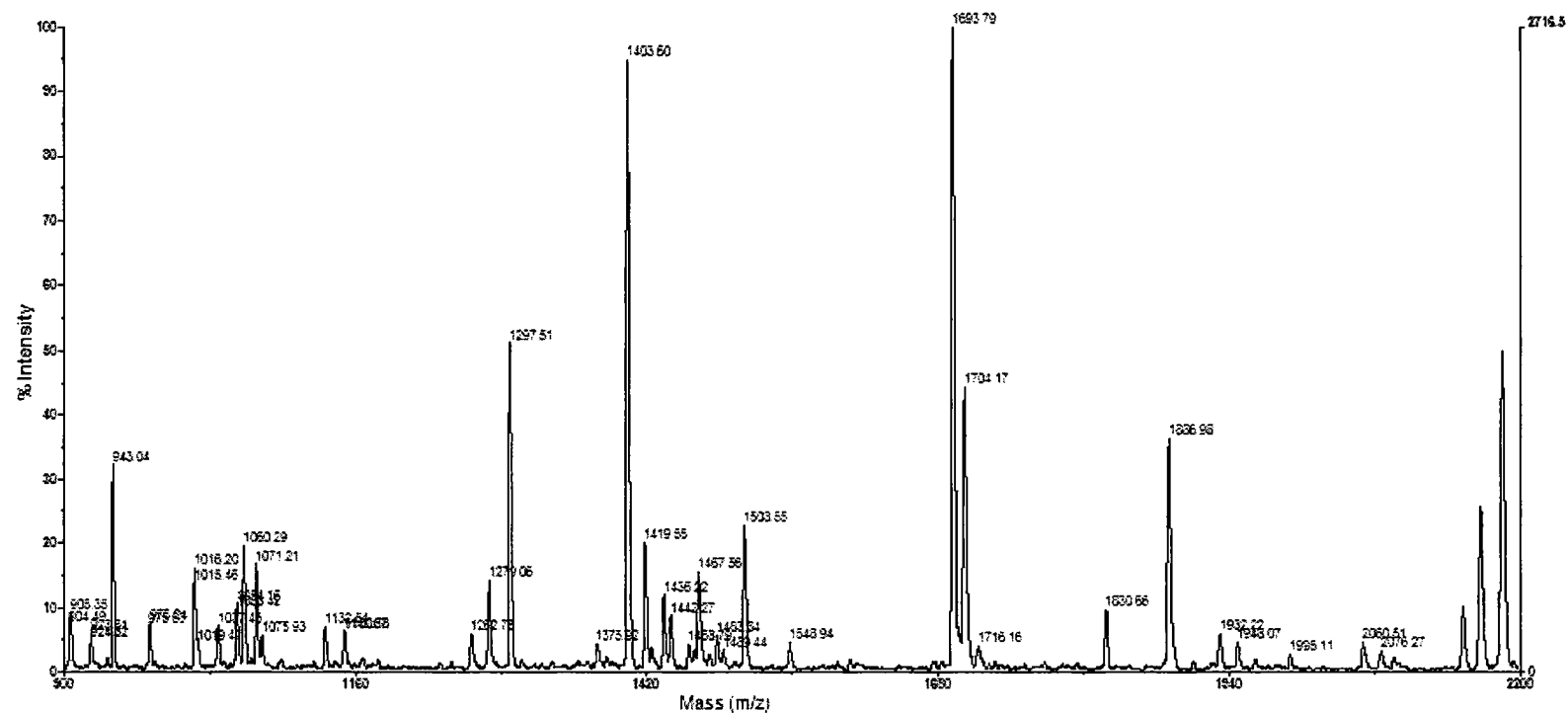


Fig. 51 - MALDI-TOF spectrum of spot 12, fragment mass 900-2200. Spot 12 was HK treated with 350  $\mu$ M ART and 100  $\mu$ M FeCl<sub>2</sub>, migrating to 55 kD and pI 7.0.

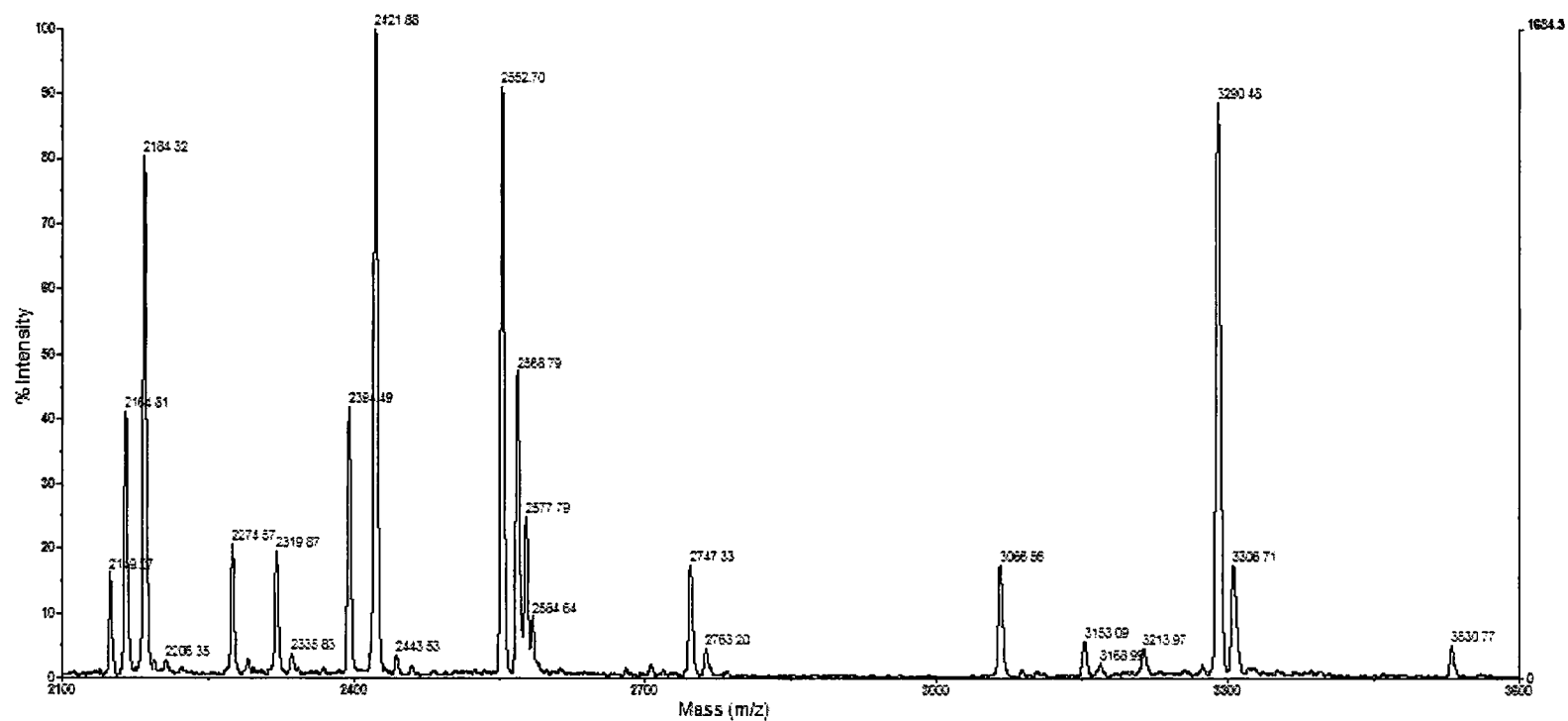


Fig. 52 - MALDI-TOF spectrum of spot 12, fragment mass 2200-3600. Spot 12 was HK treated with 350  $\mu$ M ART and 100  $\mu$ M FeCl<sub>2</sub>, migrating to 55 kD and pI 7.0.

## **VITA**

**Jennifer S. Spence**  
Old Dominion University  
Department of Biological Sciences  
Norfolk, VA

### **Educational Background**

B.S. Biological Sciences, George Washington University, May 2003  
B.A. English Language & Literature, University of Virginia, January 2001

### **Presentations**

Inhibition of Yeast Hexokinase Activity by Artemisinin: an *in vitro* Model of Drug-Protein Binding. American Society of Tropical Medicine & Hygiene Annual Meeting, Atlanta, GA, November 2006.

### **Posters**

Inhibition of Yeast Hexokinase Activity by Artemisinin: Implications for Drug-Protein Binding in the Malaria Parasite. Molecular Parasitology Meeting, Woods Hole, MA, September 2006.

### **Awards**

Board of Regents Fellowship, Tulane University, 2008-2012  
Young Investigator Award, American Society of Tropical Medicine & Hygiene, 2006